Ph.D. DISSERTATION

Highly Sensitive Pressure/Strain Sensor with Nanowire Composite for Skin-attachable Multifunctional Electronics

피부 부착 가능한 다기능 전자소자 구현을 위한

나노와이어 복합체 기반 고민감 압력/변위 센서

구현에 관한 연구

BY

YUNSIK JOO

AUGUST 2016

DEPARTMENT OF ELECTRICAL ENGINEERING AND
COMPUTER SCIENCE
COLLEGE OF ENGINEERING
SEOUL NATIONAL UNIVERSITY

Highly Sensitive Pressure/Strain Sensor with Nanowire Composite for Skin-attachable Multifunctional Electronics

피부 부착 가능한 다기능 전자소자 구현을 위한

나노와이어 복합체 기반 고민감 압력/변위 센서 구현에

관한 연구

지도교수 홍 용 택

이 논문을 공학박사 학위논문으로 제출함

2016 년 8 월

서울대학교 대학원

전기 · 컴퓨터 공학부

주 윤 식

주윤식의 공학박사 학위논문을 인준함

2016 년 8 월

위 원 장 _____ 이 창 희 ____ (인)
부위원장 _____ 홍 용 택 ____ (인)
위   원 _____ 주 영 창 ____ (인)
위   원 _____ 조 규 진 ____ (인)
위   원 _____ 방 창 현 ____ (인)

Abstract

Highly Sensitive Pressure/Strain Sensor with Nanowire Composite for Skin-attachable Multifunctional Electronics

YUNSIK JOO

DEPARTMENT OF ELECTRICAL ENGINEERING AND COMPUTER SCIENCE

COLLEGE OF ENGINEERING

SEOUL NATIONAL UNIVERSITY

In this dissertation, we describe the highly sensitive pressure/strain sensor with nanowire composite for skin-attachable and wearable electronics. Multiscale structured nanowire composite composed of silver nanowires (AgNWs) and polydimethylsiloxane (PDMS) was designed and fabricated for the high performance multifunctional sensor. Based on this multiscale structured nanowire composite, high performance pressure/strain sensors were fabricated and characterized.

Nowadays, flexible and stretchable physical sensors such as pressure, strain, and temperature sensors have been widely investigated for the application to the wearable electronics. Especially, high performance pressure/strain sensors which show high sensitivity, fast response time, and high cycle stability are required. Due to these requirements, we developed the nanowire composite, the flexible and

stretchable electrode, and introduced the multiscale structure with nanometer-sized rough surface and micrometer-sized wavy structure to the nanowire composite. By integrating this nanowire composite and polymeric dielectric layer/printed Ag electrode, we fabricated capacitive-type pressure sensors and arrays. High pressure sensitivity ($S > 3.8$ kPa^{-1}), fast response and relaxation time (t <0.15s), high cycle stability (1500-cycle of repeated loading/unloading of pressure and 5000-cycle of repeated bending with bending radius of 3mm), and multiple sensing such as pressure and bending were obtained. Nanowire composite with multiscale structure can be easily scaled up for a large area sensor array and sensor arrays with 3×3 and 5×5 pixels were fabricated. The sensor arrays can detect the spatial distribution of the applied pressure with the sensitivity as high as that of the single sensor. Wearable fingertip pressure sensor was fabricated to demonstrate the fingertip pressure sensing prototype device. We attached each pressure sensor on the four fingers except a little finger and measured the capacitance change by grabbing plastic beaker.

We developed simple method to control the pressure sensitivity of the sensor. Simply, by controlling the mixing ratio of the matrix PDMS of the nanowire composite, we can tune the pressure sensitivity of the sensor. Three types of PDMS with different mixing ratio, a 5:1, 10:1, and 15:1 mixture of liquid PDMS and curing agent, were used to fabricate nanowire composites and sensors. Owing to the difference of Young's modulus and the shape of the crest area of nanowire composites with different mixing ratio, pressure sensors showed different pressure sensitivity according to different mixing ratio.

We investigated the highly bendable pressure sensor with high bending stability and pressure sensing ability in the bending state. By introducing bending sensing part beside the pressure sensing part, the bendable sensor can detect both

pressure and bending and distinguish the pressure and bending. We used the surface functionalization method and the PDMS spacer to demonstrate the bendable sensor. Strong siloxane bonding between the surface functionalized bottom plane, PDMS spacers and patterned nanowire composite was obtained and based on this bonding, our sensor showed high bending stability. Pressure sensitivity of the bendable sensor was increased up to $9\,kPa^{-1}$ owing to the air gap from the PDMS spacer. The bendable sensor can detect ultra-low pressure of 0.7 Pa and show fast response and relaxation time below 0.075s. Even in the bending state, the bendable sensor can detect the normal pressure. By using this bendable sensor, we fabricated the wearable sensor to measure the wrist pulse and vibration of smart phone. Sensor array was also fabricated and we estimated the pressure in the bending state by calculating the capacitance change. We demonstrated the pressure sensitive transistor (PST) by integrating the bendable sensor and prined single-walled carbon nanotube thin film transistor (SWCNT TFT). PST can be operated in low voltage below 5V and ultra-low power consumption of PST below 15 nW can be achieved (I_{DS} < 15nA, V_{DS} = −1V). By using the PST and commercially available electronic devices such as LED chip, resistor, OP amp and battery, we fabricated the user inter-active pressure sensing device and pulse monitoring device.

Finally, we developed the stretchable multifunctional sensor which can detect the 3-axis force, the normal force and shear force, and strain by using nanowire composite for the application to the electronic skin. By introducing various sensing component to the sensing system, we can obtain multifunctional sensor to mimic human tactile receptors and skin. For the 3-axis sensing, four individual capacitive sensors composed single sensing cell. Our sensor can sense and distinguish the pressure and shear force by analyzing the capacitance change of four individual

capacitive sensors. For the strain sensing, flat nanowire composite was used. During the stretching process, the flat nanowire composite was deformed and this deformation resulted in the resistance change of the flat nanowire composite. Our sensor can detect the strain by analyzing the resistance change of the flat nanowire composite.

Contents

List of Tables

List of Figures

Chapter 1

Introduction

1.1 Wearable electronics

Wearing electronic devices with multi-function is one of wishes of many people and engineers and now being actualized through wearable electronics and technologies. Technologies for the realization of wearing computers and integrated sensors have been widely investigated and these technologies will be accomplished in near future. Wearable electronics began from the development of wearable computers and wearable computers are electronic devices that are worn on the clothing or our body [1]. Prototype wearable electronics have been developed and commercialized, for example, displaying textiles from CuteCircuit, wearable mouse (Mycestro), smart watches (Fitbit, Galaxy gear, etc.) and Google Glass. And much more wearable electronics will be developed and commercialized based on these prototypes. Wearable electronics can be applied to various areas. Main application is the wearable computers for infotainment. The aim of wearable computers is the ubiquitous computers and various information can be communicated from wearable computers to people or from people to wearable computers. Advanced human-machine interface, wearable sensors and health monitoring system, pattern recognition and augmented reality can be included in the researching area of

wearable computers [1].

Among them, wearable sensors and health monitoring systems have been widely investigated. For these wearable electronics, physical or mechanical sensors are necessary as core devices. Sensors which can detect the movement of human body or muscles (strain or pressure from body or muscles), the pulse, blood pressure, heat and infrared radiation are generally used and applied to these wearable electronics (Figure 1.1) [2-7]. Electrograms such as electrocardiography (ECG), electromyography (EMG), and electroencephalography (EEG), which measure electrical signals from the heart, muscles, and brain, respectively, have been used as measuring tools and sensors [8] for diagnosis, therapy, and monitoring of health [9]. Conventional sensors using these electrograms are rigid and bulky mostly. Due to rigidity and large-bulk, these sensors have some limits to realize the skin-mountable and conformable wearable electronics. Recently, physical sensors with light weight, flexibility, and stretchability have been demonstrated [2-7, 10-12]. These sensors include various types of sensors such as pressure, strain, and temperature sensors. By integrating these sensors with communication modules and self-sustainable power supply devices, wearable sensors and health monitoring systems which can be mounted on the skin have been demonstrated to detect physiological signals of human body [4, 6-7]. Also, by integrating physical sensors with chemical or bio sensors, electronic skins which mimic the human skin or show superiority beyond the human skin can be realized and applied to the prosthetic skin, robotic skin, patient rehabilitation, firefighter uniform, and military armor (Figure 1.1(c)).
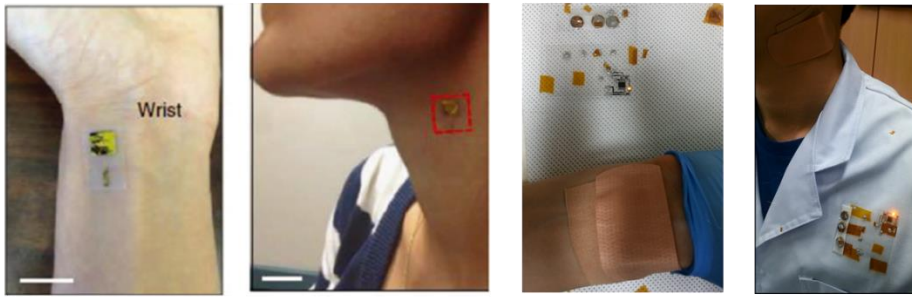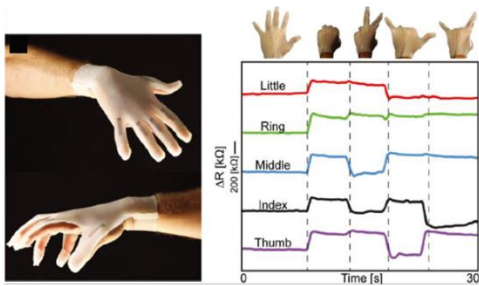
Figure 1.1 Wearable sensors and electronic skin. (a) Pulse monitoring sensors (Reference [4]).
(b) Motion detection sensor (Strain sensor) (Reference [38]). (c) Electronic skin (Reference
[3,6]).

1.2 Pressure sensor

Pressure is the force applied perpendicular to the surface of an object per unit area over which that force is distributed. Pressure is ubiquitous in nature and human activity. For example, atmospheric, gas and liquid pressure induced from the Earth's gravity, human body related pressures such as blood and intraocular pressure, gentle touch, hug, clap, etc., and crash between two objects can be pressure. Pressure sensors are pressure measuring devises and transducers that can operate in a signal transduction [13-14]. The human body related pressures are mainly distributed in low- (<10 kPa) to midum-pressure ranges (10-100 kPa) [13-14] and the human skin generally can detect these pressures (Figure 1.2). The detection of the pressures of these ranges is crucial for the wearable health monitoring system and electronic skins [13-14].

Flexible and stretchable pressure sensors have been researched widely as a core device for the wearable electronics due to their versatile applications such as wearable health monitoring system, electronic skins and human-machine interfaces [4-6,8,13-32]. Most of pressure sensors mimic the tactile receptor of the human skin which shows high pressure sensitivity, fast response time, mechanical softness and high stability and these things are the key parameters of pressure sensors. The sensitivity is one of the most important parameters of pressure sensors. The pressure sensitivity is defined as $S = dX/dP$, where S is the sensitivity and X and P denote the quantitative output signal and applied pressure, respectively [13]. High pressure sensitivity ($S > 0.1$ kPa^{-1}) is desirable to pressure sensors, because pressure sensitivity determines the measurement accuracy and effectiveness of the device and high pressure sensitivity means high accuracy and effectiveness [13]. The response

time is also an important parameter of pressure sensors. The response time is defined as the time consumption of a pressure sensor during response processes, from inputting pressure to producing a signal output [13]. Quick response of the pressure sensor from the external pressure or mechanical stimulus is desirable and needed (response time < 0.5s). Mechanical softness of pressure sensors is an important parameter for realization of the wearable electronics. Electronic devices with mechanical flexibility of stretchability only can realize the true wearable electronics without any inconvenience. Lastly, the high stability of pressure sensors must be satisfied. Pressure sensors must be robust and stable to repetitive pressures and mechanical deformations such as bending or stretching. Also, low power consumption of pressure sensors must be satisfied for the wearable electronics.

Various pressure sensing and transduction mechanisms have been demonstrated. First transduction mechanism is piezoresistive type. Piezoresistive sensors transduce a change in the resistance of a device into a measurement of pressure and have been investigated extensively because of their simple device structures and easy read-out mechanism [13-14]. The change of the resistance can be derived from several factors. Typically, the change of contact resistance between two materials and the change of the total resistance of conducting composite due to change of the distance between conducting particles have been widely used as piezoresistive sensing mechanisms. Piezoresistive polymer composites have been extensively investigated recently and piezoresistance of composite materials depends on the composition, morphology, and pressure range of the system. Mainly the modification of tunneling resistance between fillers and the break-up and reforming of percolating pathways have been used as mechanisms. In early days, PSR (pressure sensitive rubber) material have been widely used to demonstrate electronic skins. PSR has conducting carbon

5

particle fillers and elastomeric matrix. Someya and coworkers have demonstrated large area electronic skin by integrating PSR with OFETs (organic field effect transistors) [15]. Javey and coworkers also have demonstrated large area electronic skin by integrating PSR with semiconducting nanowires and SWCNTs (single-walled carbon nanotubes) [16-17]. Javey and coworkers demonstrated user-interactive electronic skin for pressure visualization by integrating pressure sensor arrays with OLEDs (organic light-emitting diodes) [17]. Recently, nano materials such as graphene, gold nanowire, PEDOT:PSS (poly(3,4-ethylenedioxythiophene–poly(styrenesulfonate)) and CNTs have been used by integrating with microstructure to surpass the sensing properties of PSR [18-21].

Second transduction mechanism is capacitive type. Capacitive sensors transduce a change in the capacitance of a device into a measurement of pressure and have been investigated extensively because of their simple device structures and low power consumption [13-14]. The capacitance (C) of a parallel plate capacitor is given by: $C = \varepsilon_0 \varepsilon_r\, A/d$, where ε_0 is the free space permittivity, ε_r is the relative permittivity, A is the area, and d is the distance between electrodes [22]. The dielectric materials for the capacitive sensors must show deformable properties to the external mechanical stimulus and based on this reason elastomeric materials have been widely used as dielectric materials. Simply, the distance d is changed from the applied pressure and this results in the change of the capacitance. Dielectric materials with elastomeric property and low modulus such as PDMS and Ecoflex have been used and stretchable and transparent capacitive sensors have been demonstrated by using these materials with CNTs or AgNWs (silver nanowires) [23-24]. However, these sensors show relatively low pressure sensitivity (S <0.1 kPa^{-1}) due to their limited compressibility. Low pressure sensitivity of capacitive sensors was overcame

6

by introducing microstructure to the dielectric material. Owing to the microstructure, the dielectric material can be compressed more easily and the pressure sensitivity of the capacitive sensors was enormously enhanced (S >0.5 kPa^{-1}) [25]. Capacitive sensors also can be integrated with transistors as a dielectric layer or gate insulator. Bao and coworkers demonstrated pressure sensitive transistors by integrating the microstructured dielectric layer with organic transistors [25-26] and they showed high pressure sensitivity. Zhu and coworkers also demonstrated the pressure sensitive transistor with suspended gate structure and organic transistor and this sensor showed ultra-high pressure sensitivity (S ~192 kPa^{-1}) [27]. However, operation voltages for these pressure sensitive transistors are somewhat high (V$_{gate}$ > 60V) and power consumptions are also high for the application to wearable electronics.

Third transduction mechanism is piezoelectric type. Piezoelectric sensors transduce the generation of electrical charges of a device into a measurement of pressure and have been investigated extensively because of their high sensitivity and fast response time [13-14]. Piezoelectricity means the electrical charge generation in certain materials from the applied mechanical stress to the materials. To generate electrical charges, electric dipole moments must occur in materials when external pressure or mechanical stress is applied. PZT (lead zirconate titanate) and ZnO (zinc oxide) have been widely investigated as piezoelectric inorganic materials [28-29]. Baik and coworkers have demonstrated piezoelectric nanogenerator and pressure sensor by using ZnO hollow hemisphere [30]. For flexible pressure senor, polymer materials with piezoelectric effect also have been investigated. PVDF (Poly(vinylidenedifluoride)) and its copolymer have been widely used due to their flexibility and easy processing (solubility in solvent) [31]. These piezoelectric

7

pressure sensors showed high sensitivity and fast response time and used to measure the vibrations of sound and slip. However, these sensors are hard to detect static pressure and exhibit drift in sensor response over time [14].

Other types of pressure sensors also have been demonstrated, including triboelectric sensor and optical sensor. Triboelectric pressure sensors use the principle of triboelectric effect. The triboelectric effect is a contact-induced electrification in which a material becomes electrically charged after it is contacted with a different material through friction and this triboelectric effect happens every day in our life [32-33]. Wang and coworkers applied this common effect to pressure sensors and nanogenerators, inversely [32-33]. Optical pressure sensors can detect the pressure from the modulation of the light intensity [14]. These sensors consist of the light source, transmission medium and light detector. Due to the deformation of the transmission medium for the applied pressure, the light intensity is modulated and the modulated light intensity was detected through the light detector. Force-sensitive waveguides or flexible optical fibers has been used for optical pressure sensors [34-36].

Figure 1.2 Pressure ranges about each application and human skin.
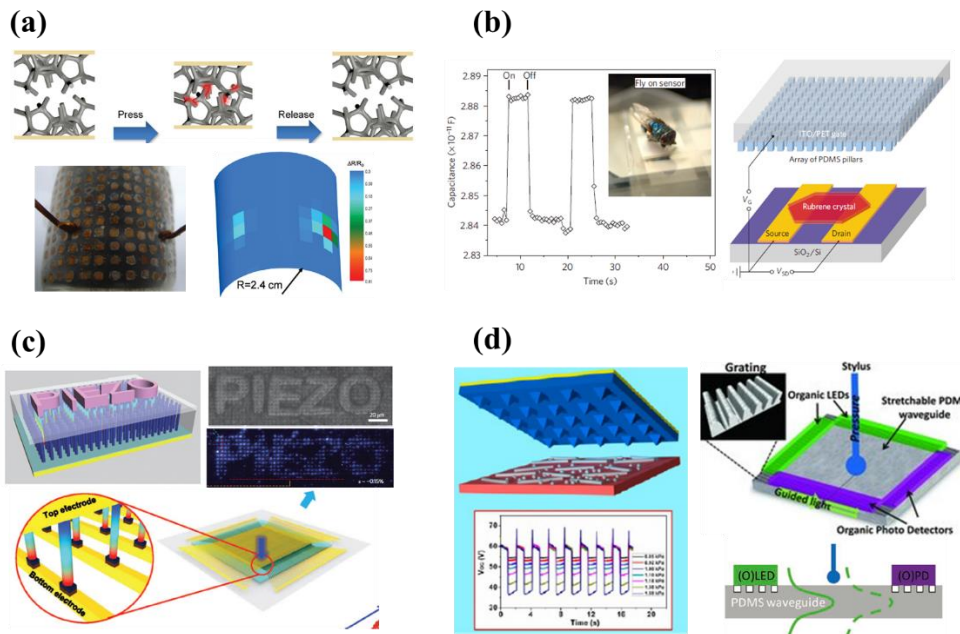
Figure 1.3 Various types of pressure sensors. (a) Piezoresistive-type sensor (Reference [18]). (b) Capacitive-type sensor (Reference [25]). (c) Piezoelectric-type sensor (Reference [28-29]). (d) Triboelectric-type sensor (left) and optical-type sensor (right) (Reference [33,36]).

1.3 Strain sensor

Strain is the deformation of the material when external force is applied to the material. Strain is also ubiquitous in nature and human activity like pressure. When we move our body, we bend a paper or plastic, we pull clothes or a rubber, or materials are pulled or pressed, strain occurs every time. Strain sensors are strain measuring devices and transducers that can operate in a signal transduction [8,37]. Recently, flexible and stretchable strain sensors have been researched widely due to their versatile applications such as human-motion monitoring and electronic skins. Most of strain sensors have been intensively researched as main devices for the human-motion monitoring. Strain levels for monitoring human-body motions can be classified two categories: 1) detection of large scale level motions (e.g., strains during bending motions of the legs, arms, and hands) and 2) detection of small scale level motions (e.g., strains during breathing, swallowing, and speaking) [8,37-39]. Detection ability of strain sensors about these strain levels is of great importance for the application in human-motion monitoring for medical area such as diagnostics for damaged vocal cords, respiratory disorders, angina, and evaluating the inner spatial gap between bones, determining the degree of change of spinal posture, monitoring Parkinson's disease, detection of posture and movement, analyzing facial expression changes, and monitoring skin sclerosis [8,37]. The sensitivity of the strain sensor is referred to as the gauge factor (GF). GF is defined as $GF = (dX/X_0)/\varepsilon$, where X denotes the quantitative output signal (X_0 means the initial value) and ε denotes the strain [37].

Various strain sensing and transduction mechanisms have been demonstrated. First transduction mechanism is piezoresistive type. This sensing type is widely investigated in both pressure and strain sensors. Conventional Si and metals based

strain sensors showed high sensitivity. However, these sensors can be used in very small strain sensing range and have low flexibility and stretchability [8,40]. Recently, various nanomaterials have been investigated for piezoresistive strain sensors with high flexibility and stretchability. Hata and coworkers demonstrated a new type of stretchable CNT strain sensor [41]. They used vertically aligned SWCNT thin films and arranged SWCNT films side by side. When these arranged films were stretched, the deformation of films was similar to the structural deformation of a string cheese when peeled. Their CNT strain sensor can be stretched up to 280% and showed high durability (10,000 cycles at 150% strain), fast response (delay time, 14 ms), and low creep (3.0% at 100% strain) [41]. Park and coworkers fabricated a piezoresistive strain sensor by using nanowire composite of AgNW and PDMS [42]. Their strain sensor showed high and tunable gauge factor of 2 to14 and a high stretchability up to 70%. Other nanomaterials graphene or PEDOT:PSS based piezoresistive strain sensors were also demonstrated [43-44].

Second transduction mechanism is capacitive type. Stretchable capacitive strain sensors generally consist of two layers of stretchable electrodes and sandwiched elastomeric dielectric layer [8,23,45]. Owing to the elastomeric dielectric layer, most of these sensors can detect both the strain and the pressure [23,45]. Bao and coworkers fabricated capacitive strain sensors by using CNT and PDMS [23]. Their sensor was transparent and can be stretched up to 150%. Zhu and coworkers fabricated capacitive strain sensors by using AgNW and PDMS [45]. Their sensor showed the multi-functionality. Their sensor can detect the pressure, strain, and touch. They also demonstrated wearable applications of the strain sensor such as monitoring human motions of walking running, squatting, and jumping.

Third transduction mechanism is piezoelectric type. Piezoelectric strain

sensors generally showed very high sensitivity based on the piezoelectric materials and nanomaterials [46-48]. Piezoelectric strain sensors using P(VDF-TrFE) and ZnO NWs have been investigated recently [46-48]. Especially, strain sensors with ZnO NWs showed ultra-high sensitivity [47-48]. Yang and coworkers reported a flexible strain sensor with vertically aligned ZnO NWs arrays and this sensor showed ultra-high gauge factor of 1813 [47]. Wang and coworkers developed strain sensors with a single $ZnSnO_3$ NW and this sensor showed an ultra-high gauge factor of 3740 [48]. Due to the limited flexibility, stretchability, and detection of low strain level, piezoelectric sensors can be restrictively applied to wearable sensors [8]. Therefore, piezoelectric sensors with high stretchability must be investigated.
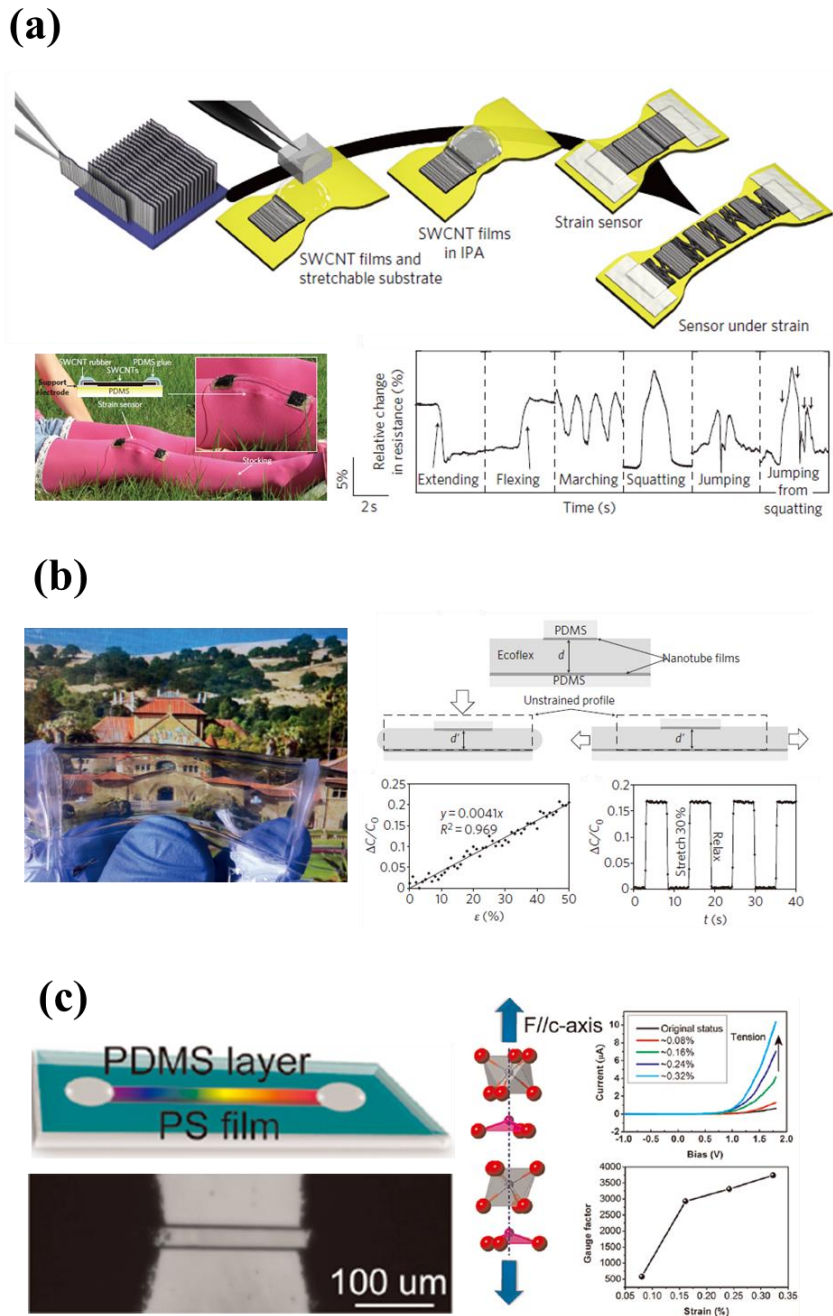
Figure 1.4 Strain sensors. (a) Piezoresistive strain sensor (Reference [41]). (b) Capacitive strain sensor (Reference [23]). (c) Piezoelectric strain sensor (Reference [48]).

13

1.4 Silver nanowire and Nanowire composite

A nanowire is nano-meter scale (10^{-9} meters) material with a wire-like shape or a rod-like shape. The diameter of the nanowire is a nano-meter scale and the length of the nanowire is much larger than the diameter, typically micro-meter scale (10^{-6} meters). The ratio of the length to diameter is greater than 100~1000. Due to this aspect ratio, nanowires are often referred to as one-dimensional (1-D) materials. Nanowires show interesting properties which are not observed in bulk materials as most nano-materials. Many different types of nanowires have been researched including semiconducting (Si, GaN, etc.), metallic (Ag, Au, Ni, etc.) and insulating (SiO_2, TiO_2, etc.).

Among these nanowires, metallic nanowires have gained exponential interest recently for the application to the transparent, flexible or stretchable electronics [49-64]. Owing to the high electrical and thermal conductivity of bulk silver, the synthesis of AgNWs (Silver Nanowires) have received great attention. AgNWs can be easily synthesized via the polyol reduction process of $AgNO_3$ [49-54]. Typically, heated ethylene glycol (EG) serves as both the solvent and a precursor to the reducing agent [51], with solutions of $AgNO_3$ and poly(vinyl pyrrolidone) (PVP) (both also in EG) being simultaneously added using a two-channel syringe pump [50]. AgNWs with high aspect ratio have been applied to the transparent and flexible electrode due to their high conductivity and optical transmittance from their random networks [52-54]. AgNWs film shows typically the sheet resistance of 20~100 ohms/sq and transmittance of 80~90% [52-54]. These AgNWs film is flexible and even foldable maintaining their transmittance and resistance [53-54] and based on these properties AgNW will be the key material for the foldable displays.

Also the AgNW is applied to highly stretchable and conducting electrode by depositing AgNW film on the stretchable substrate or embedding AgNWs into the stretchable matrix [55-57]. Stretchable electrodes based on AgNWs can be stretched up to 50% with very small change of conductance. Ko et al. showed the synthesis of very long AgNWs and this AgNWs on the Ecoflex substrate can be stretched up to 460% with small change of conductance [55]. Stretchable and flexible electrodes by embedding AgNWs into the stretchable matrix have been developed to complement the weak adhesion property of AgNWs and increase the cyclic robustness of AgNWs (Nanowire composite is generally composed of nanowires, the fillers, and matrix materials. AgNWs embedded PDMS is also the nanowire composite, because the AgNWs is the fillers and PDMS is the matrix. So, the AgNWs embedded PDMS is referred to as nanowire composite in this dissertation). PDMS (Polydimethylsiloxane) have been widely used as a stretchable matrix for the nanowire composite [57-60].

PDMS is a polymeric organosilicon compound that is well known as a silicone rubber due to its good elastic properties. PDMS is optically transparent, electrically non-conductive and mechanically stretchable. Also due to its non-toxic and bio-compatible properties, PDMS is widely investigated for the biomedical application [61-62]. Elastic modulus of the PDMS can be easily controlled by changing the mixing ratio of the liquid PDMS and crosslinking agent material [63]. Simple tuning method of the elastic modulus of PDMS make the application to the various stretchable electronics suitable. Based on these properties of PDMS, PDMS is one of the most famous materials in the field of flexible/stretchable electronics and wearable electronics.

Due to the robustness and stretchability of the nanowire composite, AgNWs embedded PDMS, nanowire composite have been applied to wearable electronics

and stretchable electronics. Also various mechanical sensors such as strain sensor, pressure sensor and bending sensor have been fabricated using nanowire composite [58,64].
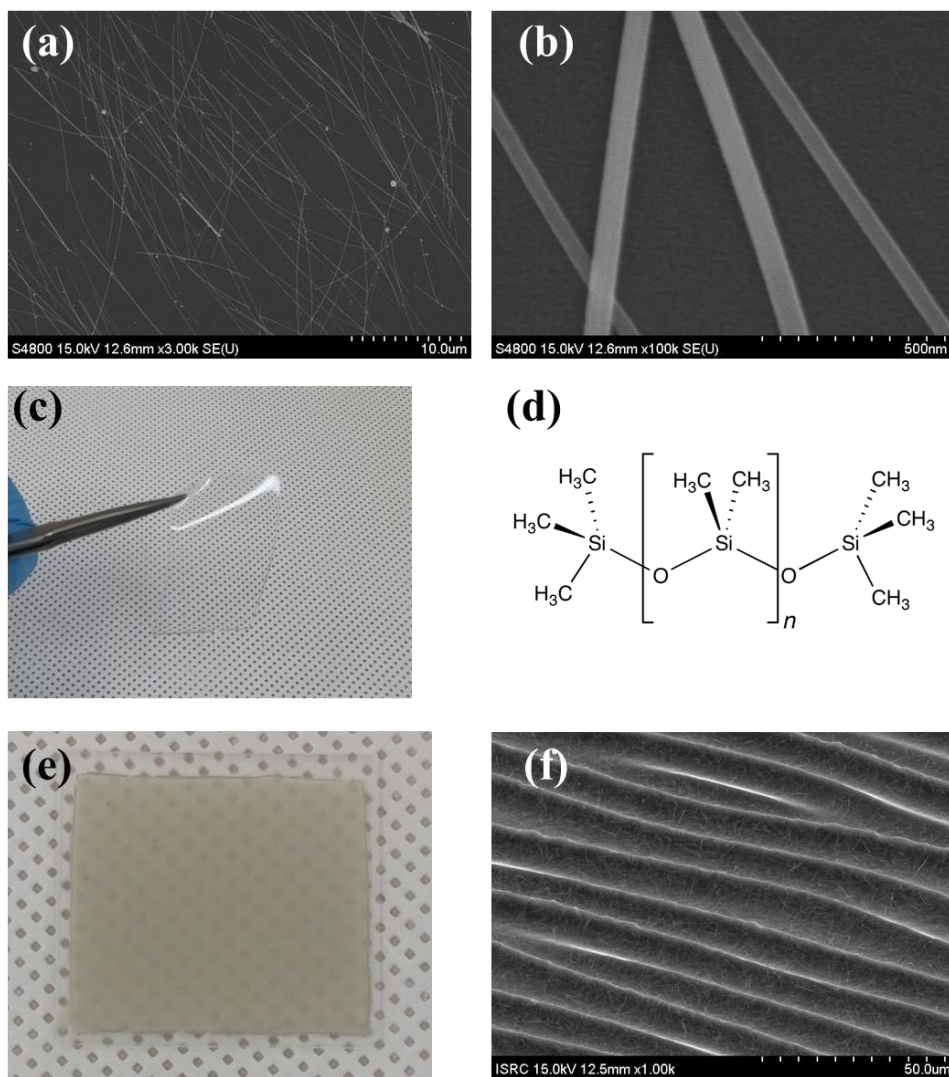
Figure 1.5 (a), (b) SEM image of AgNW. (c) Image of PDMS. (d) Chemical formula of PDMS. (e) Image of nanowire composite (multiscale structured AgNW embedded PDMS). (f) SEM image of nanowire composite.

1.5 Organization of this dissertation

This Ph.D. dissertation will present the studies on the flexible and stretchable multifunctional sensors and their applications in wearable sensing and health monitoring systems. Motivated by the urgent demand for the wearable multifunctional sensor for wearable healthcare devices and electronic artificial skins, we developed multifunctional sensors which can detect the pressure and strain by using the nanowire composite and printed electronics. By introducing the multiscale structure to the nanowire composite and air gap between the nanowire composite and dielectric layer, we can obtain highly sensitive pressure sensors.

This thesis is composed of five chapters including Introduction and Conclusion.

Chapter 1 introduces the concept and current status of wearable electronics, pressure and strain sensors, and nanowire composite.

Chapter 2 explains our approaches for the highly sensitive and flexible pressure sensors with tunable sensitivity. We fabricated the nanowire composite with multiscale structure and integrated this composite with solution-processed polymer dielectric layer/Ag electrode to demonstrate the capacitive pressure sensor.

Chapter 3 describes the bonding method for the realization of the bendable multifunctional sensor and a new method for the pressure sensitive transistor. We introduced the surface functionalization and spacer for the bendable sensor and the floating gate structure for the low voltage operation and low power consumption of the pressure sensitive transistor.

Chapter 4 covers the stretchable multifunctional sensor which can detect the pressure, strain, and shear force. This sensor was fully fabricated by using nanowire

composite and PDMS.

Chapter 5 summarizes the development of the highly sensitive flexible pressure sensor, the bendable sensor using the bonding method, and the stretchable multifunctional sensor.

Reference

[1] W. Barfield et al., *Fundamentals of Wearable Computers and Augmented Reality*, CRC Press Taylor & Francis Group, Florida, USA 2015

[2] R. C. Webb, A. P. Bonifas, A. Behnaz, Y. Zhang, K. J. Yu, H. Cheng, M. Shi, Z. Bian, Z. Liu, Y.-S. Kim, W.-H. Yeo, J. S. Park, J. Song, Y. Li, Y. Huang, A. M. Gorbach, and J. A. Rogers, *Nat. Mater.*, 12, 938 (2013)

[3] M. Kaltenbrunner, T. Sekitani, J. Reeder, T. Yokota, K. Kuribara, T. Tokuhara, M. Drack, R. Schwodiauer, I. Graz, S. Bauer-Gogonea, S. Bauer, and T. Someya, *Nature*, 499, 458 (2013)

[4] C. Dagdeviren, Y. Su, P. Joe, R. Yona, Y. Liu, Y.-S. Kim, Y. Huang, A. R. Damadoran, J. Xia, L. W. Martin, Y. Huang, and J. A. Rogers, *Nat. Commun.,* 5, 4496 (2014)

[5] C. Pang, J. H. Koo, A. Nguyen, J. M. Caves, M.-G. Kim, A. Chortos, K. Kim, P. J. Wang, J. B. H. Tok, and Z. Bao, *Adv. Mater.*, 27, 634 (2015)

[6] J. Kim, M. Lee, H. J. Shim, R. Ghaffari, H. R. Cho, D. Son, Y. H. Jung, M. Soh, C. Choi, S. Jung, K. Chu, D. Jeon, S.-T. Lee, J. H. Kim, S. H. Choi, T. Hyeon, and D.-H. Kim, *Nat. Commun.*, 5, 5747 (2014)

[7] D.-H. Kim, N. Lu, R. Ma, Y.-S. Kim, R.-H. Kim, S. Wang, J. Wu, S. M. Won, H. Tao, A. Islam, K. J. Yu, T.-i. Kim, R. Chowdhury, M. Ying, L. Xu, M. Li, H.-J. Chung, H. Keum, M. McCormick, P. Liu, Y.-W. Zhang, F. G. Omenetto, Y. Huang, T. Coleman, and J. A. Rogers, *Science*, 333, 838 (2011)

[8] T. Q. Trung and N.-E. Lee, *Adv. Mater.*, (2016) DOI: 10.1002/adma.201504244

[9] R. B. Reilly and T. C. Lee, *Technol. Health Care*, 18, 443 (2010)

[10] W.-H. Yeo, Y.-S. Kim, J. Lee, A. Ameen, L. Shi, M. Li, S. Wang, R. Ma, S. H.

Jin, Z. Kang, Y. Huang, and J. A. Rogers, *Adv. Mater.*, 25, 2773 (2013)

[11] J.-W. Jeong, W.-H. Yeo, A. Akhtar, J. J. S. Norton, Y.-J. Kwack, S. Li, S.-Y. Jung, Y. Su, W. Lee, J. Xia, H. Cheng, Y. Huang, W.-S. Choi, T. Bretl, and J. A. Rogers, *Adv. Mater.*, 25, 6839 (2013)

[12] S. Lim, D. Son, J. Kim, Y. B. Lee, J.-K. Song, S. Choi, D. J. Lee, J. H. Kim, M. Lee, T. Hyeon, and D.-H. Kim, *Adv. Funct. Mater.*, 25, 375 (2015)

[13] Y. Zang, F. Zhang, C. Di and D. Zhu, *Mater. Horiz.*, 2, 140 (2015)

[14] M. Hammock, A. Chortos, B. C.-K. Tee, J. B.-H. Tok, and Z. Bao, *Adv. Mater.*, 25, 5997 (2013)

[15] a) T. Someya , Y. Kato , T. Sekitani , S. Iba , Y. Noguchi , Y. Murase , H. Kawaguchi, and T. Sakurai, *Proc. Natl. Acad. Sci. USA*, 102, 12321 (2005); b) T. Sekitani , Y. Noguchi , K. Hata , T. Fukushima , T. Aida, and T. Someya, *Science*, 321, 1468 (2008); c) T. Sekitani , T. Yokota , U. Zschieschang , H. Klauk , S. Bauer , K. Takeuchi , M. Takamiya , T. Sakurai and, T. Someya, *Science*, 326, 1516 (2009)

[16] K. Takei, T. Takahashi, J. C. Ho, H. Ko, A. G. Gillies, P. W. Leu, R. S. Fearing, and A. Javey, *Nat. Mater.*, 9, 821 (2010)

[17] C. Wang, D. Hwang, Z. Yu, K. Takei, J. Park, T. Chen, B. Ma, and A. Javey, *Nat. Mater.*, 12, 899 (2013)

[18] H. Yao, J. Ge, C. Wang, X. Wang, W. Hu, Z. Zheng, Y. Ni, and S. Yu, *Adv. Mater.*, 25, 6692 (2013)

[19] S. Gong, W. Schwalb, Y. Wang, Y. Chen, Y. Tang, J. Si, B. Shirinzadeh, and W. Cheng, *Nat. Commun.*, 5, 3132 (2014)

[20] C. Choong, M. Shim, B. Lee, S. Jeon, D. Ko, T. Kang, J. Bae, S. Lee, K. Byun, J. Im, Y. Jeong, C. Park, J. Park, and U. Chung, *Adv. Mater.*, 26, 3451 (2014)

[21] J. Park, Y. Lee, J. Hong, M. Ha, Y. Jung, H. Lim, S. Kim, and H. Ko, *ACS nano*,

8, 4689 (2014)

[22] R. Puers, *Sens. Actuators A*, 93, 37 (1993)

[23] D. J. Lipomi , M. Vosgueritchian , B. C.-K. Tee , S. L. Hellstrom , J. A. Lee , C. H. Fox , and Z. Bao , *Nat. Nanotechnol.*, 6, 788 (2011)

[24] W. Hu, X. Niu, R. Zhao, and Q. Pei, *Appl. Phys. Lett.*, 102, 083303 (2013)

[25] S. C. B. Mannsfeld, B. C.-K. Tee, R. M. Stoltenberg, C. V. H.-H. Chen, S. Barman, B. V. O. Muir, A. N. Sokolov, C. Reese, and Z. Bao, *Nat. Mater.*, 9, 859 (2010)

[26] G. Schwartz, B. C.-K. Tee, J. Mei, A. L. Appleton, D. H. Kim, H. Wang, and Z. Bao, *Nat. Commun.*, 4, 1859 (2013)

[27] Y. Zang, F. Zhang, D. Huang, X. Gao, C. Di, and D. Zhu, *Nat. Commun.*, 6, 6269 (2015)

[28] C. Pan, L. Dong, G. Zhu, S. Niu, R. Yu, Q. Yang, Y. Liu, and Z.L. Wang, *Nat. Photonics*, 7, 752, (2013)

[29] W. Wu, X. Wen, and Z.L. Wang, *Science*, 340, 952 (2013)

[30] J. Chun, K. Lee, C. Kang, M. Kim, S. Kim, and J. Baik, *Adv. Funct. Mater.*, 24, 2038 (2014)

[31] C. Baur, J. R. DiMaio, E. McAllister, R. Hossini, E. Wagener, J. Ballato, S. Priya, A. Ballato, and D. W. Smith Jr., *J. Appl. Phys.*, 112, 124104 (2012)

[32] Z. L. Wang, *ACS nano*, 7, 9533 (2013)

[33] L. Lin, Y. Xie, S. Wang, W. Wu, S. Niu, X. Wen, and Z.L. Wang, *ACS nano*, 7, 8266 (2013)

[34] J. S. Heo , J. H. Chung, and J. J. Lee, *Sens. Actuators, A*, 126, 312 (2006)

[35] a) J. S. Heo, K. Y. Kim, and J. J. Lee, *J. Intell. Mater. Syst. Struct.*, 20, 2029 (2009); b) M. Rothmaier, M. P. Luong, and F. Clemens, *Sensors*, 8, 4318

(2008)

[36] M. Ramuz, B. C. K. Tee, J. B. H. Tok, and Z. Bao, *Adv. Mater.*, 24, 3223 (2012)

[37] M. Amjadi, K.-U. Kyung, I. Park, and M. Sitti, *Adv. Funct. Mater.*, 26, 1678 (2016)

[38] J. T. Muth, D. M. Vogt, R. L. Truby, Y. Meng, D. B. Kolesky, R. J. Wood, and J. A. Lewis, *Adv. Mater.*, 26, 6307 (2014)

[39] J. J. Park, W. J. Hyun, S. C. Mun, Y. T. Park, and O. O. Park, *ACS Appl. Mater. Interfaces*, 7, 6317 (2015)

[40] X. Li, R. Zhang, W. Yu, K. Wang, J. Wei, D. Wu, A. Cao, Z. Li, Y. Cheng, Q. Zheng, R. S. Ruoff, and H. Zhu, *Sci. Rep.*, 2, 870 (2012)

[41] T. Yamada, Y. Hayamizu, Y. Yamamoto, Y. Yomogida, A. Izadi-Najafabadi, D. N. Futaba, and K. Hata, *Nat. Nanotechnol.*, 6, 296 (2011)

[42] M. Amjadi, A. Pichitpajongkit, S. Lee, S. Ryu, and I. Park, *ACS nano*, 8, 5154 (2014)

[43] C. Yan, J. Wang, W. Kang, M. Cui, X. Wang, C. Y. Foo, K. J. Chee, and P. S. Lee, *Adv. Mater.*, 26, 2022 (2014)

[44] S. Savagatrup, E. Chan, S. M. Renteria-Garcia, A. D. Printz, A. V. Zaretski, T. F. O'Connor, D. Rodriquez, E. Valle, and D. J. Lipomi, *Adv. Funct. Mater.*, 25, 427 (2015)

[45] S. Yao and Y. Zhu, *Nanoscale*, 6, 2345 (2014)

[46] T. Q. Trung, N. T. Tien, Y. G. Seol, and N.-E. Lee, *Org. Electron.*, 13, 533 (2012)

[47] W. Zhang, R. Zhu, V. Nguyen, and R. Yang, *Sens. Actuators A*, 205, 164 (2014)

[48] J. M. Wu, C.-Y. Chen, Y. Zhang, K.-H. Chen, Y. Yang, Y. Hu, J.-H. He, and Z. L. Wang, *ACS Nano*, 6, 4369 (2012)

[49] Y. Sun, B. Gates, B. Mayers, and Y. Xia, *Nano Lett.*, 2, 165-168 (2002)

[50] K. E. Korte, S. E. Skrabalak, and Y. Xia, *J. Mater. Chem.*, 18, 437–441 (2008)

[51] F. Fievet, J. P. Lagier, and M. Figlarz, *MRS Bull.*, 14, 29–34 (1989)

[52] L. Hu, H. S. Kim, J. Lee, P. Peumans, and Y. Cui, *ACS nano*, 4, 2955-2963 (2010)

[53] C. Yang, H. Gu, W. Lin, M. Yuen, C. P. Wong, M. Xiong, and B. Gao, *Adv. Mater.*, 23, 3052-3056 (2011)

[54] X. Zeng, Q. Zhang, R. Yu, and C. Lu, *Adv. Mater.*, 22, 4484-4488 (2010)

[55] P. Lee, J. Lee, H. Lee, J. Yeo, S. Hong, K. H. Nam, D. Lee, S. S. Lee, and S. H. Ko, *Adv. Mater.*, 24, 3326-3332 (2012)

[56] J. Lee, P. Lee, H. B. Lee, S. Hong, I. Lee, J. Yeo, S. S. Lee, T. Kim, D. Lee, and S. H. Ko, *Adv. Funct. Mater.*, 23, 4171-4176 (2013)

[57] F. Xu and Y. Zhu, *Adv. Mater.*, 24, 5117-5122 (2012)

[58] W. Hu, X. Niu, R. Zhao, and Q. Pei, *Appl. Phys. Lett.*, 102, 083303 (2013)

[59] J. Liang, L. Li, X. Niu. Z. Yu, and Q. Pei, *Nat. Photonics*, 7, 817-824 (2013)

[60] S. Hong, H. Lee, J. Lee, J. Kwon, S. Han, Y. D. Suh, H. Cho, J. Shin, J. Yeo, and S. H. Ko, *Adv. Mater.*, 27, 4744-4751 (2015)

[61] Y. Chan, Y. Mi, D. Trau, P. Huang, and E. Chen, *Polymer,* 47, 5124-5130 (2006).

[62] N. Q. Balaban, U.S. Schwarz, D. Riveline, P. Goichberg, G. Tzur, I. Sabanay, D. Mahalu, S. Safran, A. Bershadsky, L. Addadi, and B. Geiger. *Nature Cell Biol.*, 3, 466-472 (2001).

[63] Z. Wang, A. A. Volinsky, and N. D. Gallant, *J. Appl. Polym. Sci.*, 131, 41050 (2014)

[64] M. Amjadi, A. Pichitpajongkit, S. Lee, S. Ryu, and I. Park, *ACS nano*, 8, 5154-5163 (2014)

Chapter 2

Multiscale structured nanowire composite for flexible pressure sensor

2.1. Highly sensitive capacitive pressure sensor

2.1.1 Introduction

Flexible, bendable or stretchable pressure sensors have gained exponential interest recently, because of their versatile application to the human oriented future technologies such as electronic skins [1-4], wearable healthcare monitors [5-8], prosthetic skins [2,9,10], patient rehabilitation [11-12], robotic skins [13-15] and touch interfaces [16-17]. For the realization of most of the aforementioned technologies that mimic human skin or human tactile receptors, highly sensitive pressure sensors for low pressure-regime (<10 kPa, gentle touch) [18] with mechanical flexibility or strecthability are required. Various sensing mechanisms have demonstrated the possibility to fabricate highly sensitive and flexible pressure sensors. They includes piezoresistive sensing [5,19-24], piezoelectric sensing [25-27], triboelectric sensing [27,28], and capacitive sensing mechanisms [9,16,30-34]. The piezoresistive sensors based on pressure sensitive rubber (PSR) have been widely investigated by being integrated with organic field effect transistors [1,4,15] or inorganic semiconducting nanowire-based transistors [3] for large area artificial electronic skins.

24

Recently, a PSR based pressure sensor array fabricated with semiconducting carbon nanotube transistors and organic light-emitting diodes [35] and a piezoelectric nanowire light-emitting diode-based pressure sensor array [27] demonstrate the real-time visualization of pressure mapping. However, vacuum processes are needed for these sensor arrays and PSR based sensors are susceptible to hysteresis and show low stability [13,36].

Capacitive pressure sensors with elastomeric dielectric materials also have been widely investigated [17,30,32,34]. The elastomeric dielectric layer is deformed (e.g., the thickness of the dielectric layer is reduced) when an external pressure is applied to the sensor and this deformation induces the capacitance change of the sensor. Various metals (gold, silver) or liquid metal have been used as electrodes of the capacitive pressure sensor [17,34]. Nanomaterials such as silver nanowires (AgNWs) or carbon nanotubes which have been widely investigated for stretchable electronics were also used with elastomeric dielectric layers for stretchable capacitive pressure sensors [16,30,32,37]. Although these sensors have mechanical stretchability, their pressure sensitivity is low. To enhance the pressure sensitivity of capacitive-type sensors, recently, microstructured elastomeric dielectric layers have been introduced and the pressure sensors with them show high pressure sensitivity and mechanical flexibility [9,31]. By integrating organic field effect transistors with the microstructured elastomer as a gate insulator, pressure sensitive active sensor devices have been fabricated [9,31]. However, the manufacturing process of the mould for microstructured elastomers is based on the photolithography and chemical etching, which are expensive and complicated processes.

In this work, we present a highly sensitive and flexible capacitive pressure sensor with the multiscale-structured elastomeric electrode by using a simple and

low-cost process. The spontaneous buckle formation of ultraviolet/ozone (UV/O$_3$) treated pre-strained PDMS [38] was used as a simple and low cost mould fabrication method. Through this mould, the AgNWs embedded multiscale-structured PDMS electrode was fabricated. By sandwiching the multiscale-structured electrode and a solution processed dielectric layer/electrode template, the flexible capacitive pressure sensor can be obtained. The sensor shows high sensitivity (3.8 kPa^{-1}), fast response and relaxation time (< 150 ms), high flexibility and high stability. In addition, the pixel-type pressure sensor array can be easily fabricated and scaled up from the simple cutting and attaching process. The fingertip grip pressure sensing device is also demonstrated by attaching each sensor onto the fingertips.

2.1.2 Experimental

The multiscale-structured PDMS electrode was fabricated as schematically illustrated in Figure 2.1. To obtain the multiscale-structured electrode, we used the spontaneous buckle formation of PDMS surface due to the relaxation of pre-stretched PDMS with stiff silicon oxide film [38] as a mould. The mould PDMS was prepared by mixing the liquid PDMS elastomer (Sylgard 184, Dow corning) and a curing agent in the ratio 10:1 by weight. The liquid mixture was poured onto a glass substrate and thermally cured at 130 ℃ for 20 min. The cured PDMS was cut into rectangles (8 cm × 10 cm) and placed onto the glass substrate. After that, we stretched the PDMS uniaxially up to 40% with tweezers, and fixed the both ends of PDMS with binder clips. The stretched PDMS was UV/O$_3$-treated (power = 28 mW cm^{-2}) for 30 minutes to form the SiO$_X$ thin film on the PDMS surface. AgNWs (SLV-NW-90, Blue Nano inc.) were tip-sonicated (52 W, 10 minutes) to obtain the length of 5 ~ 10 μm. AgNWs were bar-coated onto the stretched and UV/O3 treated PDMS several times through the Arylite mask (3 cm × 4 cm) to obtain the resistance below 30 Ω. The bar-coated AgNW film was dried at 60 ℃ for 30 min. After the heat treatment, AgNW coated PDMS was released to its original condition (no strain) to introduce the spontaneous buckle formation. Due to the preformed silicon oxide thin film on the mould PDMS surface, the buckled structure was introduced on the PDMS surface [38] and the AgNW film also showed the buckled surface as shown in Figure 2.1(b). The mixture of a liquid PDMS elastomer and a curing agent (10:1, w/w) was poured on the buckled AgNW film, and then cured at 65 ℃ for 12 h in air. Due to the penetration of the liquid PDMS into the AgNW network, the AgNW film was embedded tightly into the cured PDMS [38]. After the curing process, we inverted

the cured PDMS/mould PDMS and then peeled off the mould PDMS from the AgNW-embedded PDMS while the AgNW-embedded PDMS is attached to the glass by using tweezers. Finally we obtained the AgNW-embedded multiscale-structured PDMS as shown in Figure 2.1(b). The AgNW-embedded surface of PDMS is conductive and the opposite surface of PDMS is non-conductive. The resistances of the AgNW film (20Ω) and the multiscale-structured electrode (45Ω) at each fabrication stage are indicated in Figure 2.1(b). The resistance of the AgNW film was increased slightly after strain releasing (25Ω) due to the rearrangement of each AgNW and AgNW junctions. The resistance of the AgNW-embedded multiscale-structured PDMS electrode was increased over 100% after peeling off due to the penetration and filling of the AgNW junctions of PDMS and the peel-off stress [39,40].

The Ag ink (Sigma-Aldrich) was printed on the flexible Arylite substrate (200 μm thickness, Ferrania Corp.) by using a piezoelectric inkjet-printer (DMP-2831, Dimatix Corp.), and then sintered at 100 ℃ for 1 h. A PMMA solution containing 10 wt% of PMMA (Mw ~120,000, Sigma-Aldrich) dissolved in propylene glycol methyl ether acetate (PGMEA) or a PVP solution containing 10 wt% of PVP (Mw ~30,000, Sigma-Aldrich) and 2 wt% of poly(melamine-co-formaldehyde) as a cross-linking agent dissolved in PGMEA was spin-coated on the Ag printed Arylite substrate for the formation of the dielectric layer. Afterward, the PMMA film was dried at 120 ℃ for 1h and the PVP film was cross-linked at 200 ℃ for 1 h. The capacitive pressure sensor was fabricated by laminating the multiscale-structured electrode (A pressure of 10 kPa was applied to the multiscale-structured electrode before the lamination) on top of the dielectric layer/Ag printed Arylite substrate (Figure 2.2) (We will call the dielectric layer coated bottom electrode as the bottom

28

plane) and thin PET film (50, 100 μm thickness, Toray Corp.) was placed on top of
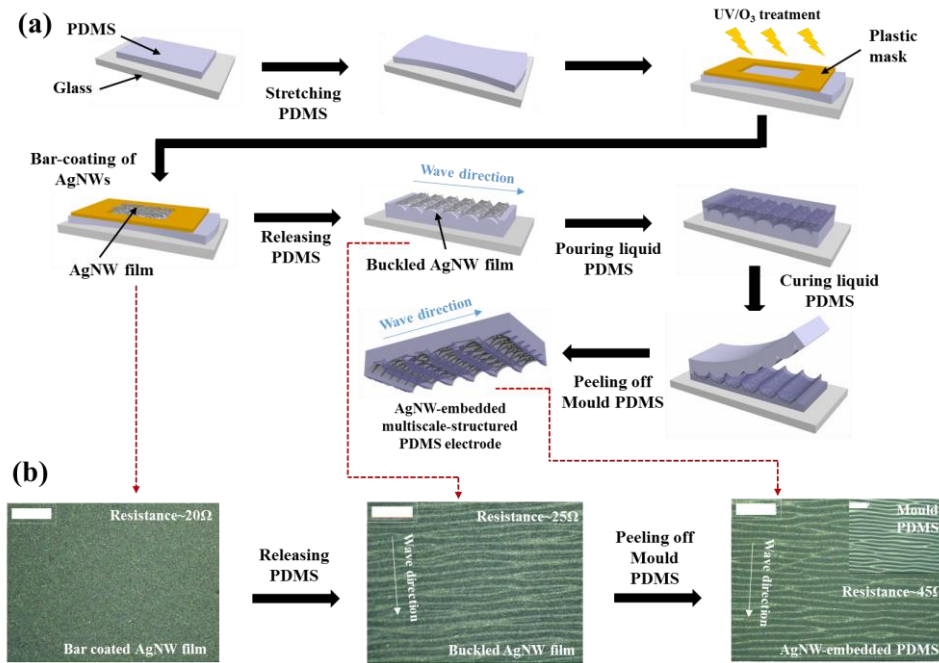
Figure 2.1 Fabrication process of the multiscale-structured electrode and the capacitive pressure sensor. (a) Schematic diagrams of the fabrication process of the AgNW-embedded multiscale-structured PDMS electrode. (b) Microscopic images of the AgNW film at each fabrication step. AgNW film was bar-coated on the PDMS (left). Buckled AgNW film was formed after strain releasing (middle). The buckled AgNWs were totally embedded into the PDMS and AgNWs were hardly left on the mould PDMS (right). (Scale bar = 100 μm).

(a)

AgNW-embedded PDMS

Multiscale-structured electrode

(c)

AgNW-embedded PDMS

PMMA or PVP
Ag electrode
Plastic substrate

Capacitive pressure sensor

(b)

Inkjet printing of Ag electrode

Spin coating of dielectric layer

PMMA or PVP

Ag electrode

Plastic substrate
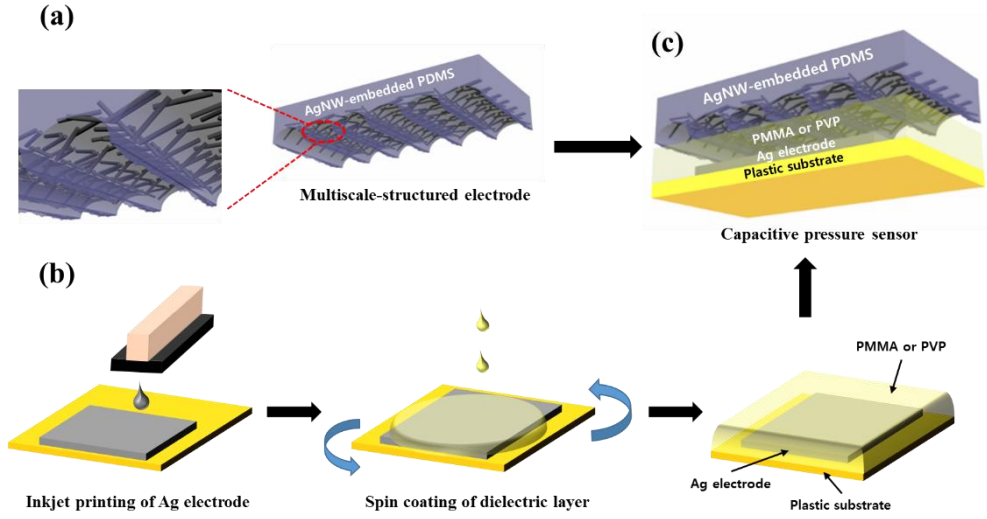
Figure 2.2 Fabrication process of the capacitive pressure sensor. (a) The multiscale-structured electrode for a top electrode. (b) Schematic diagrams of the fabrication process of the bottom plane. Inkjet-printed Ag electrode and spin coated dielectric layer compose the bottom plane. (c) The capacitive pressure sensor is obtained by laminating the multiscale-structured electrode onto the bottom plane.

the multiscale-structured PDMS to avoid the stickiness of PDMS during the pressure sensing tests. Both electrodes were connected to copper wire with silver paste for electrical measurements. For 3×3 and 5×5 sensor arrays, the multiscale-structured electrodes were cut into 2 mm $\times$ 22 mm and 4 mm $\times$ 22 mm respectively by a razor blade and attached to PET film to form pixel type arrays. For the fingertip pressure sensors, we stuck elastomeric foam-tape (3M[TM] VHB[TM] Tape) on the poly glove and laminated each bottom plane on the tape. After that, we sandwiched the multiscale-structured electrode on the bottom plane by using Kapton tape to fabricate the pressure sensors.

The microstructure of the AgNW-embedded multiscale-structured PDMS electrode was characterized by a field emission scanning electron microscope (FE-SEM, Hitachi S-48000), a 3-D surface profiler (NanoFocus) and AFM (XE-100, Park Systems Corp.). For the 3-D surface profiler measurement, thin gold layer (20nm) was deposited on the PDMS and AgNW-embedded PDMS by using thermal evaporator. The microscopic images were obtained by an optical microscope (EGTECH). Capacitance was measured at 1 kHz with a 0.1 V a.c. signal by using the Agilent 4284A LCR meter. IMADA force gauge with z-axis stage was used to apply the pressure to the sensor and metal or plastic weights were used to apply the pressure to the arrays and the sensor. A mechanical bending test was performed using a home-made bending apparatus.

2.1.3 Results and Discussion

The multiscale structure of the AgNW-embedded PDMS electrode was characterized by using scanning electron microscopy (SEM), 3-D surface profiler and atomic force microscopy (AFM). The multiscale structure consists of the wavy structure (micrometer-size) obtained from the buckled PDMS mould and the rough surface of the crest of the wavy structure (nanometer-size) obtained from the relaxation of peel-off stress, as shown in Figure 2.3. The uniform wavy structure of the AgNW-embedded PDMS was characterized by using SEM. The average wavelength and amplitude of the wavy structure are about 22 μm and 6 μm, respectively, as shown in Figure 2.3(a) and 2.3(b). Figure 2.3(a) and 2.3(b) also show that the wavy structure was formed uniformly over the entire region and AgNWs were totally embedded into the PDMS matrix. The rough surface of the crest was observed from 3-D surface profiler and AFM images (see Figure 2.3(c) and 2.3(d)). When peeling off the cured PDMS, the peel-off stress was applied to the entire domain of the AgNW-embedded PDMS. More excessive peel-off stress was applied to the sharp crest of the wavy structure among the entire domain and the rough surface was formed spontaneously to release the peel-off stress at the crest [39, 40]. However, no rough surface of the crest was observed from the structured PDMS without AgNWs as shown in Figure 2.3(c) and 2.3(f). The root-mean-square (RMS) values of the measured line roughness at the crest are about 350 nm for AgNW-embedded PDMS and 30 nm for only PDMS, respectively. The AgNW-embedded PDMS is still flexible, bendable and deformable as reported elsewhere [16,30,39]. The resistance of the wavy structured electrode was hardly changed from its original value during the repeated pressing (up to 10 kPa) as shown in Figure 2.4.
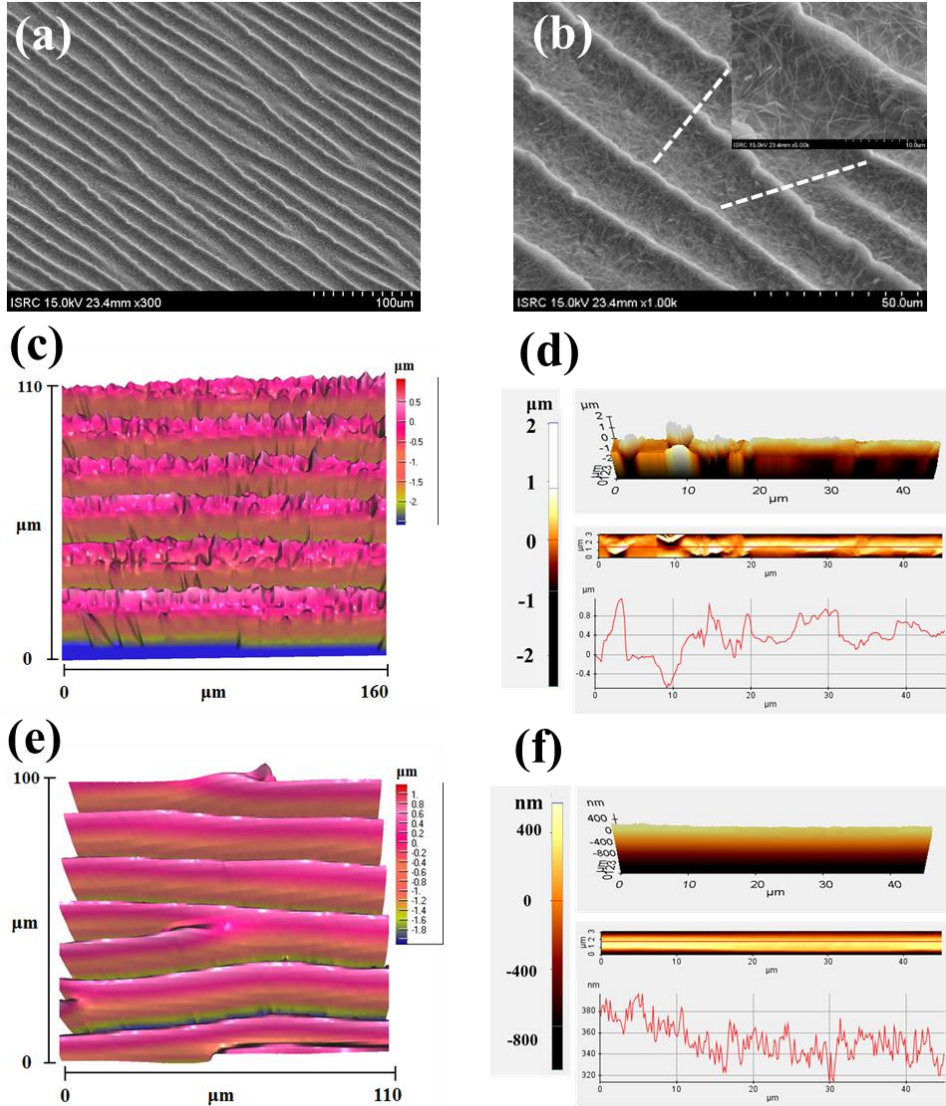
Figure 2.3 The microstructure of the multiscale-structured electrode. (a) SEM image of the multiscale-structured electrode with high uniformity. (b) AgNWs are totally embedded into the PDMS and the high magnification inset image shows that AgNWs are embedded well even in the crest of the wavy structure. (c) 3-D surface profiler image of the multiscale-structured electrode. The rough surface at the crest of wavy structure is formed. (d) AFM image and line profile of the crest of the multiscale-structured electrode. In this crest, the root-mean-square (RMS) value of the measured line roughness is about 350 nm. (e) 3-D surface profiler image of the structured PDMS (AgNWs were not bar-coated onto the mould PDMS. It means that the bar-coating of AgNWs is omitted from the fabrication process in Fig. 1a). (f) AFM image and line profile of the crest of the structured PDMS. In this crest, the root-mean-square (RMS) value of the measured line roughness is about 30 nm.

(a)

(b)
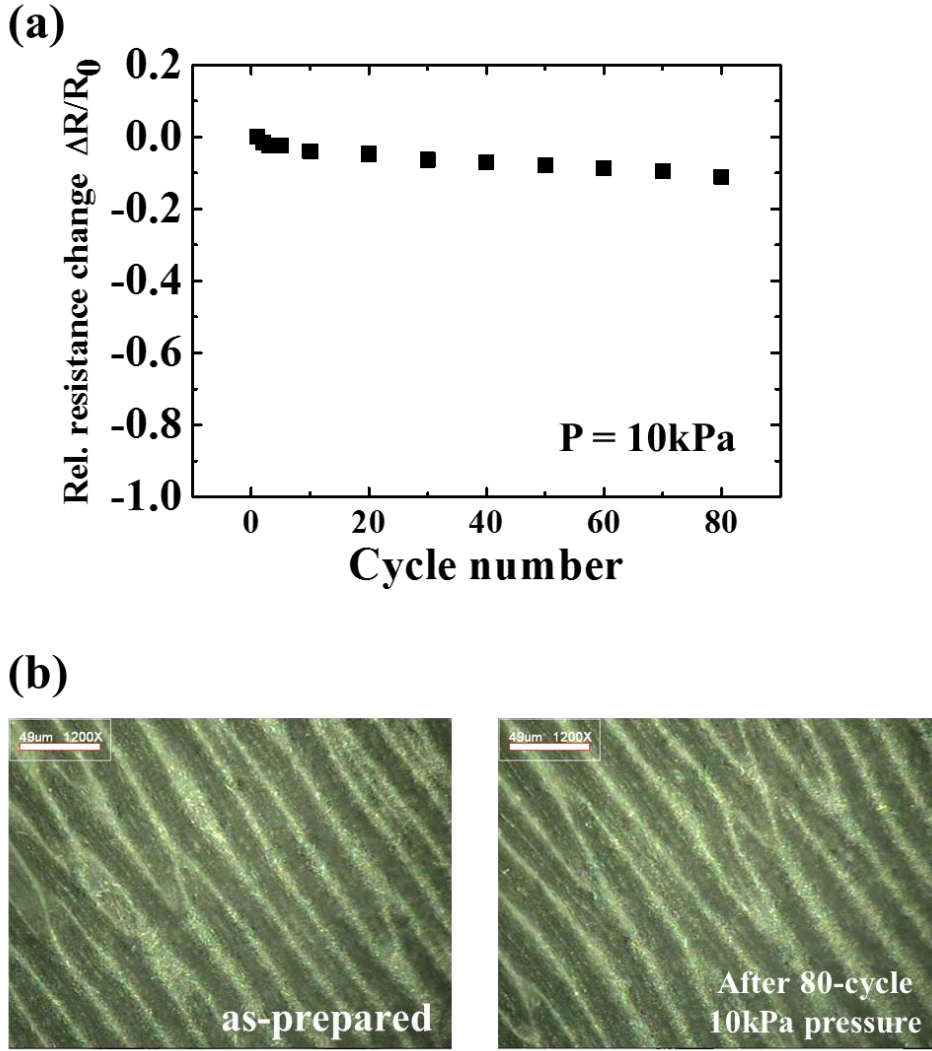
Figure 2.4 (a) The resistance change of the multiscale-structured electrode during the repeated loading/unloading of the pressure of 10 kPa. (b) The microscopic images of the as-prepared multiscale-structured electrode and the multiscale-structured electrode after 80-cycle test, respectively.

Pressure was applied to the capacitive pressure sensor to test the pressure sensitivity. The force gauge with z-axis motor stage and weights were used as pressure applying tools. The size of the square pressure sensitive capacitor was 16 mm^2 (the size of the multiscale-structured electrode is 4×10 mm^2). To avoid the

stickiness of PDMS that could hinder the pressure sensor test, the poly(ethylene terephthalate) (PET) film (100 μm) was attached on the PDMS surface and thin glass slide was placed onto the PET film. The pressure from the multiscale-structured electrode with PET film and glass slide (180 mg) is defined as the base pressure (45 Pa) and the capacitance at the base pressure is defined as the base capacitance C_0. The external pressure was applied from 0 Pa to 4.5 kPa. Figure 2.5(a) shows the pressure sensitivities of the sensors with the multiscale-structured electrode and non-structured flat electrode, respectively. The pressure sensitivity of the pressure sensor (S) can be defined as the slope of the relative capacitance change-pressure curve in Figure 2.5(a) ($S=\delta(\Delta C/C_0)/\delta p$, $\Delta C = C-C_0$, where C and C_0 denote the capacitance with the applied pressure and the base capacitance, respectively, and p denotes the applied pressure). The sensor with non-structured electrode (flat electrode in Figure 2.5(a)) shows no change of capacitance according to the applied pressure. However, the sensor with the multiscale-structured electrode shows high sensitivity of 3.8 kPa^{-1} in the low pressure regime (45 ~ 500 Pa), 0.8 kPa^{-1} in the mid pressure regime (500 Pa ~ 2.5 kPa) and 0.35 kPa^{-1} in the high pressure regime (2.5 ~ 4.5 kPa). The sensitivity of our sensor surpassed that of the previously reported capacitive pressure sensors for a wide pressure regime (0 ~ 4.5 kPa) [9,31]. The pressure sensor with the multiscale-structured electrode shows very small hysteresis as shown in Figure 2.6(a). The pressure sensor can detect the loading and unloading of a paper ship of very small weight (40 mg) as shown in Figure 2.5(b). The pressure of the paper ship is about 15 Pa. The capacitance change of the sensor is large enough to detect the small pressure. Ten independent sensors were measured to check the sample-to-sample variation in pressure sensitivity and the average capacitance values at each pressure are plotted with error bars (standard deviation) as shown in Figure 2.6(b).
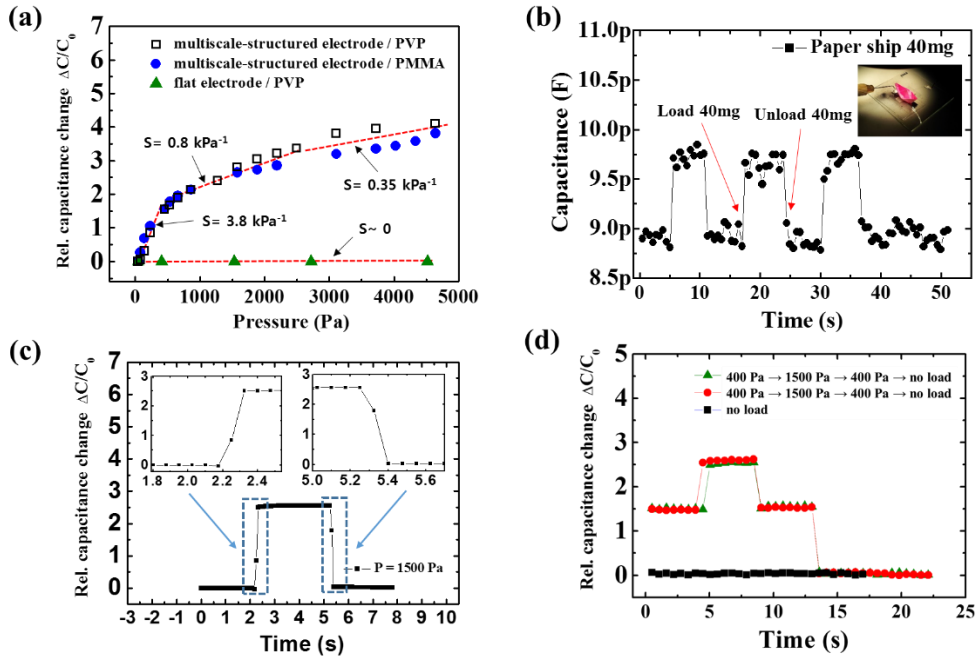
Figure 2.5 Characterization of the capacitive pressure response of the pressure sensor. (a) Relative capacitance change-pressure curve for the multiscale-structured electrode with PVP or PMMA dielectric layer and the non-structured flat electrode with PVP dielectric layer. The sensors with the multiscale-structured electrode exhibit higher pressure sensitivity than the sensor with non-structured electrode. (b) Capacitance-time curve for the detection of very small pressure (15 Pa) according to the loading and unloading of a paper ship (40mg). (c) Fast response and relaxation time (< 150 ms) of the sensor. (d) Stair-like pressure loading and unloading. The sensors show fast response and relaxation regardless of the previous pressure.

36
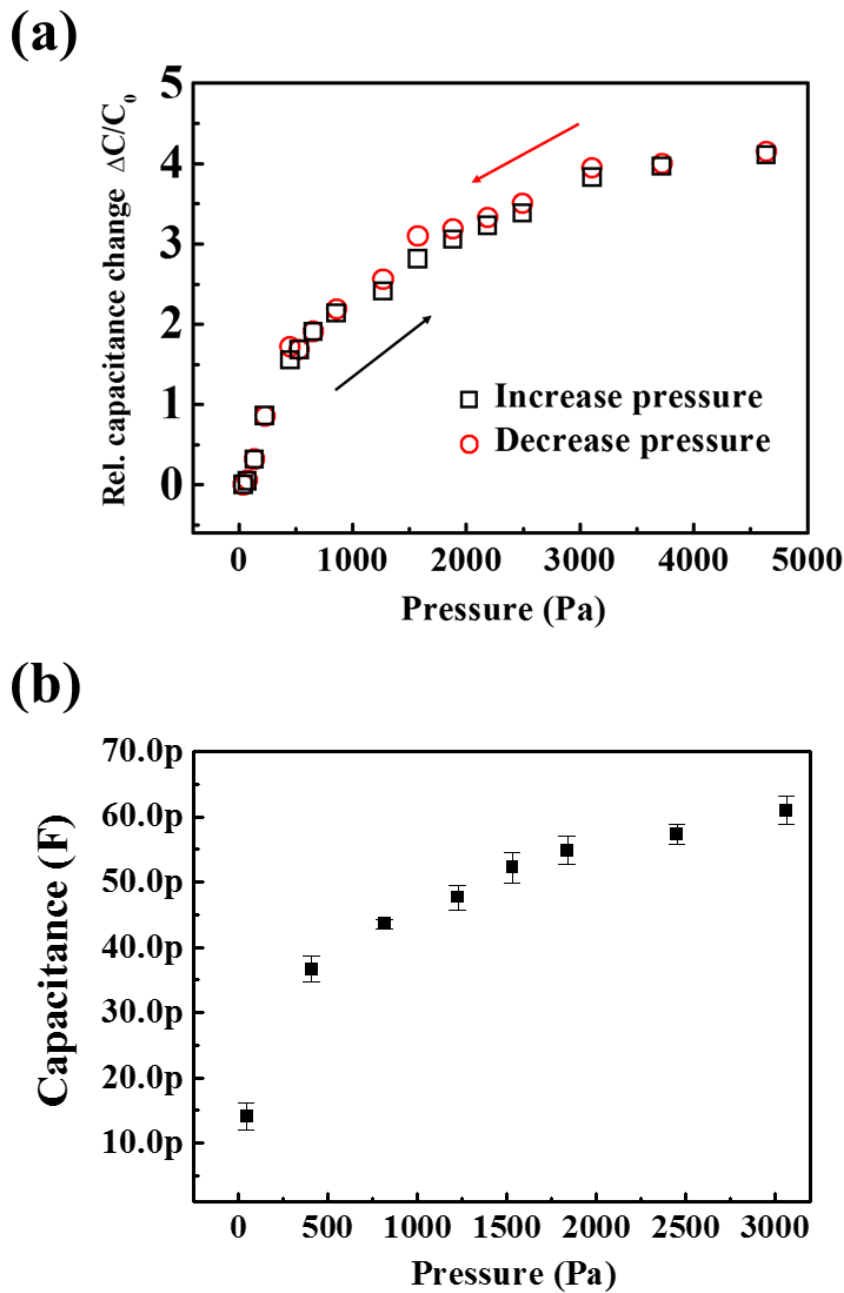
Figure 2.6 (a) Relative capacitance change-pressure curves from the consecutive loading-unloading cycles. (b) The capacitance-pressure curve of the pressure sensor. We tested ten independent samples and the error bars represent the standard deviation from ten samples.
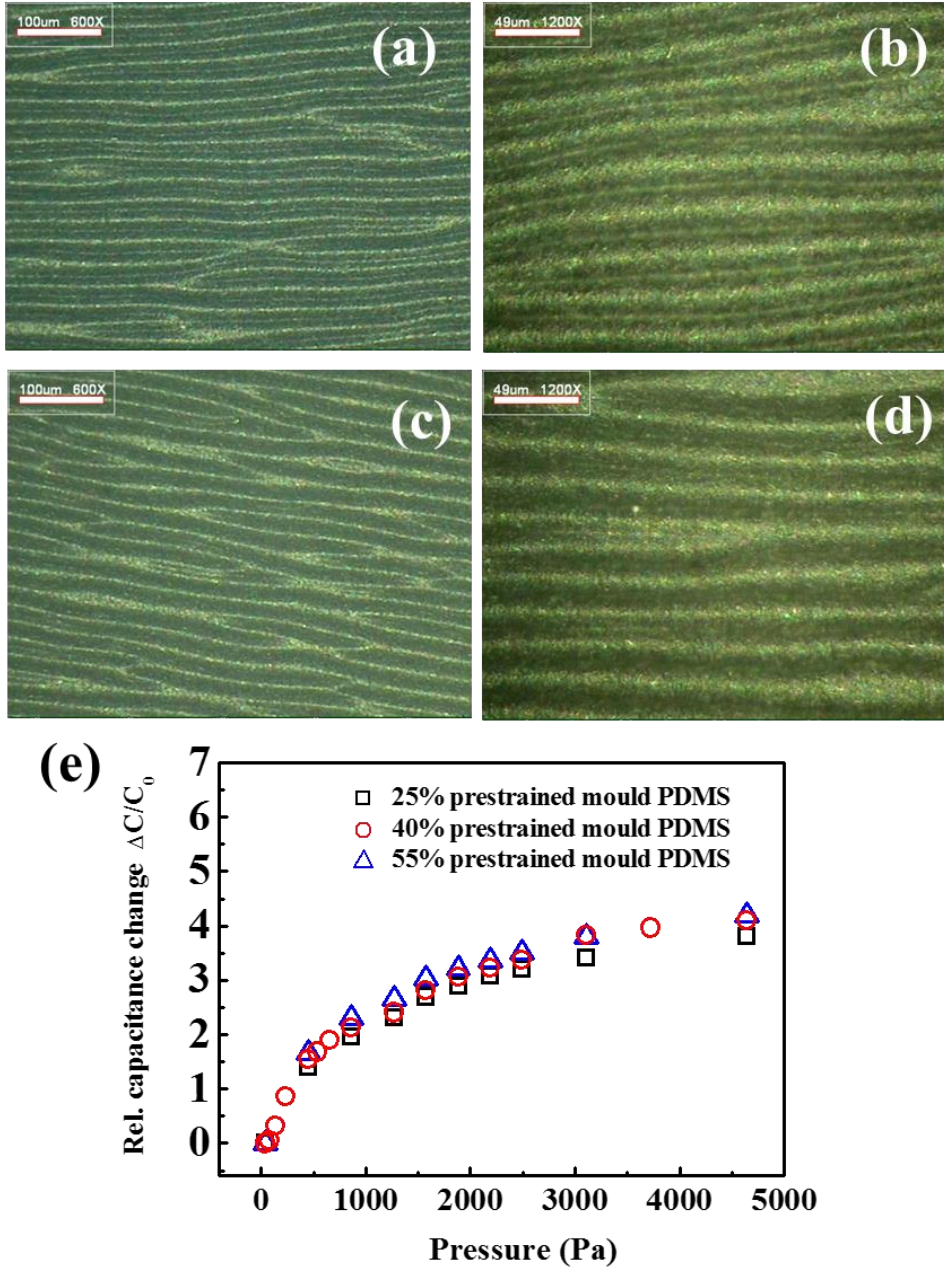
Figure 2.7 (a,b) Microscopic images of the multiscale-structured electrode obtained from the mould with pre-strain level of 25%. The average wavelength and amplitude are about 25 μm and 5 μm, respectively. (c,d) Microscopic images of the multiscale-structured electrode obtained from the mould with pre-strain level of 55%. The average wavelength and amplitude are about 22 μm and 7 μm, respectively. (e) Relative capacitance change-pressure curve of the sensors from the mould PDMS with different pre-strain level.

Pressure sensors fabricated by using multiscale-structured electrodes obtained from the mould PDMS with different pre-strain level were also tested to check the variation of pressure sensitivity according to the pre-strain level of the mould PDMS, as shown in Figure 2.7. The variation of pressure sensitivity was small. Therefore, we used the mould PDMS with pre-strain level of 40% only based on this result.

This dramatic high pressure sensitivity of the pressure sensor can be based on the multiscale structure (it consists of the wavy structure and the rough surface of the crest) and the deformable property of the electrode. The AgNW-embedded PDMS electrode can be deformed by the applied pressure or external force. From this property, the contact area and the volume of air gap between the multiscale-structured electrode and dielectric layer are changed by the applied pressure. Therefore, when the pressure is applied to the sensor, the sharp contact edges of the wavy structure and the rough surface of the crest provide dramatic changes of the contact area and the volume of air gap. Through these changes of the contact area and the volume of air gap, the capacitance of the sensor changes dramatically and the sensor shows high pressure sensitivity. Due to the rubberlike property of the multiscale-structured electrode, any kind of the dielectric layer that shows higher mechanical rigidity than the multiscale-structured electrode can be used to the sensor. Polymer dielectric materials such as PMMA and PVP can be applied to the sensor as a dielectric layer as shown in Figure 2.5(a). Even oxide dielectric material can be used to the sensor. (Figure 2.8). Each sensitivity of the sensors was similar, with the variation below 10 %, regardless of the kind of polymer dielectric layer.

Figure 2.5(c) and insets show the response and relaxation times of the sensor. When the pressure of 1.5 kPa was loaded and unloaded to the sensor, the response and relaxation times were less than 150 ms, respectively. When the pressure like stair

shape, a rising and falling pressure (400 Pa → 1500 Pa → 400 Pa → no load), is applied, the response and relaxation times are less than 500 ms and the capacitance shows the same value for the same pressure regardless of the previous pressure (Figure 2.5(d)). The capacitance of the sensor does not change for the static pressure, which means the stable operation of the sensor for the static pressure and demonstrates the accurate measurement for the applied pressure (Figure 2.5(c) and (d)).
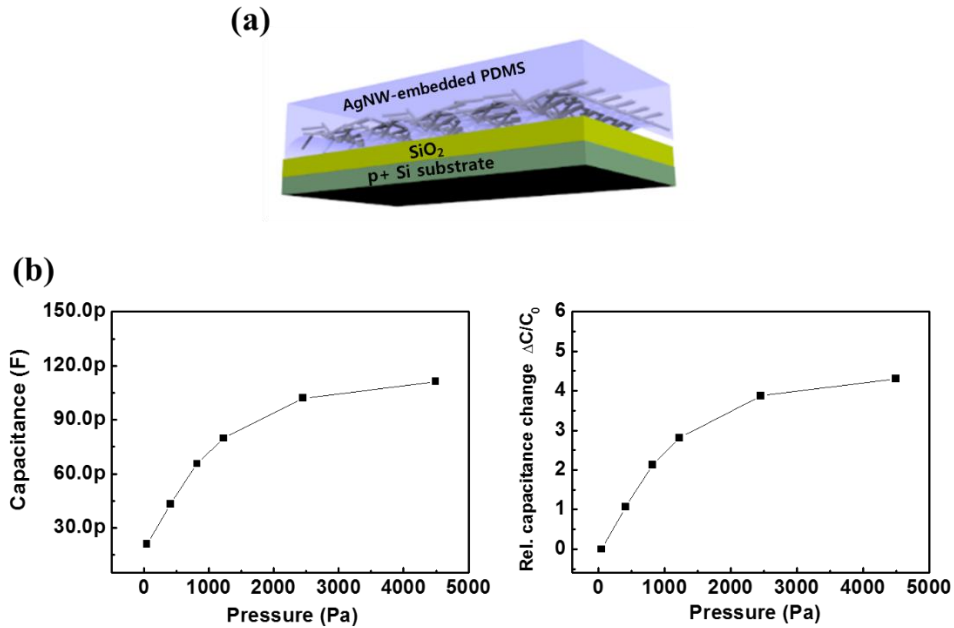
Figure 2.8 The pressure sensor with oxide dielectric layer. (a) Schematic diagram of the pressure sensor fabricated with the multiscale-structured electrode, SiO2 dielectric layer (thermally grown, 200 nm) and p+ silicon substrate (b) Pressure-response curves of the pressure sensor.
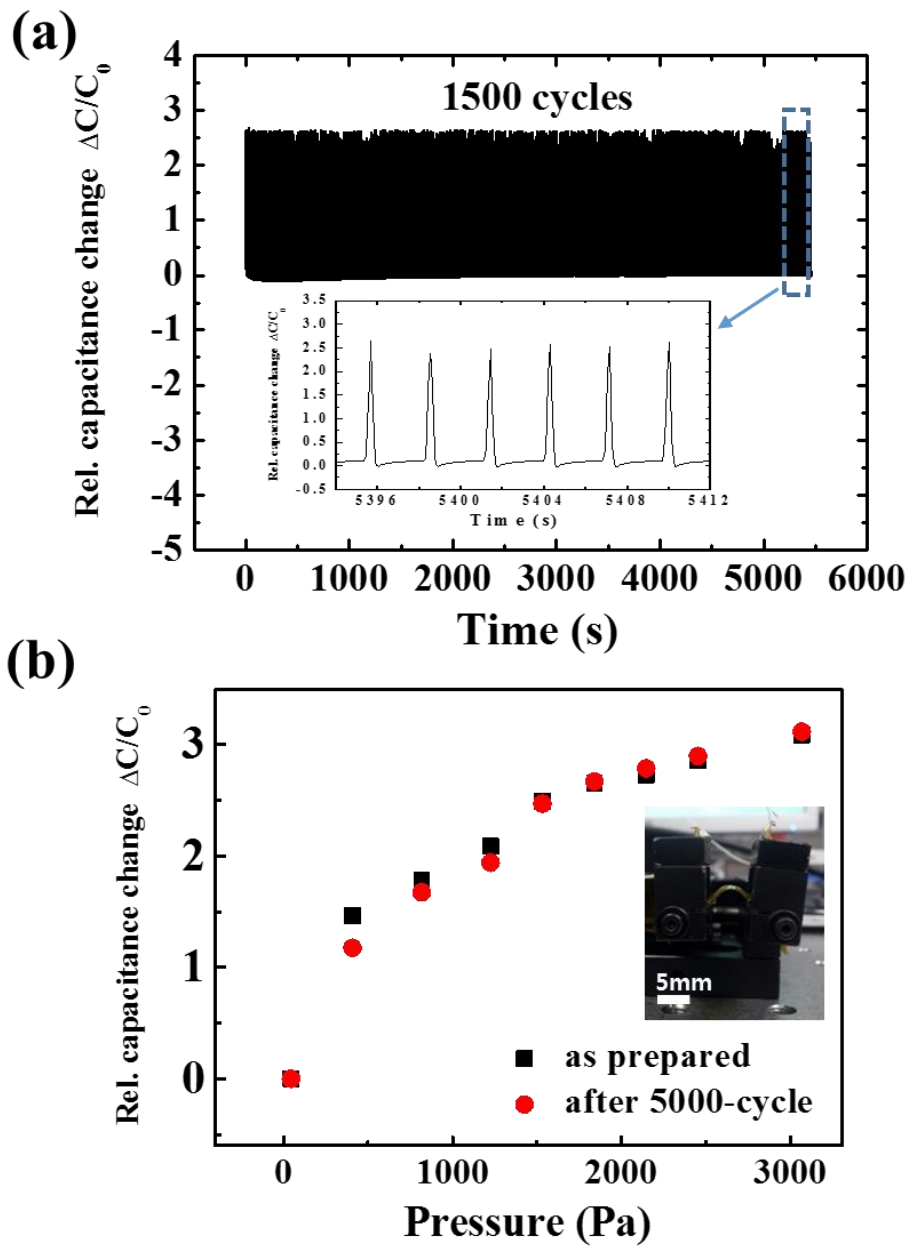
Figure 2.9 Stability of the pressure sensor. (a) Stability of pressure response to the 1500-cycle loading/unloading pressure of 1500 Pa. (b) Bending stability of pressure response after 5000-cycle bending test.

The stability of the pressure sensor was investigated from the repeated loading/unloading cycling test. The capacitance changes of the sensor were measured when the pressure of 1.5 kPa was loaded and unloaded repeatedly up to 1500 times as shown in Figure 2.9(a). The capacitance of the sensor at each pressure was hardly changed for repeated cycles. The result indicates that the pressure sensor has high stability for the repeated loading/unloading. In addition, the bending stability of the sensor was tested by using a home-made bending apparatus. For the bending test, the multiscale-structured electrode was fastened to the bottom plane by using a Kapton tape. The relative capacitance change- pressure curve of the sensor were measured before bending and after 5000-cycle bending with 3 mm radius of curvature. The relative capacitance changes of the 5000-cycle bending tested sensor at each pressure show no appreciable degradation in comparison with the as-prepared sensor (Figure 2.9(b)). The pressure sensor with the multiscale-structured electrode is robust and stable to the repeated loading/unloading and bending cycles based on the above results.

The AgNW-embedded multiscale-structured PDMS electrode can be easily handled and scaled up for a large-area fabrication. Simply, by cutting and attaching the multiscale-structured PDMS electrode of desired size onto the PET substrate (50 µm thick), we fabricated pixel-type capacitive pressure sensor arrays. The bottom Ag electrode was inkjet-printed and PVP dielectric layer was spin-coated. As shown in Figure 2.10(a) and 2.10(d), sensor arrays with 3×3 pixels and 5×5 pixels were obtained (size of the sensor array is 24×24 mm^2) and the sizes of each capacitor were 4×4 mm^2 and 2×2 mm^2, respectively. To investigate the sensing ability of the sensor arrays, a small weight (5 g, 8 mm diameter) was loaded to the marked site of the sensor array with 3×3 pixels as shown in Figure 2.10(a) and 2.10(b).
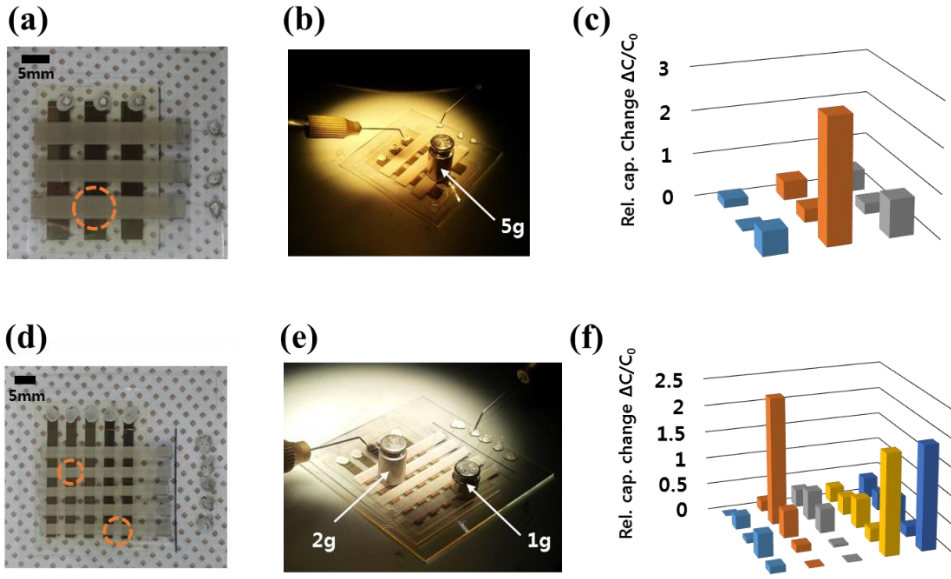
Figure 2.10 Pixel-type pressure sensor arrays. (a) Photograph of the sensor array with 3×3 pixels. (b,c) 5g weight is loaded onto the 3×3 sensor array and the corresponding two-dimensional intensity profile is shown. (d) Photograph of the sensor array with 5×5 pixels. (e,f) 1g and 2g weights are loaded onto the 5×5 sensor array and the corresponding two-dimensional intensity profile is shown.

The corresponding result is visualized to a two-dimensional intensity profile as shown in Figure 2.10(c). It is notable that the loaded site only shows a large increment of capacitance and other sites show small increments of capacitances. Also, the large increment value that obtained from this array device is similar to that of the single sensor device for 1.5 kPa pressure. We also fabricated the sensor array with 5×5 pixels that has much smaller size of pixel (2×2 mm^2). This 5×5 sensor array has a smaller sensing area per pixel than 3×3 array (Figure 2.10(d)). Small weights (1 g, 6 mm diameter and 2g, 6mm diameter) were loaded onto the marked sites as shown in Figure 2.10(d) and 2.10(e). The corresponding result is visualized to a two-dimensional intensity profile as shown in Figure 2.10(f). The capacitances of the sites with weights only increase dramatically. The increment value of the site

43

with 2g weight is higher than those of the sites with 1g weight and the increment values of the sites with 1g weight are almost same. These results from sensor arrays of 3 × 3 pixels and 5 × 5 pixels demonstrate that the sensor arrays can detect the spatial distribution of the applied pressure with the sensitivity as high as that of the single sensor and be applied to the electronic skins or large area wearable sensing devices.

Our pressure sensor can be used to measure the pressures of fingertips when an object is grabbed with fingers. To realize the fingertip pressure sensing prototype device, each sensor was attached on the four fingers except a little finger as shown in Figure 2.11(a). The capacitor size of each finger sensor was 4×4 mm^2 and PMMA was used as a dielectric layer. The plastic beaker (28.11 g) was grabbed tightly not to drop it down by the four fingers (Figure 2.11(b)). Figure 2.11(c) shows each capacitance change ratio ($\Delta C/C_0$) of the pressure sensors attached on the four fingers. The capacitance change ratio of the sensor on the thumb is about 7.6, the largest value among the fingertip sensors, which means that the highest pressure was applied to the thumb among the four fingers when the beaker was grabbed. The capacitance change ratio of the index finger is the second largest (5), that of the middle finger is third (4.6) and that of the ring finger is forth (3.2). The result demonstrates that the pressure sensor can be used to sense the fingertip pressure distribution, when grabbing an object. Our pressure sensor can be applied to the finger or hand muscles rehabilitation treatment to measure the degree of the grip strength of the patient and the sportswear to measure the distribution of pressures or forces of people's hands when grabbing a ball, a bat, a racket, a golf club, etc.
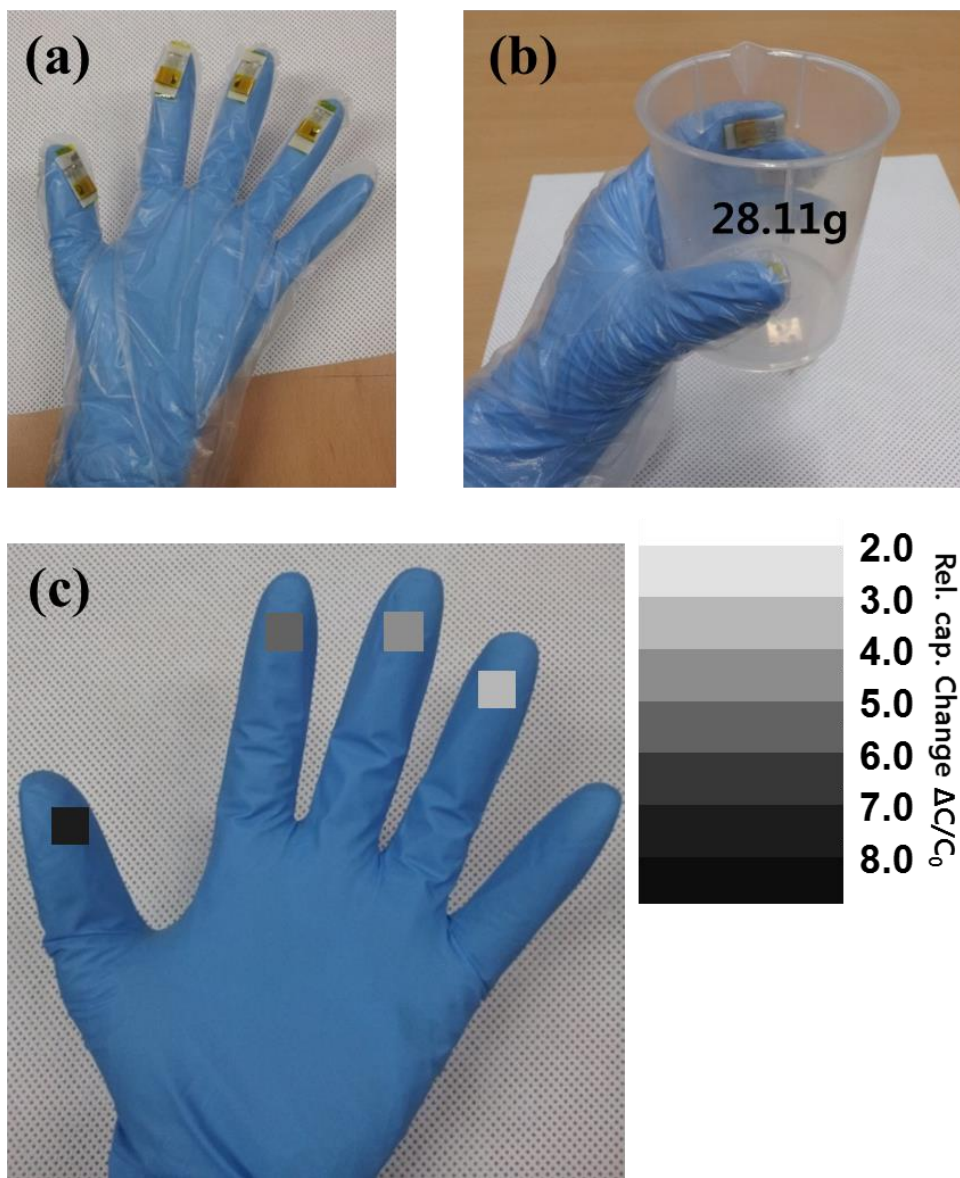
Figure 2.11 Fingertip grip pressure sensing device. (a) Photograph of the fingertip grip pressure sensor. Each pressure sensor is attached on the fingertips. (b,c) Grabbing a plastic beaker with four fingertips and the corresponding relative capacitance changes are visualized.

2.1.4 Conclusion

In summary, we developed capacitive pressure sensors based on the robust and elastomeric AgNW-embedded multiscale-structured PDMS electrode with a low-cost and simple fabrication process for the first time. The capacitive pressure sensor has high pressure sensitivity 3.8 kPa^{-1} (45 ~ 500Pa), 0.8 kPa^{-1} (500 Pa ~ 2.5 kPa) and 0.35 kPa^{-1} (2.5 ~ 4.5 kPa) and can detect very small pressure of 15 Pa. The sensor also shows fast response and relaxation times (< 150 ms), high stability for repeated cycles over 1500 times and high bending stability. We demonstrated easy handling and scaling up of our sensor by fabricating 3×3 and 5×5 arrays. These arrays also show high pressure sensitivity similar to the single sensor device and can detect the spatial distribution of the applied pressure. We also fabricated the fingertip pressure sensing device to detect the pressure distribution of fingers, when grabbing an object. The highly sensitive and stable capacitive pressure sensor with a low-cost fabrication and easy handling may open and broaden its application to wearable electronic skins for rehabilitation treatment of patients and pressure mapping in sports activities or daily activities.

2.2. Pressure sensor with tunable sensitivity

2.2.1 Introduction

Wearable electronics have gained huge interest nowadays, because of their versatile applications such as human-machine interface, real-time health monitoring, patient rehabilitation and wearable displays. Flexible pressure sensor or tactile sensor, one of the core device of wearable electronics, has been widely investigated due to its multifunctional application to wearable electronics [1,5-6,9,16]. Flexible pressure sensors can detect wide range pressure from gentle touch (<10kPa) to body pressure mapping (>1MPa) and even very small pressure (<10Pa) [5-6,9,16]. Based on these properties, flexible pressure sensors can be applied to human-machine interfaces, next generation touch interfaces for wearable displays and health care system [5-7,9,16,20,43,44]. For these applications, pressure sensors must have high pressure sensitivity, flexibility, stability and also tunable sensitivity like human skin. Because pressure sensors with customized sensitivity which is suitable for versatile application are desirable, the tunable pressure sensitivity of the sensor is needed [44]. A number of flexible pressure sensors with high sensitivity have been reported [1,5-7,9,16,20,43]. However, only a few papers have been reported for the pressure sensors with tunable sensitivity [24,44]. Bao et al. reported tunable flexible pressure sensor using different microstructured elastomer geometries [44]. They used different microstructured moulds to obtain different microstructured elastomers. However, the preparation of different moulds leads to complexity of the fabrication process and increase of the fabrication cost.

Recently, our group reported a capacitive flexible pressure sensor with

47

elastomeric nanowire composite [43]. However, the pressure sensitivity of the reported sensor was fixed and not tunable. In this paper, we report highly sensitive and flexible pressure sensor with tunable sensitivity. By controlling the mixing ratio of the matrix PDMS of the nanowire composite, we can tune the pressure sensitivity of the sensor easily. Three types of PDMS with different mixing ratio, a 5:1, 10:1 and 15:1 mixture of liquid PDMS and curing agent, were used to fabricate pressure sensor. All the sensors show different pressure sensitivity in the wide pressure range (0 ~ 2500 Pa).

2.2.2 Experimental

AgNW ink (SLV-NW-90, Blue Nano inc.) was spray-coated onto the mould PDMS to obtain AgNW film. After heat treatment of the spray-coated AgNW film, the AgNW film coated mould PDMS was released to zero strain condition to obtain buckled structure. Finally, the mixtures of a liquid PDMS and a curing agent (5:1, 10:1, and 15:1, w/w) were casted onto the buckled surface of the AgNW film, followed by curing at 100 °C for 2 h. After the curing process, the mould PDMS was detached to obtain the AgNW-embedded PDMS, nanowire composite, with buckled structure as shown in Figure 2.12(a). No delamination and increase of resistance were observed to the AgNW-embedded PDMS after 3M tape test [39,43]. The fabrication process of buckled mould PDMS and the bottom plane (dielectric layer/inkjet printed Ag on poly(ethylene 2,6- naphtharate) (PEN) substrate) were explained in detail in our previous work [43]. The pressure sensors were fabricated by sandwiching the AgNW-embedded PDMS with buckled surface and the bottom plane. For the bending test, the AgNW-embedded PDMS was fastened onto the bottom plane by using Kapton tape and the sensor was bent by using home-made bending test machine. The microstructure of the AgNW-embedded PDMS was characterized by 3D surface profiler (NanoFocus) and an optical microscope (EGTECH). Capacitance was measured at 1 kHz with a 0.5 V a.c. signal by using the Agilent 4284A LCR meter. IMADA force gauge with z-axis stage was used to apply the pressure to the sensor and metal or plastic weights were used to apply the pressure to the sensor.
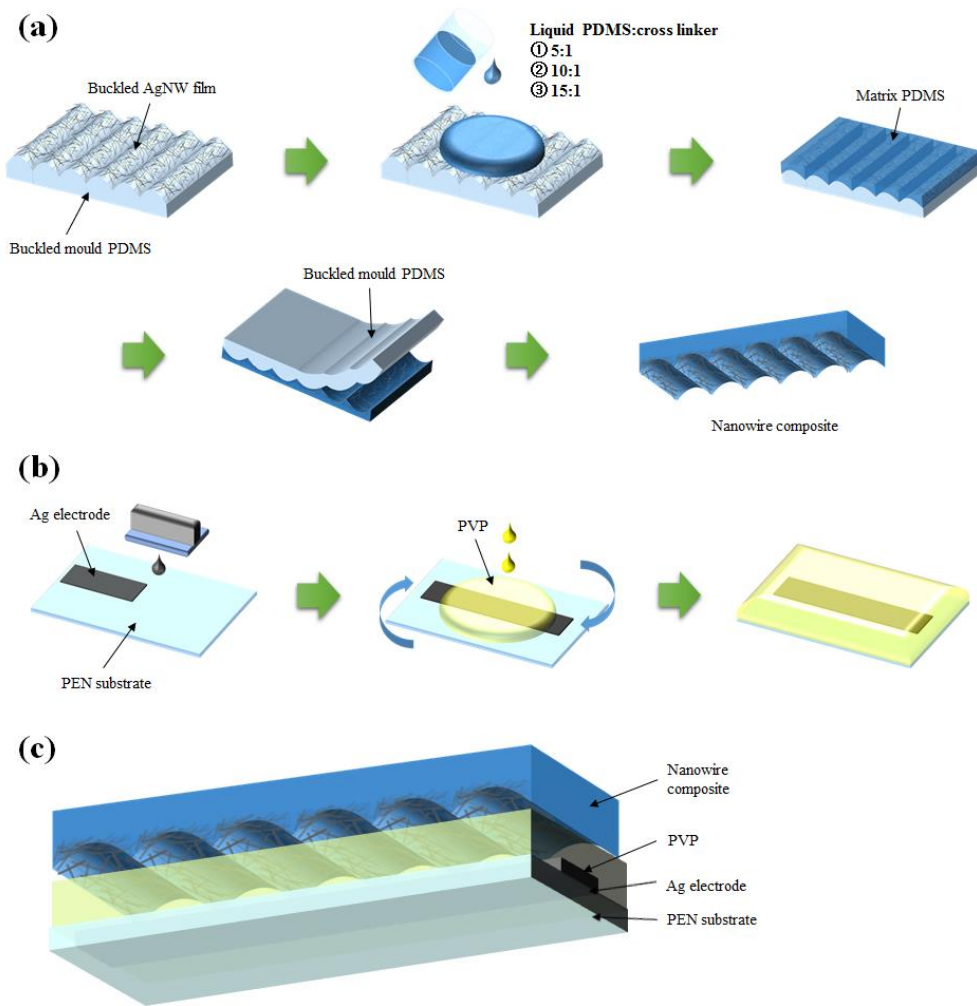
Figure 2.12 Fabrication process. (a) Fabrication process of nanowire composites with different mixing ratio of matrix PDMS. (b) Fabrication process of bottom plane: Inkjet printing of Ag electrode onto the PEN substrate and spin coating of PVP dielectric layer. (c) Capacitive flexible pressure sensor with nanowire composite and bottom plane.

2.2.3 Results and discussion

Microstructure of the AgNW-embedded PDMS was characterized by using 3D surface profiler and optical microscopy (OM). As shown in Figure 2.13, the buckled structure was introduced successfully onto the AgNW-embedded PDMS surface and the AgNWs were totally embedded into the matrix PDMS, even into the sharp crest area of the matrix PDMS [43]. All the nanowire composites showed wavy structure regardless of the mixing ratio of matrix PDMS. However, the shape of the buckled structure was different according to the mixing ratio of the matrix PDMS as shown in Figure 2.12 and Table 2.1. Surface roughness value of the crest area of the wavy structure was different according to the mixing ratio. Nanowire composite with mixing ratio of 10:1 showed the highest roughness value about 0.3μm. For the nanowire composite with mixing ratio of 15:1, the crest area of the buckled structure looked like crumpled and blunt compared to the mixing ratio of 5:1 and 10:1 as shown in Figure 2.12(c). The smallest amplitude of the wavy structure and the largest width of crest area (width of crest area at top 5 % of amplitude) in the Table 1 supported the crumpled crest area of the nanowire composite of 15:1. Differences of the buckled structure including surface roughness, width of crest and amplitude according to the different mixing ratio resulted from the different peeling-off stress, which is related to the mechanical property of the matrix PDMS of nanowire composite, during the detaching process from the mould PDMS.
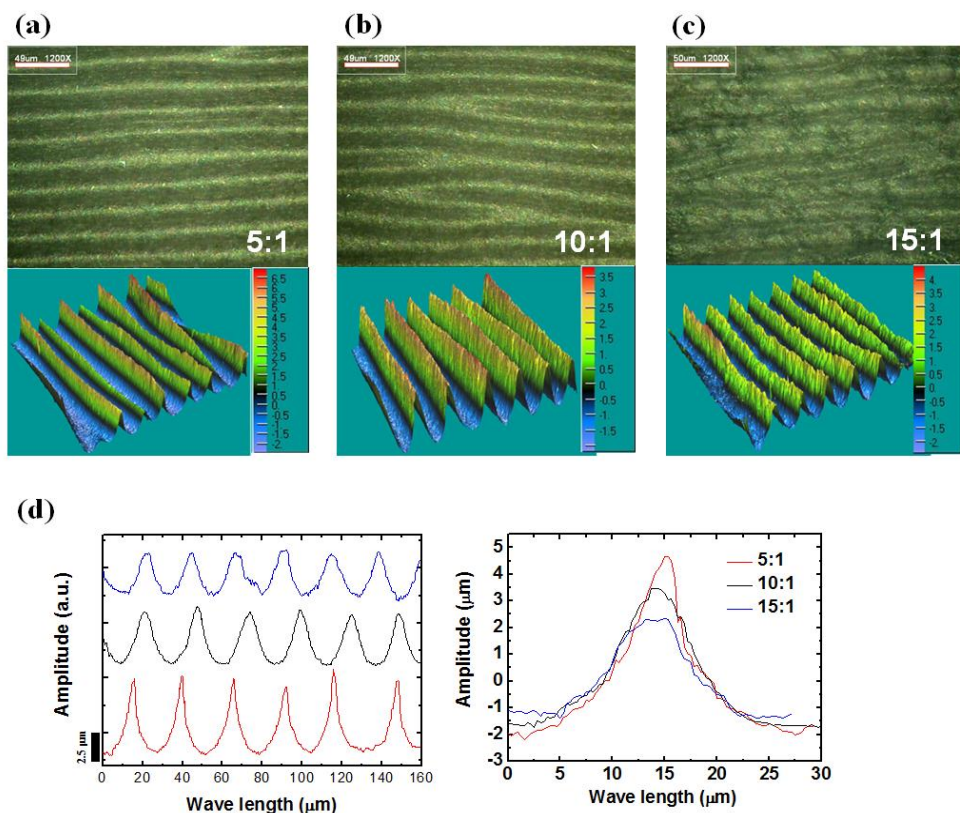
Figure 2.13 Optical images and 3D surface profiler images: (a) nanowire composite with mixing ratio of 5:1, (b) nanowire composite with mixing ratio of 10:1 and (c) nanowire composite with mixing ratio of 15:1. (d) Wavy structures of nanowire composites (left) and single wavy structures of nanowire composites (right).

PDMS : cross linker	5:1	10:1	15:1
Crest area surface roughness	0.22 μm	0.3 μm	0.15 μm
Width of crest (5%)	1.3 μm	1.7 μm	2.5 μm
Wavelength & Amplitude	25 & 7 μm	24 & 5 μm	24 & 4 μm

Table 2.1 Microstructure of nanowire composites

Elastic modulus of the matrix PDMS and the nanowire composite was predicted by using modified Halpin-Tsai equation [45,46]

$$E_{random\ 3D\ fiber} \cong 0.184E_{\parallel} + 0.816E_{\perp} \qquad (1)$$

$$E_c = E_m \frac{E_f + \xi[(1-\phi)E_m + \phi E_f]}{[(1-\phi)E_f + \phi E_m + \xi E_m\ ]} \qquad (2)$$

Where ϕ is the volume fraction of fiber, E_f is the modulus of fiber and E_m is the modulus of matrix PDMS. The parameter ξ is the shape factor for a solicitation parallel to the wire orientation, $\xi = 2(L/d)$, and for a transverse solicitation, $\xi = 2$. By using equation (1) and (2), we calculated the elastic modulus of nanowire composite as shown in Figure 2.14. Each modulus of nanowire and PDMS with different mixing ratio was referred [47]. As shown in Figure 2.14, a nanowire composite with mixing ratio of 5:1 showed the highest modulus at the condition of the same nanowire volume fraction. The higher the modulus of matrix PDMS is, the higher the modulus of nanowire composite is. Difference of the elastic modulus of the nanowire composite according to the mixing ratio resulted in difference of the microstructure of the nanowire composite after the peeling-off process.
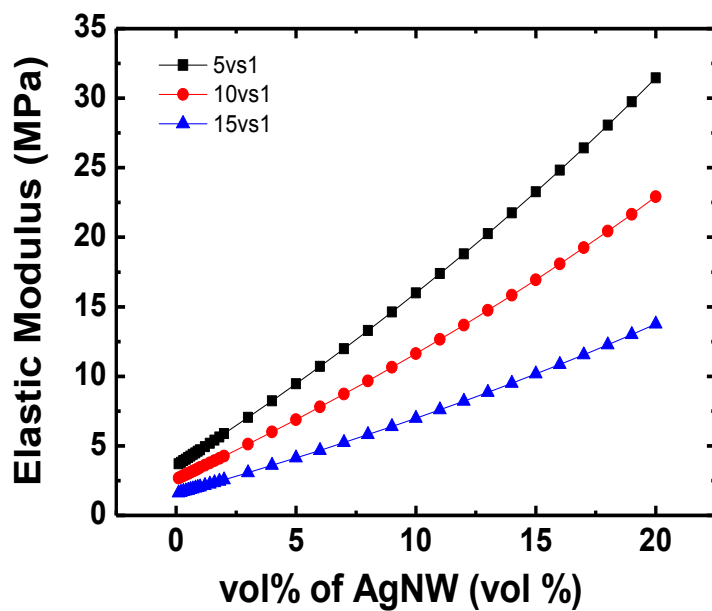
Figure 2.14 Elastic modulus – AgNW volume fraction curve of nanowire composites calculated from the modified Halpin-Tsai equation.
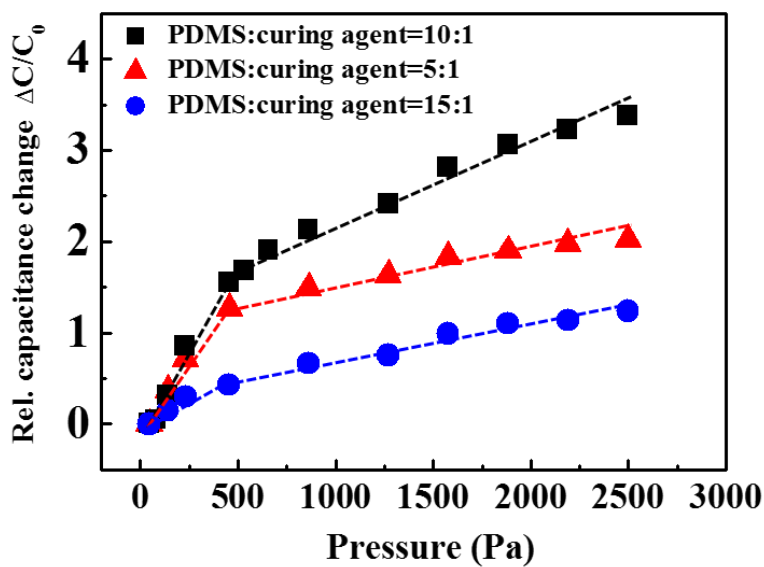
Figure 2.15 Relative capacitance change–pressure curve for the pressure sensors of nanowire composites with different mixing ratio.

The structure of the flexible capacitive pressure sensor is illustrated in Figure 2.12 (c). AgNW-embedded area was facing PVP dielectric layer and the air gap was formed between AgNW-embedded PDMS and PVP as shown in Figure 2.12 (c). The pressure sensitivity of each sensor with different PDMS mixing ratio was tested by applying pressure as shown in Figure 2.15. The pressure sensitivity of the sensor can be defined as the slope of the relative capacitance change-pressure curve in Figure 2.15, $S = \delta(\Delta C / C_0)/\delta p$, $\Delta C = C - C_0$ where C and C_0 denote the capacitance with the applied pressure and base pressure, respectively, and p denotes the applied pressure. The pressure sensor with mixing ratio of 10:1 showed highest sensitivity among the sensors. This sensor showed very high pressure sensitivity, 4 kPa^{-1} (0~450Pa) and 0.6 kPa^{-1} (450~2500Pa) in the wide pressure regime. The pressure sensitivity of the sensor with mixing ratio of 5:1 was 3 kPa^{-1} (0~450Pa) and 0.4 kPa^{-1} (450~2500Pa) and the pressure sensitivity of the sensor with mixing ratio of 15:1 was 1 kPa^{-1} (0~450Pa) and 0.4 kPa^{-1} (450~2500Pa). The pressure sensitivity of the sensor was dramatically changed by simply changing the mixing ratio of the liquid PDMS and curing agent of the matrix PDMS. This simply tunable pressure sensitivity resulted from the mechanical property of the matrix PDMS and the shape of the crest area of the buckled structure. For the sensors with the mixing ratio of 5:1 and 10:1, these sensors had relatively smooth crest area and similar buckled structure as shown in Figure 2.13(a) and 2.13(b). However, the pressure sensitivities were different due to the difference of mechanical property of the matrix PDMS, specifically, the elastic modulus of the PDMS. According to the mechanical property of the matrix PDMS, the degree of deformation of the nanowire composite was different in the same pressure and this difference induced the

difference pressure sensitivity. For the sensor with the mixing ratio of 15:1, this sensor had crumpled crest area as shown in Figure 2.13(c) and this crumpled shape of the buckled structure induced lower pressure sensitivity. Due to the crumpled and blunt crest area of the nanowire composite with 15:1, the base capacitance of the sensor, C_0, was highest among the three sensors and this sensor shows the lowest pressure sensitivity due to the highest base capacitance (C_0 =17 pF (5:1), 16 pF (10:1) and 24 pF (15:1)). Based on these results we can conclude that the mechanical property of the matrix PDMS and the shape of the crest area of the buckled structure affect the pressure sensitivity.

The response and relaxation properties of the sensor were also measured. As shown in Figure 2.16, the sensors with nanowire composites of mixing ratio 5:1 and 10:1 showed fast response and relaxation properties below 0.15 seconds. However, the sensor with nanowire composite of mixing ratio 15:1 showed very slow relaxation property. The relaxation time was almost 8 seconds. This slow relaxation is related to the viscoelastic property of the nanowire composite [9].

Our pressure sensor can also detect the bending strain and the capacitance change of the sensor according to the bending radius is shown in Figure 2.17(a). As the moving distance increased and the bending radius decreased, the capacitance of the sensor was increased. The bending stability of the pressure sensor was also tested by using a bending machine. The capacitance change and pressure sensitivity of the sensor were measured before bending and after 5000-cycle bending with 3 mm radius of curvature. We calculated the relative capacitance change of the sensors before and after bending cycle (Relative capacitance change $=(C_{after\ bending} - C_{before\ bending})/C_{before\ bending}$). At 400 Pa, the sensor showed slightly decreased

capacitance value about 20% after bending process. However, in the other pressure ranges, the sensor showed no appreciable degradation in comparison with the as-prepared sensor as shown in Figure 2.17(b). Our sensor is sensitive to the bending strain and is robust and stable to the repeated bending strain.
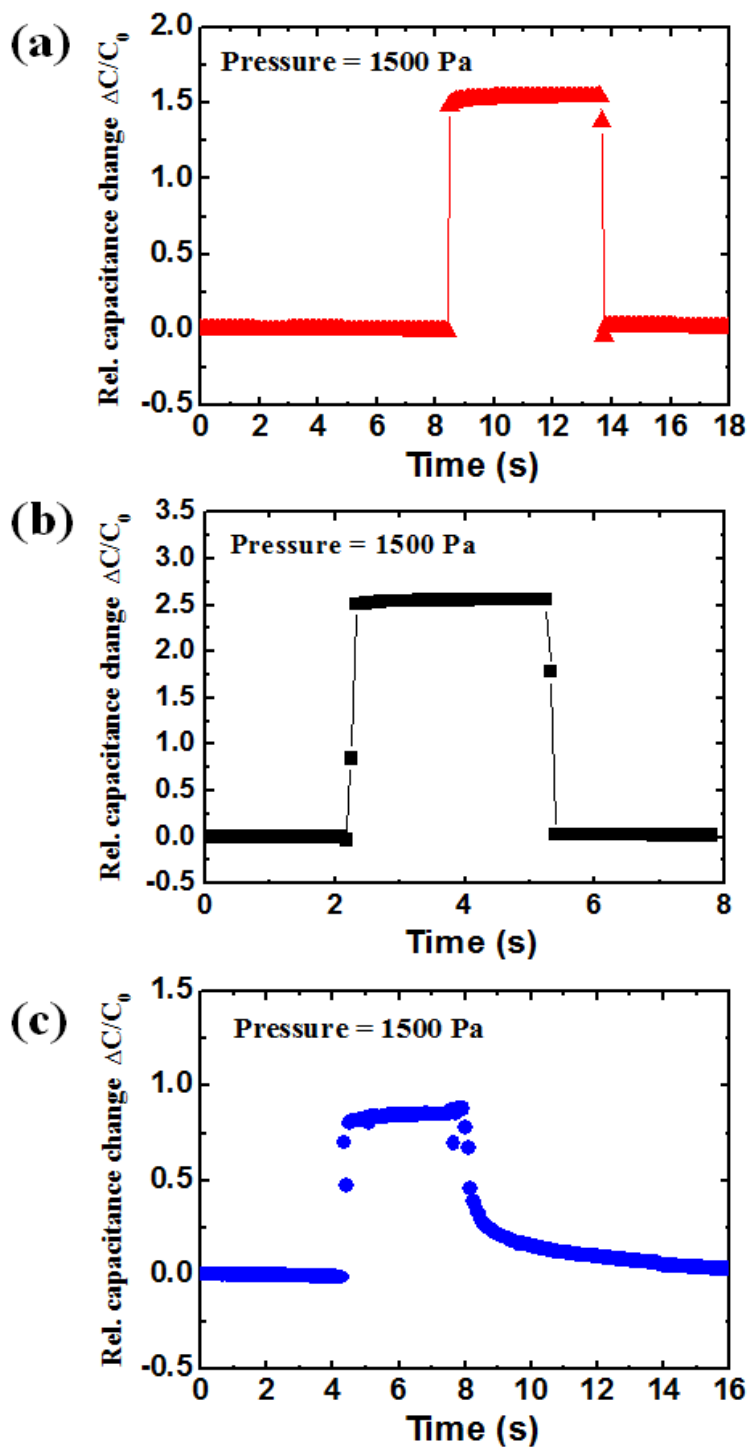
Figure 2.16 Response and relaxation properties of the pressure sensor: (a) nanowire composite with mixing ratio of 5:1, (b) nanowire composite with mixing ratio of 10:1 and (c) nanowire composite with mixing ratio of 15:1.
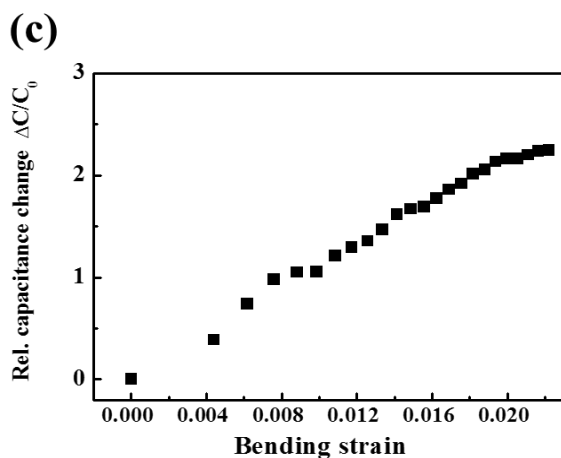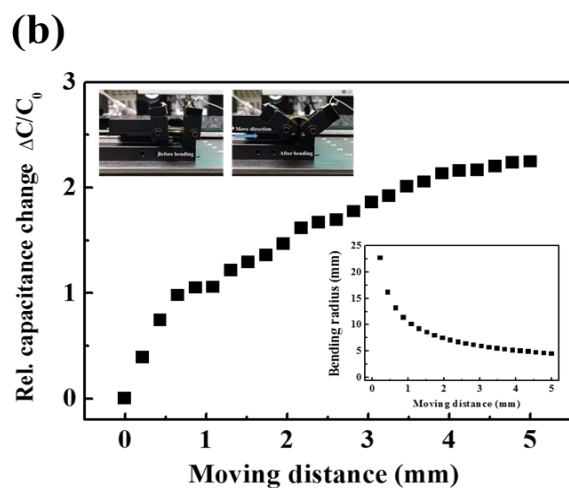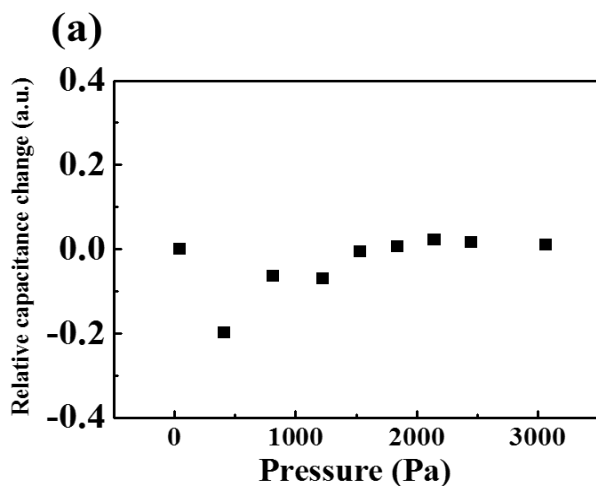
Figure 2.17 (a) Bending stability of the pressure sensor after 5000-cycle bending test (nanowire composite with mixing ratio of 10:1). (b) Relative capacitance change-moving distance curve; Inset: The bending radius-moving distance curve (nanowire composite with mixing ratio of 10:1). (c) Relative capacitance change-bending strain curve.

2.2.4 Conclusion

In summary, we fabricated sensitivity tunable pressure sensors by controlling the mixing ratio of the matrix PDMS. Due to the difference of the mechanical property of the matrix PDMS and the shape of the crest area of the buckled structure, we can easily tune the pressure sensitivity of the sensor. Our sensor can also detect the bending strain and is very stable to the repeated bending condition. This pressure sensor can be applied to the next generation human-machine interface for wearable or flexible/foldable displays and electronics.

Reference

[1] T. Someya, T. Sekitani, S. Iba, Y. Kato, H. Kawaguchi and T. Sakurai, *Proc. Natl. Acad. Sci. USA*, 101, 9966 (2004)

[2] A. N. Sokolov, B. C.-K. Tee, C. J. Bettinger, J. B.-H. Tok and Z. Bao, *Acc. Chem. Res.*, 45, 361 (2012)

[3] K. Takei, T. Takahashi, J. C. Ho, H. Ko, A. G. Gillies, P. W. Leu, R. S. Fearing and A. Javey, *Nat. Mater.*, 9, 821 (2010)

[4] T. Sekitani and T. Someya, *MRS Bull.*, 37, 236 (2012)

[5] C. Pang, G.-Y. Lee, T.-I. Kim, S. M. Kim, H. N. Kim, S.-H. Ahn and K-Y. Suh, *Nat. Mater.*, 11, 795 (2012)

[6] X. Wang, Y. Gu, Z. Xiong, Z. Cui and T. Zhang, *Adv. Mater.*, 26, 1336 (2014)

[7] G. Schwartz, B. C.-K. Tee, J. Mei, A. L. Appleton, D. H. Kim, H. Wang and Z. Bao, *Nat. Commun.*, 4, 1859 (2013)

[8] W. Honda, S. Harada, T. Arie, S. Akita and K. Takei, *Adv. Funct. Mater.*, 24, 3299 (2014)

[9] S. C. B. Mannsfeld, B. C.-K. Tee, R. M. Stoltenberg, C. V. H.-H. Chen, S. Barman, B. V. O. Muir, A. N. Sokolov, C. Reese and Z. Bao, *Nat. Mater.*, 9, 859 (2010)

[10] E. Biddiss and T. Chau, *Med. Eng. Phys.*, 28, 568 (2006)

[11] L. Masia, H. I. Krebs, P. Cappa and N. Hogan, *IEEE/ASME Trans. Mechatronics*, 12, 399 (2007)

[12] M. Donati, N. Vitiello, S. M. M. D. Rossi, T. Lenzi, S. Crea, A. Persichetti, F. Giovacchini, B. Koopman, J. Podobnik, M. Munih and M. C. Carrozza, *Sensors*, 13, 1021 (2013)

[13] N. Lu and D.-H. Kim, *Soft Robotics*, 1, 53 (2013)

[14] H.-K. Lee, S.-I. Chang and E. Yoon, *J. Microelectromech. Syst.*, 15, 1681 (2006)

[15] T. Someya, Y. Kato, T. Sekitani, S. Iba, Y. Noguchi, Y. Murase, H. Kawaguchi and T. Sakurai, *Proc. Natl. Acad. Sci. USA*, 102, 12321 (2005)

[16] S. Yao and Y. Zhu, *Nanoscale*, 6, 2345 (2014)

[17] D. P. J. Cotton, I. M. Graz and S. P. Lacour, *IEEE Sens. J.*, 9, 2008 (2009)

[18] E. S. Dellon, R. Mourey and A. L. Dellon, *J. Plast. Reconstr. Surg.*, 90, 112 (1992)

[19] B. C.-K. Tee, C. Wang, R. Allen and Z. Bao, *Nat. Nanotechnol.*, 7, 825 (2012)

[20] H.-B. Yao, J. Ge, C.-F. Wang, X. Wang, W. Hu, Z.-J. Zheng, Y. Ni and S.-H. Yu, *Adv. Mater.*, 25, 6692 (2013)

[21] L. Pan, A. Chortos, G. Yu, Y. Wang, S. Isaacson, R. Allen, Y. Shi, R. Dauskardt and Z. Bao, *Nat. Commun.*, 5, 3002 (2014)

[22] B. Zhu , Z. Niu , H. Wang , W. R. Leow , H. Wang , Y. Li , L. Zheng, J. Wei, F. Huo and X. Chen, *Small*, 10, 3625 (2014)

[23] J. Lee , S. Kim, J. Lee, D. Yang, B. C. Park, S. Ryu and I. Park, *Nanoscale*, 6, 11932 (2014)

[24] Q, Shao, Z. Niu, M. Hirtz, L. Jiang, Y. Liu, Z. Wang and X. Chen, *Small*, 10, 1466 (2014)

[25] J. Chen, K. Y. Lee, C.-Y. Kang, M. W. Kim, S.-W. Kim and J. M. Baik, *Adv. Funct. Mater.*, 24, 2038 (2014)

[26] C. Hou, T. Huang, H. Wang, H. Yu, Q. Zhang and Y. Li, *Sci. Rep.*, 3, 3138 (2013)

[27] C. Pan, L. Dong, G. Zhu, S. Niu, R. Yu, Q. Yang, Y. Liu and Z. L. Wang, *Nat. Photonics,* 7, 752 (2013)

[28] F.-R. Fan, L. Lin, G. Zhu, W. Wu, R. Zhang and Z. L. Wang, *Nano Lett.*, 12, 3109 (2012)

[29] L. Lin, Y. Xie, S. Wang, W. Wu, S. Niu, X. Wen and Z. L. Wang, *ACS Nano*, 7,

8266 (2013)

[30] W. Hu, Z. Niu, R. Zhao and Q. Pei, *Appl. Phys. Lett*., 102, 083303 (2013)

[31] J. Kim, T. N. Ng and W. S. Kim, *Appl. Phys. Lett*., 101, 103308 (2012)

[32] D. J. Lipomi, M. Vosgueritchian, B. C.-K. Tee, S. L. Hellstrom, J. A. Lee, C. H. Fox and Z. Bao, *Nat. Nanotechnol*., 6, 788 (2011)

[33] K. F. Lei, K.-F. Lee and M.-Y. Lee, *Microelectron. Eng*., 99, 1 (2012)

[34] H. Vandeparre, D. Watson and S. P. Lacour, *Appl. Phys. Lett*., 103, 204103 (2013)

[35] C. Wang, D. Hwang, Z. Yu, K. Takei, J. Park, T. Chen, B. Ma and A. Javey, *Nat. Mater.*, 12, 899 (2013)

[36] M. Hussain, Y.-H. Choa and K. Niihara, *J. Mater. Sci. Lett*., 20, 525 (2001)

[37] Z. Niu, H. Dong, B. Zhu, J. Li, H. H. Hng, W. Zhou, X. Chen and S. Xie, *Adv. Mater.*, 25, 1058 (2013)

[38] C. Yu and H. Jiang, *Thin Solid Films*, 519, 818 (2010)

[39] F. Xu and Y. Zhu, *Adv. Mater*., 24, 5117 (2012)

[40] C. H. Lee, D. R. Kim and X. Zheng, *Proc. Natl. Acad. Sci. USA*, 107, 9950 (2010)

[41] S. Chung, S. O. Kim, S.-K. Kwon, C. Lee and Y. Hong, *IEEE Electron Device Lett.*, 32, 1134 (2011)

[42] S. Chung, M. Jang, S.-B. Ji, H. Im, N. Seong, J. Ha, S.-K. K, Y.-H. Kim, H. Yang and Y. Hong, *Adv. Mater*., 25, 4772 (2013)

[43] Y. Joo, J. Byun, N. Seong, J. Ha, H. Kim, S. Kim, T. Kim, H. Im, D. Kim and Y. Hong, *Nanoscale*, 7, 6208 (2015)

[44] B. C.-K. Tee, A. Chortos, R. R. Dunn, G. Schwartz, E. Eason and Z. Bao, *Adv. Funct. Mater.*, 24, 5427 (2014)

[45] J.C. Halpin, J.L. Kardos, *J. Appl. Phys*., 43, 2235 (1972)

[46] A. Lonjon, P. Demont, E. Dantras and C. Lacabanne, *J. Non-Cryst. Solids*, 358, 236, (2012)

[47] Z. Wang, A. A. Volinsky and N. D. Gallant, *J. Appl. Polym. Sci*., 131, 41050, (2014)

Chapter 3

Bendable sensor and its application to pressure sensitive transistor

3.1. Introduction

Flexible pressure sensor is one of the most important devices for human oriented future technologies such as wearable health monitoring systems, touch interfaces and electronic skins [1-20]. For these application, pressure sensors must mimic sensing abilities of human tactile receptors such as high sensitivity, fast response, flexibility, stretchability and distinguishment of different mechanical stimuli. Micro- or nano-structured soft materials with various sensing mechanisms that include capacitive [1-6], piezoresistive [7-13], piezoelectric [14,15], and triboelectric sensing [16,17] have been introduced to satisfy these demands. Pressure sensors based on these materials can detect very small pressure (P < 20 Pa) and the movement of human muscles caused by pulse or vibration during speech [2,7-10,12-14]. Also they show fast response (t < 1 s) to the change of the pressure and they are flexible or stretchable [2,7-10,12-14].

Among these soft materials, micro-structured polydimethylsiloxane (PDMS) has been widely investigated due to its elastomeric property and biocompatibility [1,2,4,6,7,9,21]. Pressure sensors with micro-structured PDMS show high pressure sensitivity and fast response. Small contact area and air gap between the micro-structured PDMS and substrate enabled the high sensitivity and fast response

[1,2,4,7,9,21]. However, due to this small contact area and air gap, micro-structured PDMS is physically separated from the substrate in most flexible sensors. Micro-structured PDMS is just sandwiched or endpiece of the micro-structured PDMS is only bonded to the substrate by using temporary methods such as epoxy bonding or taping [1,2,4,9,21]. Due to these reasons, pressure sensing of the flexible pressure sensor in the bending state is more difficult than pressure sensing in the flat state and only a few paper have reported the pressure sensing in the bending state [8]. Flexible pressure sensors with micro-structured PDMS can detect not only pressure but also bending and twisting [2,6,7,9,21]. However, the distinguishment of each stimulus, when multiple mechanical stimuli were simultaneously applied to the sensor, still remains a challenge [6]. Thus, the development of flexible pressure sensor that can detect pressure even in the bending state and distinguish the type of applied mechanical stimuli is needed.

Pressure sensors have been integrated with various electronic devices to demonstrate active sensor array, user-interactive sensing system and wearable sensing system [1-3,14,18,19]. Among these devices, thin film transistors (TFTs) with organic semiconductors or semiconducting carbon nanotubes have been widely integrated with pressure sensors as active elements in the pressure sensing system [1-3,18,19,22,23]. Capacitive-type pressure sensors have been generally integrated with organic thin film transistors (OTFTs) as dielectric layers and these OTFTs are pressure sensitive due to the dependence of the output current on the capacitance of the dielectric layer [1-3,22]. These pressure sensitive transistors (PSTs) enable the amplification of the pressure sensitivity and easy integration with other electronic devices as the output value of the sensor from the change of the pressure is not capacitance but current. However, the operation voltage of PSTs integrated with

capacitive-type pressure sensors is above tens or even hundreds volt due to the low capacitance value of the dielectric layer ($C < 1$ nF cm^{-2}) [1-3,22]. This voltage level is too high to fabricate wearable sensing system by using the commercially available batteries ($V \leq 5$ V). Hence, for the realization of the wearable sensing system, the operation voltage of PSTs must be reduced.

In this chapter, we demonstrate a highly sensitive and bendable pressure sensor with the ability of distinguishment of pressure and bending and a PST which can be operated below 5V [24]. By introducing the PDMS spacer and surface treatment, the patterned AgNW (Silver nanowire) embedded PDMS electrode can be strongly bonded to the bottom plane (PMMA/Ag/PEN) and this results in high pressure sensitivity and high bending stability of the pressure sensor. Our bendable pressure sensor shows high pressure sensitivity of 9 kPa^{-1} and can detect the pressure and operate stably even in the bending state. Also our sensor can distinguish the pressure and bending by the aid of the additional bending sensor. By integrating the bendable pressure sensor and inkjet printed single-walled carbon nanotube TFT (SWCNT TFT), we fabricated the PST with low voltage device operation of $\leq$ 5V. The low voltage operation of the PST enables to demonstrate the wearable user-interactive pulse monitoring system by using commercial available electronic devices.

3.2 Experimental

PDMS with buckled patterns was used as a mold for the patterned electrode. The mold PDMS (Sylgard 184, Dow corning. Liquid PDMS and a curing agent were mixed in the ratio 10:1 by weight) was stretched uniaxially up to 40% and UV/O_3 treatment (power = 28 mW/cm^2) was conducted to form the patterned SiO_x thin film on the mold PDMS surface by using patterned mask. Then, AgNW solution (YURUI chemical, AgNW length 5~10μm) was spray-coated onto the mold PDMS. Spray-coated AgNW film was dried at 50℃ for 30min. After heat treatment, the mold PDMS was released to its initial state (zero strain) and the buckled patterns was introduced to the AgNW film and mold PDMS. Due to the mask during UV/O_3 treatment, SiO_x thin film was formed selectively and buckled structure was also selectively introduced onto the area of SiO_x. AgNW film followed well the buckled structure. We poured the mixture of liquid PDMS and curing agent (10:1 ratio of weight) on the AgNW film and then cured it at 100℃ for 60min. Due to the void between the AgNW networks, the liquid PDMS can penetrate into the AgNW film and the AgNW film can be embedded into the cured PDMS tightly. After curing, we peeled off the mold PDMS from the AgNW embedded PDMS and finally obtained the patterned AgNW embedded PDMS electrode (the patterns consist of the wavy structure (from buckled structure) and flat structure).

Bottom plane was fabricated using inkjet printing and spin coating process. The Ag metal-organic ink (Jet600C, Hisense Electronics, Kunshan, China) was printed on the PEN substrate (Q65H, Teijin DuPont Films) using a piezoelectric inkjet-printer (DMP-2831, Dimatix Corp.) and annealed at 100℃ for 1h. PMMA (M_w ~ 120000, Sigma-Aldrich) layer, the dielectric layer, was deposited on the Ag

electrode by using spin coating (PMMA solution containing 10 wt % of PMMA dissolved in propylene glycol methyl ether acetate (PGMEA)) and heated at 100℃ for 1h. For the APTES surface treatment, UV/O$_3$ treatment was conducted to the bottom plane and after UV/O$_3$ treatment, APTES solution (Sigma-Aldrich) was spin-coated at 3000rpm for 30 s. After baking the APTES coated bottom plane on hot plate at 80℃ for 0.5h, APTES-functionalized PMMA surface was obtained (A silylated layer was formed on the PMMA surface as shown in Figure 3.3(a)). To bond PDMS spacer and APTES-functionalized PMMA, both surfaces are activated using the oxygen plasma (CUTE-1MP, Femto Science) for 1 min and activated surfaces of PDMS spacer and APTES-functionalized PMMA were sandwiched together. Then, we heated sandwiched sample at 80℃ for 30min and irreversible strong chemical bonding was successfully introduced between the PDMS spacer and APTES-functionalized PMMA. To fabricate the bendable sensor, patterned electrode and PDMS spacer bonded bottom plane were activated through the oxygen plasma treatment (CUTE-1MP, Femto Science) and they were sandwiched together to introduce the strong chemical bonding between the PDMS spacer and flat area of patterned electrode. Finally we obtained the bendable pressure sensor.

Bottom plane for PST was fabricated using inkjet printing. UV/O$_3$ treatment was conducted to the PEN substrate and Poly-L-Lysine (PLL, Sigma-Aldrich) was drop-casted on the PEN for surface functionalization. And then, semiconducting SWCNT (IsoNanotubes-S^{TM} 95%, NanoIntegris) was inkjet-printed on the PLL-functionalized PEN substrate (PLL enhance the anchoring and deposition of the semi-SWCNT on the substrate). Source/drain Ag electrode was printed on the semi-SWCNT printed substrate and annealed 100℃ for 1h. BTO ink (PD-100; Paru

Corporation, Korea) was inkjet-printed on to the active region of semi-SWCNT to form insulating layer. BTO composite was sintered at 100℃ for 1h. Ag electrode, top gate electrode, was also inkjet-printed on the BTO composite insulating layer. This top gate was integrated with both semi-SWCNT transistors and bendable sensor. To integrate with bendable sensor, PMMA layer and APTES was deposited on the Ag electrode by using spin coating, respectively. And the same processes to bond PDMS spacer and patterned electrode were conducted to fabricate the pressure sensitive transistor.

The microstructure of the patterned electrode was characterized by using a field emission scanning electron microscope (FE-SEM, Hitachi S-48000), a 3-dimensional surface profiler (NanoFocus) and optical microscope (EGTECH). Pressure was applied to the sensors by using IMADA force gauge with a z-aixs stage and metal weights. The capacitance of the bendable sensor was measured at 1 kHz with a 0.1 V a.c. signal by using Agilent 4284A LCR meter and electrical characteristics of semi-SWCNT transistor and PST were measured by using Agilent 4145B analyzer in ambient air. Bending test of the sensor was performed using a home-made bending apparatus.
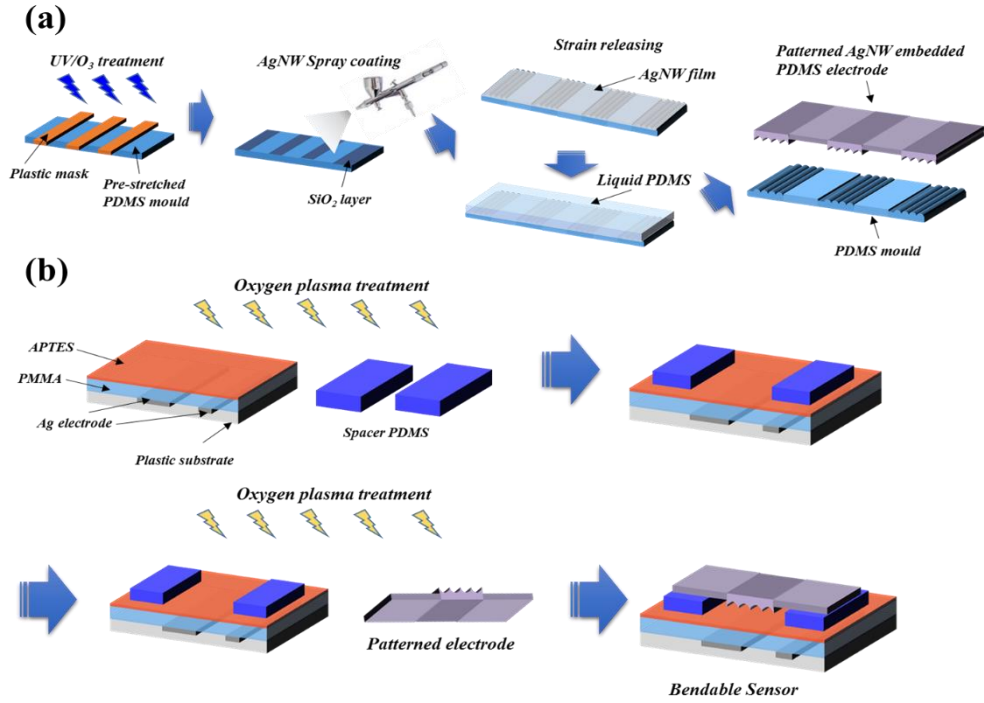
Figure 3.1 Fabrication process of our bendable sensor. (a) Schematic illustration of the fabrication of the patterned electrode. (b) Schematic illustration of the fabrication of the bendable sensor. First, we bonded the bottom plane and the spacer by using oxygen plasma treatment. Next, we bonded the patterned electrode and the spacer bonded bottom plane to fabricate the bendable sensor.

3.3 Results and Discussion

3.3.1 Bendable sensor

A schematic illustration of the bendable pressure sensor is shown in Figure 3.2(a) Our sensor consists of the patterned AgNW embedded PDMS electrode (patterned electrode), spacers and the bottom plane. By using the (3-Aminopropyl)triethoxysilane (APTES) surface treatment and spacer, the patterned electrode can be combined with bottom plane tightly. Due to the strong siloxane bonding (Si-O-Si) between the APTES treated bottom plane, PDMS spacers and patterned electrode [25,26], the combined sensor is bendable (see Figure 3.3(a) and 3.3(b)). The bonding is so strong that our sensor can lift the 50g metal weight as shown in Figure 3.3(c). Patterned electrode consists of the wavy and flat patterns as shown in Figure 3.4. The average wavelength and amplitude of the wavy pattern were about 22μm and 6μm, respectively. Wavy area of the AgNW embedded PDMS is introduced for the pressure sensing with high sensitivity [4]. Flat area of AgNW embedded PDMS is introduced for the bonding between the PDMS spacers and patterned electrode. Figure 3.2(c) shows SEM image of the bonding area and the spacer bonds patterned electrode and bottom plane tightly. Air gap was introduced between patterned electrode and bottom plane as shown in Figure 3.2(b) and 3.2(c).
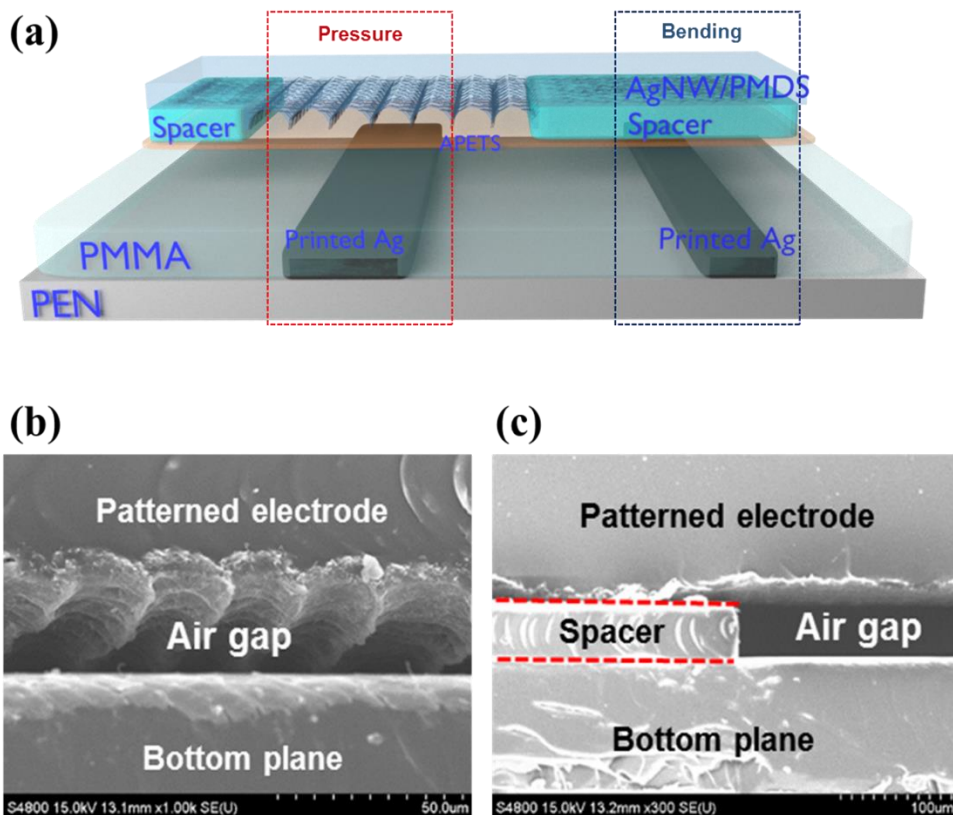
Figure 3.2 Device structure and microstructures. (a) Schematic illustration of the bendable pressure sensor with description of each layer. (b) SEM image of the pressure sensing area. Wavy patterned electrode, air gap, and bottom plane are shown. (c) SEM image of the bonding and bending sensing area. Flat patterned electrode, PDMS spacer, air gap, and bottom plane are shown.
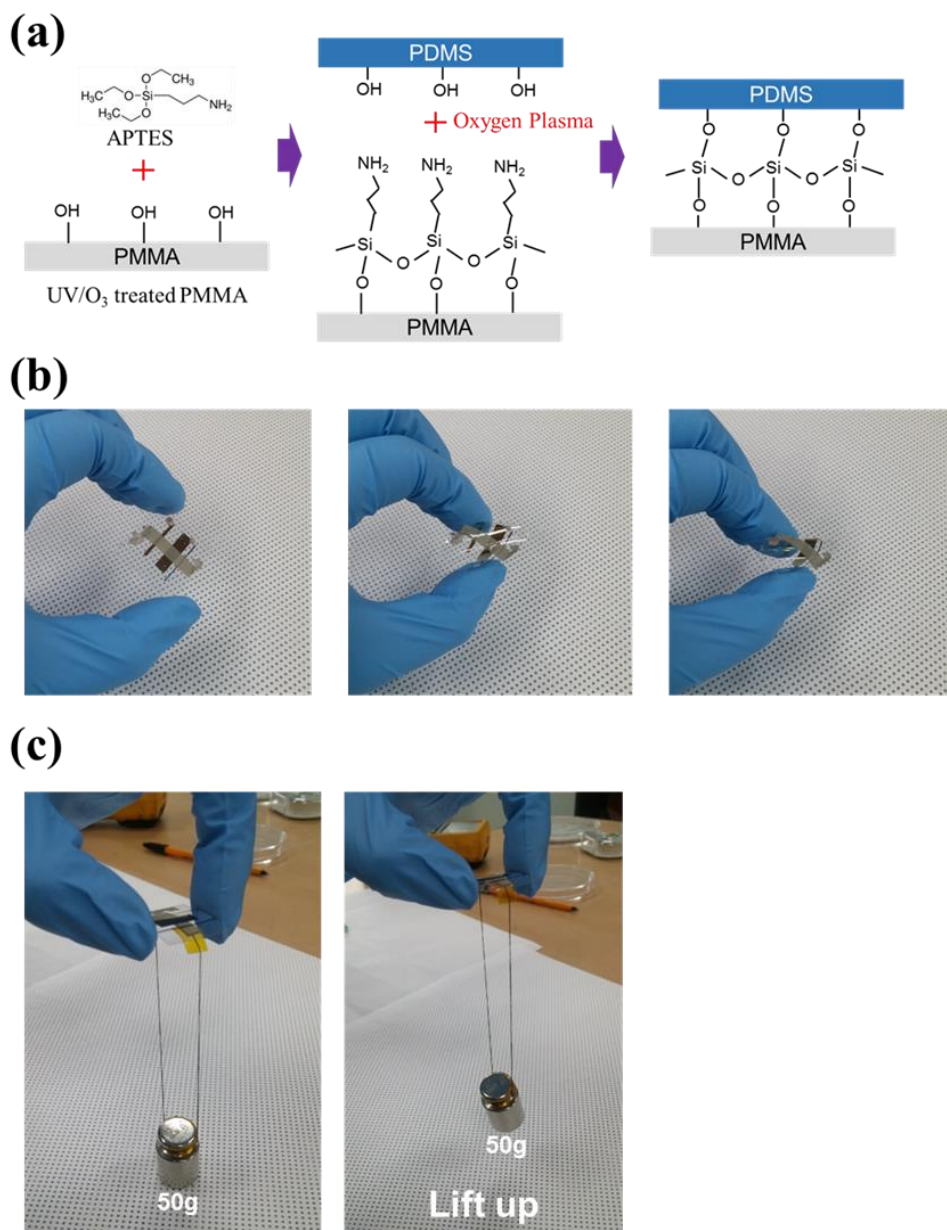
Figure 3.3 Siloxane bonding and bonding strength. (a) Schematic representation of the bonding process. Irreversible strong bonding was formed between the PMMA layer and PDMS spacer. (b) Bending of the bendable sensor with hand. (c) Lift up of metal weight of 50g.
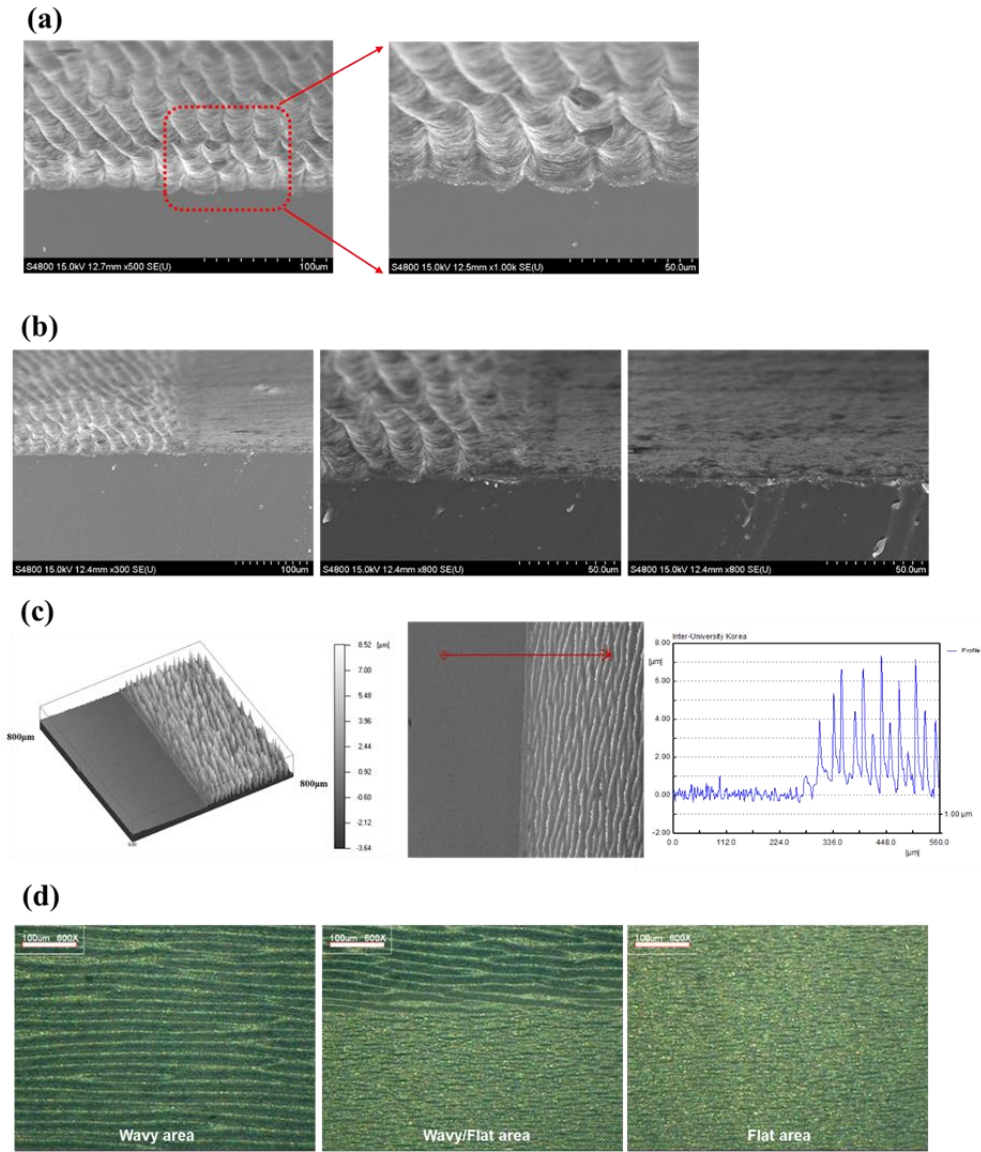
Figure 3.4 Microstructures of the patterned electrode. (a) SEM image of the wavy patterned area. (b) SEM images of the patterned electrode with wavy structure and flat structure. SEM mages in left and middle show the boudary area of wavy and flat structure. SEM image in right shows the flat patterned area. (c) 3-D surface profiler image of the patterned electrode at the boundary area. (d) Optical microscopic images of the patterned electrode. Wavy area (left), boundary area (middle), and Flat area (right).

Bendable pressure sensor consists of two parts with different function. First part is the pressure sensing part which consists of wavy patterned electrode/air gap/bottom plane (Figure 3.2(a)). This part can detect the pressure from the capacitance change. Pressure was applied to the sensing part to measure the pressure sensitivity. Relative capacitance change of the sensor ($\Delta C/C_0$, $\Delta C = C - C_0$) according to the pressure change is shown in Figure 3.5(a). We measured the capacitance change of the sensor by changing the spacer thickness. As the thickness of the spacer increased, the pressure sensitivity of the sensor increased (Pressure sensitivity $S = \delta(\Delta C/C_0)/\delta p, \Delta C = C - C_0$, where C and C_0 denote the capacitance with the applied pressure and the base capacitance, respectively, and p denotes the applied pressure). The sensor with 50μm spacer shows the highest sensitivity, $S = 9 \text{ kPa}^{-1}(0\sim0.6\text{kPa})$ and $S = 0.6 \text{ kPa}^{-1}(0.6\sim6.6\text{kPa})$. This sensor can detect very small pressure of only 0.7 Pa as shown in Figure 2b. Repeated loading/unloading of very small pressure of 0.7 Pa can be detected by using our sensor. Due to the air gap between the patterned electrode and bottom plane, the pressure sensitivity of the sensor with spacer is enhanced at low pressure region (P=0~0.6kPa) when it is compared to the sensor without spacer ($S = 3.8 \text{ kPa}^{-1}(0\sim0.5\text{kPa})$) [4]. Base capacitance of the sensor with spacer is smaller due to the air gap and this results in the higher pressure sensitivity. Also, the air gap enables the distance between the patterned electrode and dielectric layer to be decreased easily even under low pressures and this increased the pressure sensitivity [6]. At high pressure region (P=0.6~6kPa), the wavy structure of the patterned electrode touched the dielectric layer and the pressure sensitivity was decreased. In this pressure region, wavy structure of the patterned electrode was deformed by the applied pressure and based on this deformation, the contact area and air gap between

76

the wavy structure and dielectric layer were changed [4]. According to these changes, the capacitance of the sensor changed to the applied pressure. Pressure sensing part is not only sensitive to the pressure but also sensitive to the bending. As the bending radius decreased, the capacitance of the sensor increased as shown in Figure 3.6(a).
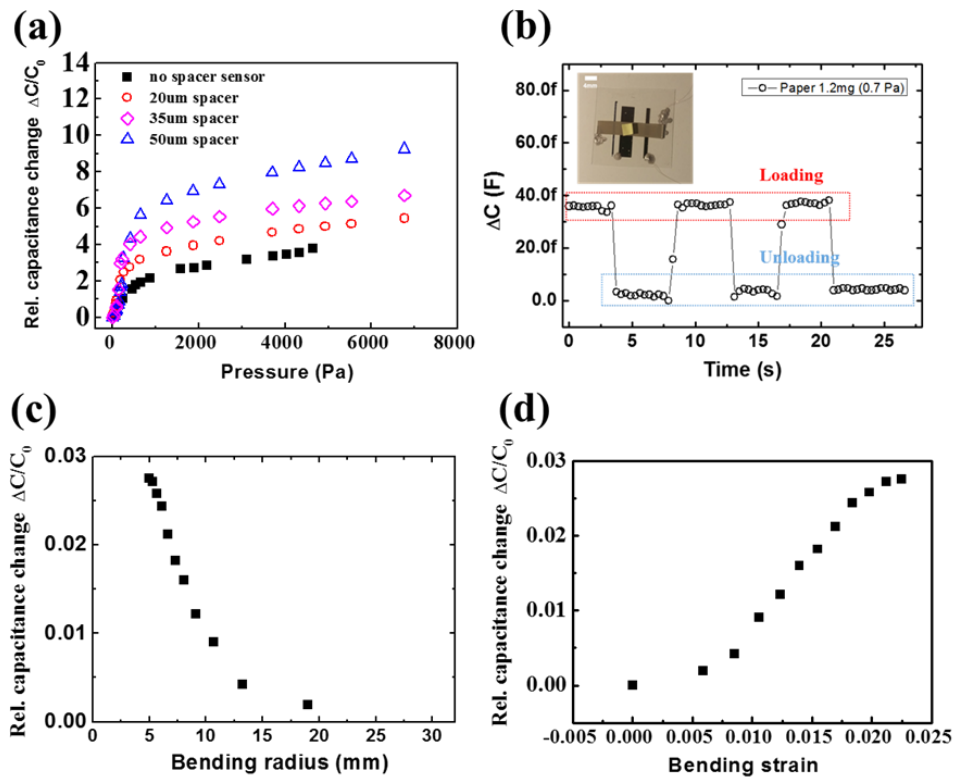
Figure 3.5 Sensing performance of our bendable sensor. (a) Relative capacitance change-pressure curve of pressure sensing part with different spacer thickness. (b) Capacitance change-time curve for the detection of very small pressure (0.7 Pa) according to the repeated loading/unloading of a paper (1.2 mg) (spacer thickness = 50μm). (c) Relative capacitance change-bending radius curve of bending sensing part (spacer thickness = 50μm). (d) Relative capacitance change-bending strain curve of bending sensing part (spacer thickness = 50μm).

However, we cannot distinguish which one among pressure or bending caused the capacitance change of the sensor, because of the property of the pressure sensor that the pressure sensor is sensitive to both pressure and bending. For this reason, we introduced the second part, the bending sensing part to classify the pressure and bending as shown in Figure 3.2(a). The bending sensing part is sensitive to the bending as shown in Figure 3.5(c) and 3.5(d) (The bending sensing part is relatively less sensitive to the pressure than bending as shown in Figure 3.6(b) and based on this property, we introduced the bending sensing part). By the aid of the bending sensor, the sensor can notice that it is in the bending state or not and classify the pressure and bending from the capacitance change.

Our sensor operates stably in the bending state and can detect the pressure even in the bending state as shown in Figure 3.7(a) and 3.7(b). We attached our sensor onto the home-made bending machine and bent our sensor with bending radius of 8.5 and 5 mm, respectively. After bending our sensor, we applied pressure to the sensor and the capacitance of the sensor was changed as shown in Figure 3.7(a). The capacitance change of the sensor was linearly increased to the change of the pressure in both bending states with bending radius of 8.5 and 5mm. However, the capacitance change value at the same pressure is larger in the smaller bending radius as shown in Figure 3.7(a) inset. As shown in Figure 3.6(a), the base capacitance of the pressure sensing part increased as the bending radius decreased and this increased capacitance caused by bending became the base capacitance value of the sensor in the bending state. We plotted the capacitance-pressure curve and compared the capacitance change of the sensor according to the change of the pressure in the bending state and in the flat state as shown in Figure 3.6(c). The capacitance change

behavior of the bent sensor to the applied pressure is almost same with that behavior of the flat sensor.
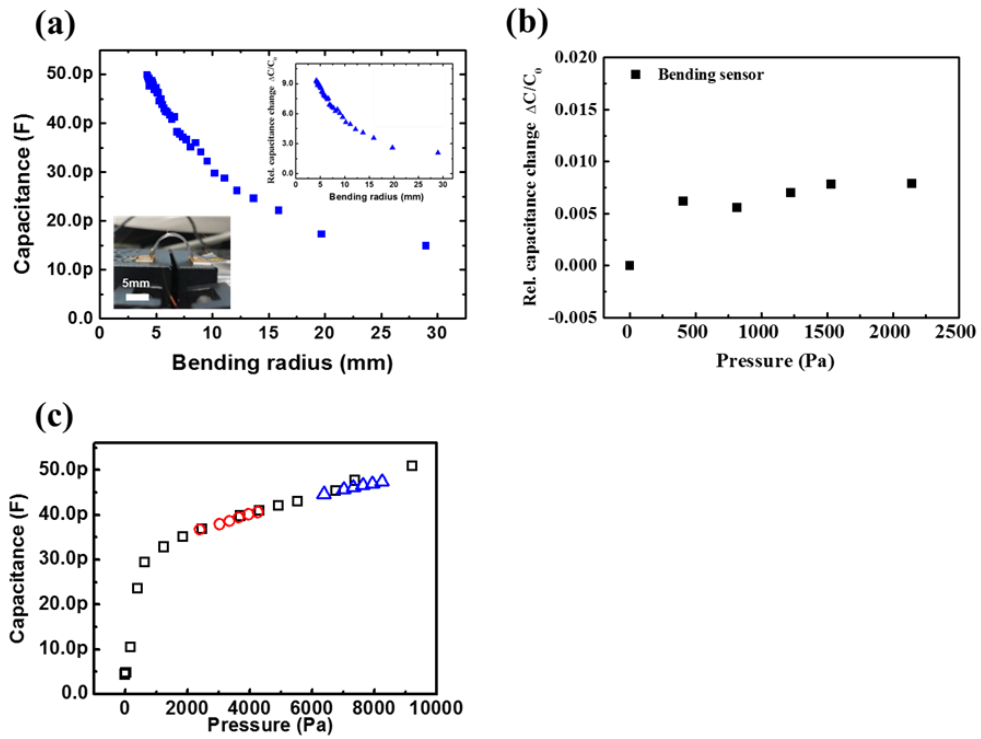
Figure 3.6 (a) Capacitance-bending radius curve of the pressure sensing part. Inset shows the relative capacitance change-bending radius curve of the pressure sensing part. (b) Relative capacitance change-pressure curve of the bending sensing part. Relative capacitance change value is below 0.75% up to 2.3 kPa. (c) Capacitance-pressure curves of the sensing part in the flat state (black squar), the sensing part in the bending state of bending radius of 8.5 mm (red circle), and the sensing part in the bending state of bending radius of 5 mm (blue triangle), respectively.
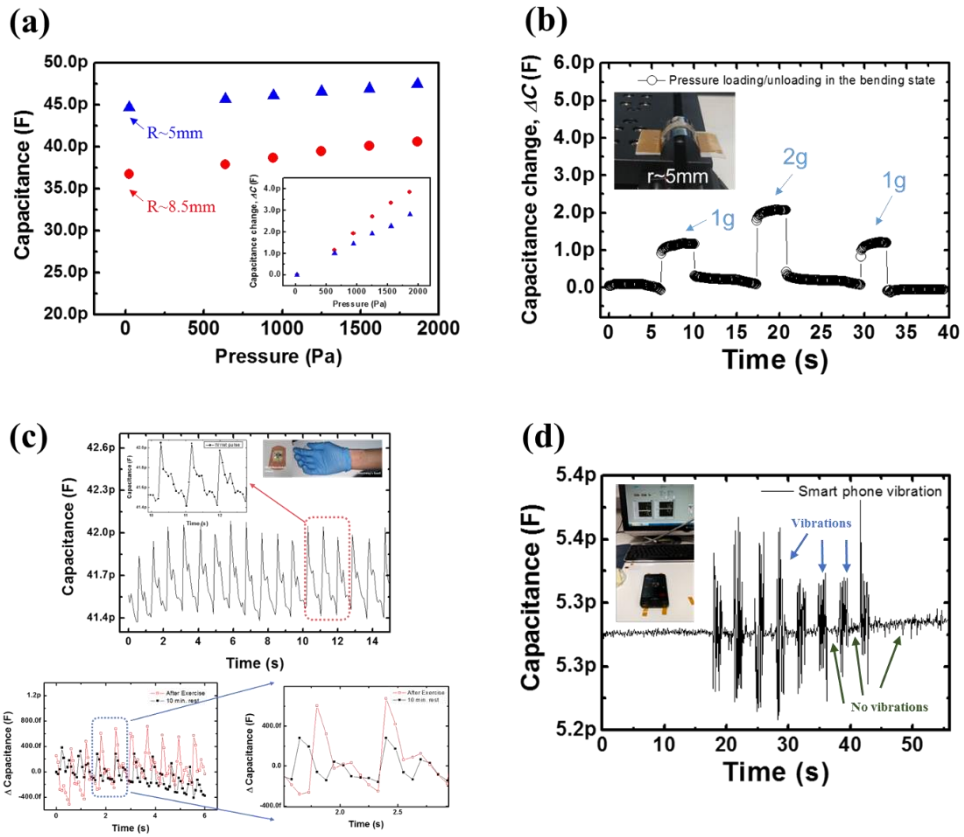
Figure 3.7 Pressure sensing in various conditions. (a) Capacitance-pressure curve of pressure sensing part in the bending state. Inset is a capacitance change-pressure curve in the bending state. (b) Capacitance change-time curve for the detection of loading/unloading of pressure in the bending state (bending radius ~5mm). (c) Wrist pulse measurements by using our bendable sensor. Upper capacitance-time curve: wrist pulse measurement in normal condition of health man. Lower capacitance change-time curves: wrist pulse measurement in exercise and rest condition of health man. (d) Vibration measurement by using our bendable sensor. Capacitance-time curve: measurement of vibration caused from the smart phone.

The capacitance value of the sensor can be increased from the bending or applied pressure and if we applied additional pressure to the sensor with the same increased capacitance value, the capacitance change behavior to the applied pressure is almost same regardless of the source of the initially increased capacitance value as shown in Figure 3.6(c). This means that the pressure sensing performance of our sensor is maintained even in the bending state. Also, we loaded different weights onto the sensor in the bending state with bending radius of 5mm as shown in Figure 3.7(b). Our sensor can distinguish the difference of the pressure even in the bending state with small bending radius. The response and relaxation of the sensor were also fast and the capacitance change of the sensor was almost same for the same pressure even in the bending state as shown in Figure 3.7(b). We monitored the wrist pulse by using our sensor. Our sensor was fixed onto the commercial plaster by using $3M^{TM}$ VHB^{TM} tape and then we wrapped wrist area with this plaster. As shown in Figure 3c, our sensor can detect wrist pulse with three distinguishable peaks [2,9] and his heart rate was about 75 bpm from the measured data. We also monitored the wrist pulse after exercise and rest. After exercise (sixty push-ups) and 10 minutes rest, we monitored the wrist pulse, respectively, as shown in Figure 3.7(c). From the capacitance change time curve (Figure 3.7(c)), we can notice two differences. First, wrist pulse rate (or heart rate) is faster in exercise condition than in rest condition. Wrist pulse rates (or heat rate) were 101 and 90 bpm for exercise and rest condition, respectively. Second, capacitance change is larger in exercise condition than in rest condition and it means that the blood pressure is higher in exercise condition than in rest condition. We also measured the vibration of the smart phone by using our sensor. We placed our sensor onto the smart phone and then called to the smart phone to vibrate the smart phone. As shown in Figure 3.7(d), our sensor can detect the vibration of the smart phone.
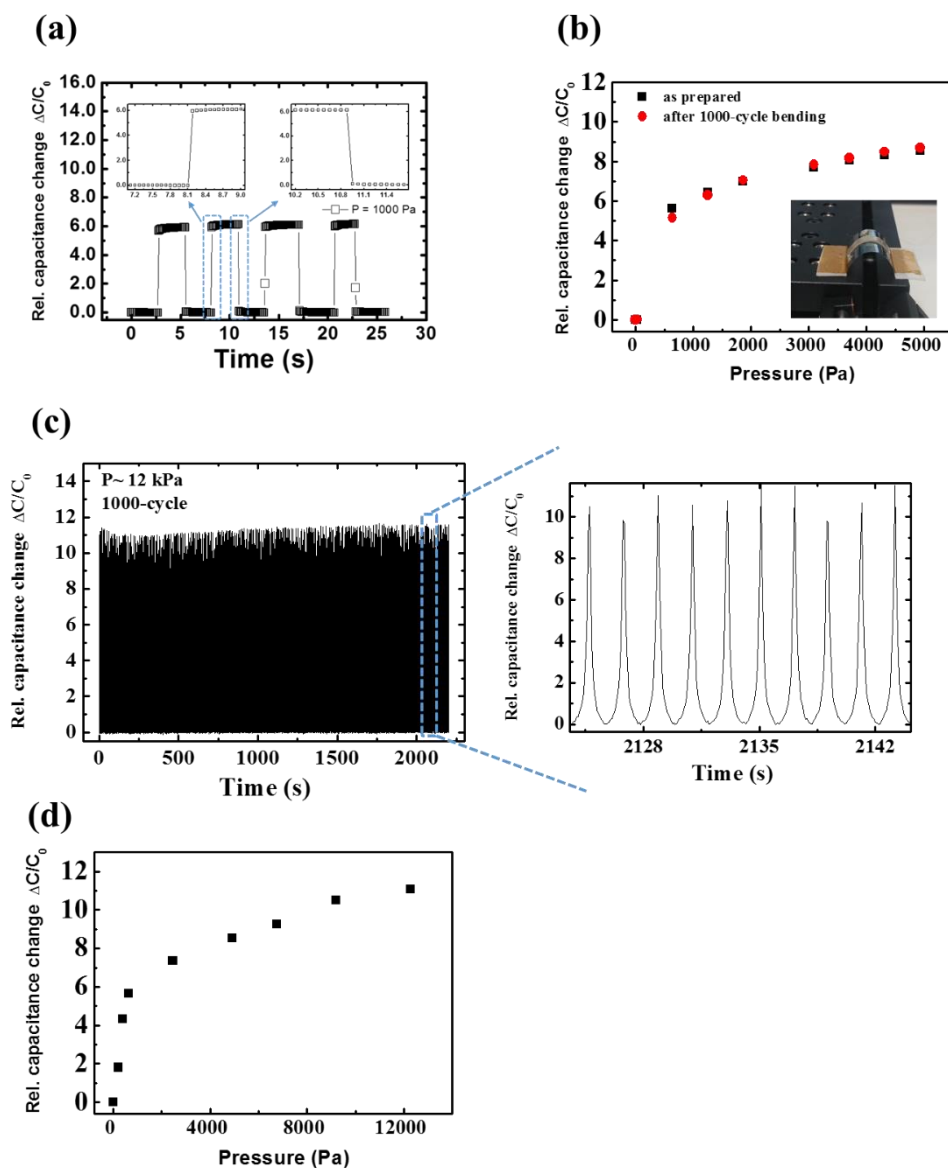
Figure 3.8 (a) Response and relaxation property of our bendable sensor to the pressure of 1000 Pa. Response and relaxation time of our sensor is below 75 ms. (b) Relative capacitance change-pressure curves of our bendable sensor for as-prepared and 1000-cycle bending with 5mm bending radius, respectively. Our sensor shows high bending stability. (c) Relative capacitance change-time curve of our bendable sensor for the 1000-cycle loading/unloading of the pressure of 12 kPa. Our sensor shows high repeated cycle stability. (d) Relative capacitance change-pressure curves of our bendable sensor up to 12 kPa.

The response and relaxation times of our sensor were measured as shown in Figure 3.8(a). We applied the pressure of 1000 pa repeatedly and both the response and relaxation time were less than 75ms. Bending cycle stability of the sensor was also measured by using home-made bending machine. Before the bending and after 1000-cycle bending with a 5mm radius of curvature, we measured the capacitance change of the sensor by applying pressure as shown in the relative capacitance change–pressure curves of Figure 3.8(b). Relative capacitance change values at each pressure show no appreciable difference before bending and after bending. Repeated loading/unloading of the pressure was also performed to investigate the cycle stability of our sensor. We loaded and unloaded a pressure of 12 kPa repeatedly up to 1000 times and measured the capacitance changes of the sensor as shown in Figure 3.8(c). Our sensor operates robustly to the repeated pressure cycle up to 12 kPa and this indicates that our bendable sensor has high stability to the repeated loading/unloading of the pressure. Our sensor is robust to the repeated pressure loading/unloading and bending cycle based on these results.

Our sensor can be easily scaled up for large-area sensor array. We fabricated 3×3 pixel type sensor array with sensing area of 4 mm $\times$ 4mm as shown in Figure 3.9. Metal weight of 2g (6mm diameter) was loaded on the sensor array to investigate the sensing ability of the sensor array and the corresponding two-dimensional mapping with color contrast was illustrated in Figure 3.9(a). Dramatic increment of capacitance occurred only in the weight loaded site and very small increment of capacitance occurred in other sites. We loaded the same weight to the same site of the sensor array which is in the bending state (bending radius ~25mm) as shown in Figure 3.9(b). Based on the measured data from the pressure sensor and bending sensor, we calculated the pressure of the weight. Figure 3.9(b) shows the calculated

pressure and its corresponding two-dimensional mapping. Highest pressure value was only obtained from the loaded site and calculated pressures from other site were small. The calculated pressure in the bending state was about 820 Pa and the pressure in the flat state was about 700 Pa. This discrepancy may come from the reduction of the pressing area of the weight according to the bending. These results demonstrate that our sensor array can detect the spatial distribution of the pressure not only in the flat state but also in the bending state.
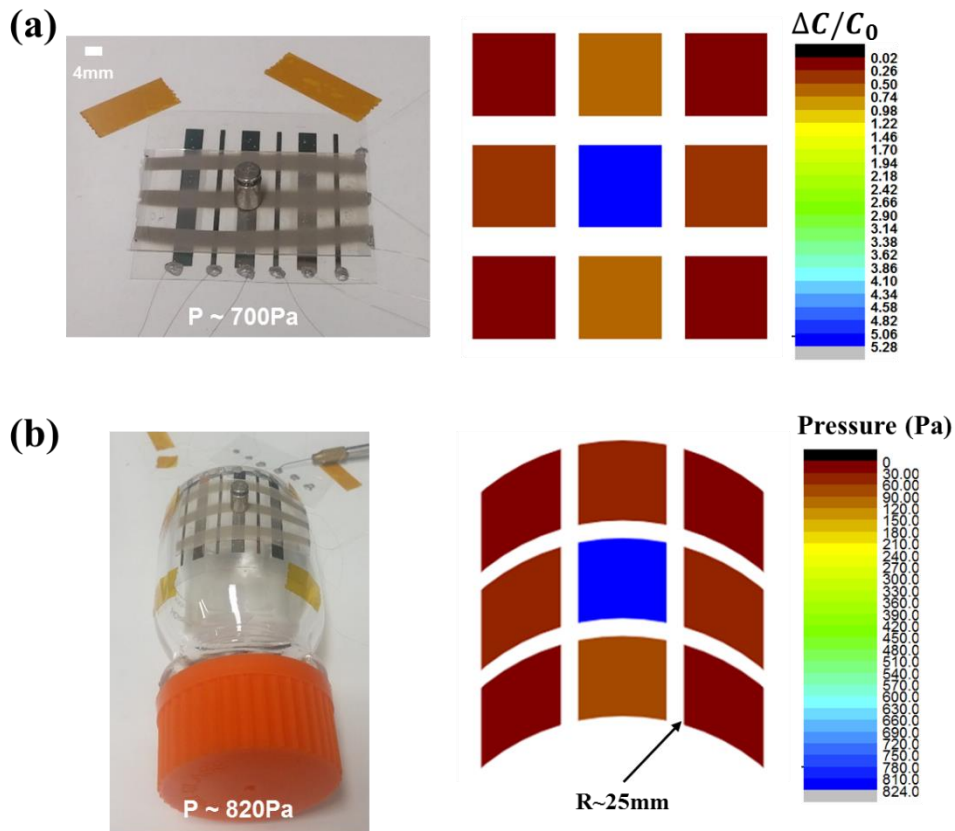
Figure 3.9 Bendable sensor array and pressure sensing. (a) Photograph of the sensor array with 3 × 3 pressure sensing pixels and 3 × 3 bending sensing pixels and pressure loading (left). Corresponding two-dimensional mapping with color contrast (right). (b) Photograph of the sensor array in the bending state (bending radius ~25mm) and pressure loading (left). Corresponding two-dimensional mapping with color contrast (right).

3.3.2 Pressure sensitive transistor

We fabricated the pressure sensitive transistor (PST) using the bendable pressure sensor. To demonstrate the low voltage operation (also low power consumption) and wearable sensing device, we used the floating gate transistor connected with the capacitive bendable pressure sensor as shown in Figure 3.10(a). For low voltage operation of the floating gate transistor ($V_{GS}, V_{DS} < 5V$), we used semiconducting single-walled carbon nanotube (s-SWCNT) and high-k oxide dielectric material, $BaTiO_3$. All the components of the floating gate transistor were fabricated using inkjet printing method on the PEN substrate. After obtaining the floating gate transistor, bendable sensor was fabricated onto the transistor. Top gate of the floating gate transistor which functioned as a floating gate was connected with bendable sensor as an electrode of the capacitor. Operation mechanism of the PST is based on the modulation of the voltage of the floating gate and its corresponding field effect to the transistor [24]. If we are considering Gauss equation, the total charge of the floating gate can be written as

$$Q_0 = C_D(V_{FG} - V_D) + C_S(V_{FG} - V_S) + C_{sensor}(V_{FG} - V_{sensor}) \qquad (1)$$

where C_D and C_S are the parasitic capacitances of drain and source electrodes, respectively, and C_{sensor} is the capacitance of the bendable pressure sensor. Drain and source electrodes were biased by V_D and V_S, respectively, and the top electrode of the bendable pressure sensor was biased by V_{sensor}. If the floating gate is totally floated, the total charge of the floating gate, Q_0, is constant. And therefore, V_{FG} changes to maintain Q_0 constant if the pressure is applied to the bendable sensor. The floating gate voltage can be extracted from equation (1) as

$$V_{FG} = \frac{C_D}{C_{sum}}V_D + \frac{C_S}{C_{sum}}V_S + \frac{C_{sensor}}{C_{sum}}V_{sensor} + \frac{Q_0}{C_{sum}} \quad , \quad (C_{sum} = C_D + C_S + C_{sensor})$$

(2)

From the equation (2), we can notice that V_{FG} can be modulated by changing the capacitance of the bendable sensor, C_{sensor}. And this change of V_{FG} affect the current of the floating gate transistor. Drain current of the floating gate transistor in the linear region can be written as

$$I_{DS} = \frac{W}{L}\mu C_{OX}(V_{FGS} - V_{TH} - \frac{V_{DS}}{2})V_{DS}, \quad (V_{FGS} = V_{FG} - V_S) \qquad (3)$$

where W and L are the channel width and length respectively, μ is the mobility of the s-SWCNT (average field effect mobility ~ 3.5 cm^2 V^{-1} s^{-1}), C_{OX} is the capacitance per unit area of the dielectric layer (20 nF cm^{-2}), and V_{TH} is threshold voltage. From the equation (2) and (3), we can conclude that drain current of the floating gate transistor can be modulated by changing the capacitance of the bendable sensor, C_{sensor}.
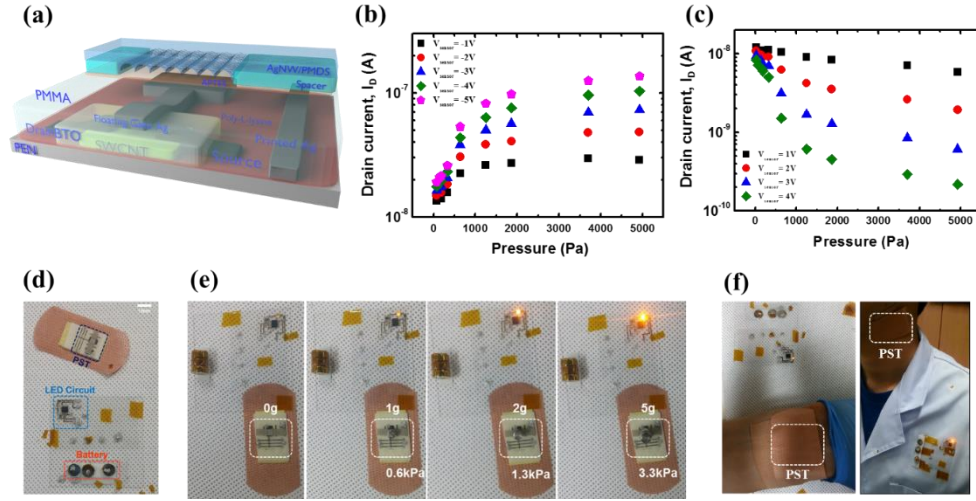
Figure 3.10 Pressure sensitive transistor and its application to wearable user inter-active pressure sensing device. (a) Schematic illustration of the pressure sensitive transistor (PST) with description of each layer. (b) Drain current-pressure curve of the PST for the negative bias of the sensor, Vsensor < 0. (c) Drain current-pressure curve of the PST for the positive bias of the sensor, Vsensor > 0. (d) Photographs of wearable user inter-active pressure sensing device. It consists of the PST, LED circuit, and batteries. (e) Light emitting of LED according to the pressure. (f) Wearable user inter-active pulse monitoring system. Wrist pulse measuring (left) and neck pulse measuring (right).
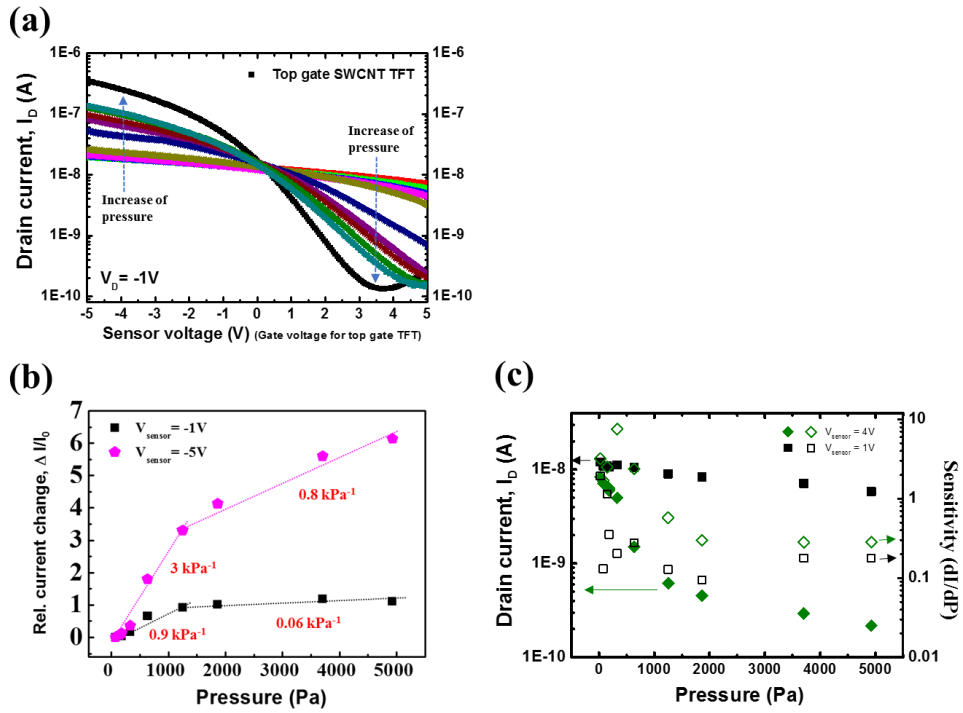
Figure 3.11 Transfer curves of the PST and pressure sensitivity of the PST. (a) Transfer curves of the PST by increasing the applied pressure. Black curve is for the top gate SWCNT TFT and color curves are for the PST at different pressure. (b) Relative current change-pressure curves of the PST at Vsensor of -1V and -5V, respectively. Pressure sensitivity at each Vsensor were calculated. (c) Drain current-pressure curves of the PST at Vsensor of 1V and 4V, respectively. Pressure sensitivity at each Vsensor were also calcualted. Pressure sensitivity was calculated by using different equation compared to the (b) due to the different behavior of current according to the pressure. Pressure sensitivity S is defined as the slope of the current versus pressure ($S=dR/dP$).

We measured and plotted transfer curves of the PST by applying pressure as shown in Figure 3.11(a) and we demonstrated that the PST can operate at low voltages below 5V as shown in Figure 3.10(b) and 3.10(c). Shape of the transfer curve was changed by changing the applied pressure. As shown in Figure 3.10(b) and 3.11(a), when the top electrode of the bendable pressure sensor was negatively biased, drain current was increased by increasing the applied pressure and as shown in Figure 3.10(c) and 3.11(a), when the top electrode of the bendable pressure sensor was positively biased, drain current was decreased by increasing the applied pressure. This means that the transfer curve of the PST follows the transfer curve of the top gate s-SWCNT TFT as increasing the applied pressure as shown in Figure 3.11(a). Figure 3.10(b) and 3.10(c) show the drain current-pressure curves at negatively biased V_{sensor} and positively biased V_{sensor}, respectively. PST can operate below 5V and even in the low voltage of 1V. When PST operates at a voltage of 1V ($V_{sensor} = 1V$), ultra-low power consumption of < 15 nW can be achieved ($I_{DS} <$ 15nA, $V_{DS} = -1V$) as shown in Figure 3.10(c). The higher the absolute value of V_{sensor} is, the higher the pressure sensitivity is as shown in Figure 3.10(b) and 3.10(c). The pressure sensitivity of the PST at certain voltages is shown in Figure 3.11(b) and 3.11(c). Based on these results, we can notice that the pressure sensitivity of the PST can be tunable simply by controlling the voltage of the bendable pressure sensor, V_{sensor} and the direction of the change of the drain current can be controlled by biasing V_{sensor} negatively or positively. Further studies about the operation of the PST are now under investigation. Because the output of the PST to external pressure is not capacitance but current, the PST enables easy integration with various electronic devices such as LED chip, OLED, resistor, battery and so on. Also, due to the tunable sensitivity and controllability of the direction of the current change, the

PST can be applied to the wearable sensors or electronic skins which need customized sensitivity and function depending on the type of application.

We fabricated pressure sensing devices by integrating the PST with certain electronic devices such as LED chip, resistor, OP amp and battery to demonstrate low voltage operation of the PST and wearable sensing device. We integrated the PST with LED chip, resistor, OP amp and battery to demonstrate the user inter-active pressure sensing device. We used commercially available resistors, OP amp, LED chip and batteries and the circuit was fabricated onto the PEN substrate. Schematic images of the circuit of the pressure sensing device are shown in Figure 3.12(a) and 3.12(b). The PST operated below 3V and the total device operated below 4.5V. We designed the circuit to emit brighter light as the applied pressure increases. We tested the sensing performance of the pressure sensing device to the pressure by applying the pressure from 0 to 3.3 kPa. As shown in Figure 3.10(e), the emitted light from LED chip became brighter as the applied pressure increased. We measured the voltage of the node at each pressure and Figure 3.12(c) shows the relationship between the luminance and the pressure and the current and the pressure, respectively. Also we demonstrated the wearable user inter-active health monitoring system by combining the light emitting and pulse measuring. We designed the circuit like Figure 3.12(b) and in this condition the brightness of the LED chip was decreased as the applied pressure increased. Wrist and neck pulse were measured as shown in Figure 3.10(f), respectively. We can see the change of the brightness of the LED chip according to the change of the pressure induced from the pulse.
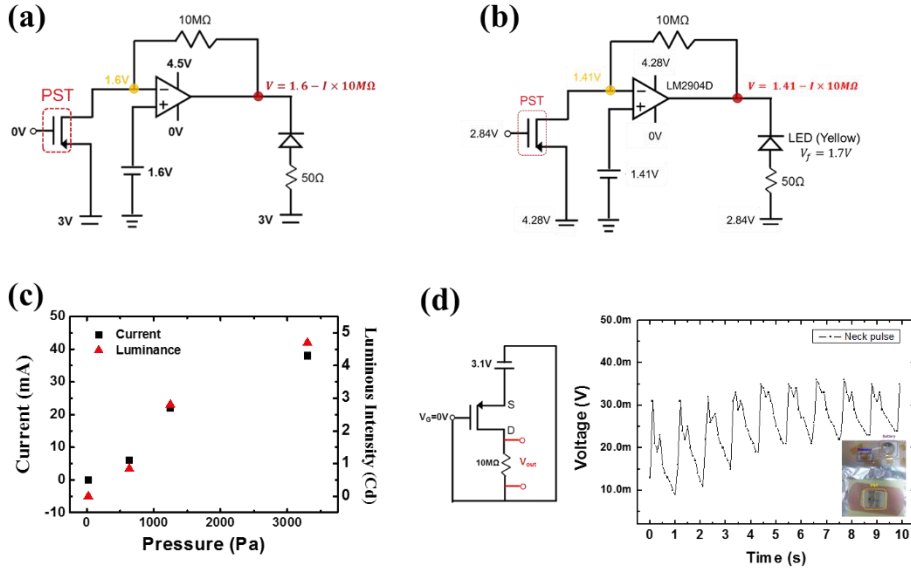
Figure 3.12 (a) Schematic image of the circuit to emit brighter light as the applied pressure increases. (b) Schematic image of the circuit to emit brighter light as the applied pressure decreases. This design was used for the wearable user inter-active pulse monitoring system. (c) The current and luminous intensity of LED chip as a function of the applied pressure. (d) Schematic image of the circuit to measure the neck pulse by using battery, resistor, and PST (left). Voltage-time curve for the neck pulse measurment by using the device from this circuit design.

Type	Manufacturer part number
Op-Amp	LM2904
Resistor (10 MΩ)	R3216G1005F1-4W50V
Resistor (50 Ω)	R3216G51R0F1-4W50V
LED	XZM2CYK78W

Table 3.1 Chip Information.

3.4 Conclusion

In summary, we have demonstrated a highly sensitive and bendable sensor capable of pressure sensing in flat and bending state and distinguishment of pressure and bending and PST with ultra-low power consumption below 15 nW for the first time. Based on the APTES surface functionalization and spacer, the bendable sensor can be operated stably and detect the pressure exactly in the bending state. Also, by introducing the bending sensing part beside the pressure sensing part, the bendable sensor can detect both pressure and bending and distinguish the pressure and bending. We integrated the bendable sensor with the inkjet-printed SWCNT TFT for the fabrication of the pressure sensitive transistor (PST). PST can be operated in low voltage below 5V and ultra-low power consumption of PST below 15 nW can be achieved (I_{DS}< 15nA, V_{DS}= −1V). By using the PST and commercially available electronic devices such as LED chip, resistor, OP amp and battery, we fabricated the user inter-active pressure sensing device and pulse monitoring device. Our bendable sensor and PST may open and broaden their application to the wearable health monitoring/sensing system or electronic skins with low power consumption.

Reference

[1] S. C. B. Mannsfeld, B. C.-K. Tee, R. M. Stoltenberg, C. V. H.-H. Chen, S. Barman, B. V. O. Muir, A. N. Sokolov, C. Reese, and Z. Bao, *Nat. Mater.*, 9, 859 (2010)

[2] G. Schwartz, B. C.-K. Tee, J. Mei, A. L. Appleton, D. H. Kim, H. Wang, and Z. Bao, *Nat. Commun.*, 4, 1859 (2013)

[3] Y. Zang, F. Zhang, D. Huang, X. Gao, C.-A. Di, and D. Zhu, *Nat. Commun.*, 6, 6269 (2015)

[4] Y. Joo, J. Byun, N. Seong, J. Ha, H. Kim, S. Kim, T. Kim, H. Im, D. Kim, and Y. Hong, *Nanoscale*, 7, 6208 (2015)

[5] L. Viry, A. Levi, M. Totaro, A. Mondini, V. Mattoli, B. Mazzolai, and L. Beccai, *Adv. Mater.*, 26, 2659 (2014)

[6] S. Park, H. Kim, M. Vosgueritchian, S. Cheon, H. Kim, J.H. Koo, T.R.Kim, S. Lee, G. Schwartz, H. Chang, and Z. Bao, *Adv. Mater.*, 26, 7324 (2014)

[7] C. Pang, G.-Y. Lee, T.-I. Kim, S. M. Kim, H. N. Kim, S.-H. Ahn, and K-Y. Suh, *Nat. Mater.*, 11, 795 (2012)

[8] H.-B. Yao, J. Ge, C.-F. Wang, X. Wang, W. Hu, Z.-J. Zheng, Y. Ni, and S.-H. Yu, *Adv. Mater.*, 25, 6692 (2013)

[9] X. Wang, Y. Gu, Z. Xiong, Z. Cui, and T. Zhang, *Adv. Mater.*, 26, 1336 (2014)

[10] L. Pan, A. Chortos, G. Yu, Y. Wang, S. Isaacson, R. Allen, Y. Shi, R. Dauskardt, and Z. Bao, *Nat. Commun.*, 5, 3002 (2014)

[11] B. Zhu, Z. Niu, H. Wang, W.R. Leow, H. Wang, Y. Li, L. Zheng, J. Wei, F. Huo, and X. Chen, *Small*, 10, 3625 (2014)

[12] C.-L. Choong, M.-B. Shim, B.-S. Lee, S. Jeon, D.-S. Ko, T.-H. Kang, J. Bae, S.H. Lee, K.-E. Byun, J. Im, Y.J. Jeong, C.E. Park, J.-J. Park, and U.-I. Chung, *Adv. Mater.*, 26, 3451 (2014)

[13] S. Gong, W. Schwalb, Y. Wang, Y. Chen, Y. Tang, J. Si, B. Shirinzadeh, and W. Cheng, *Nat. Commun.*, 5, 3132 (2014)

[14] C. Dagdeviren, Y. Su, P. Joe, R. Yona, Y. Liu, Y.-S. Kim, Y. Huang, A. R. Damadoran, J. Xia, L. W. Martin, Y. Huang, and J. A. Rogers, *Nat. Commun.*, 5, 4496 (2014)

[15] C. Pan, L. Dong, G. Zhu, S. Niu, R. Yu, Q. Yang, Y. Liu, and Z.L. Wang, *Nat. Photonics*, 7, 752 (2013)

[16] F.-R. Fan, L. Lin, G. Zhu, W. Wu, R. Zhang, and Z. L. Wang, *Nano Lett.*, 12, 3109 (2012)

[17] L. Lin, Y. Xie, S. Wang, W. Wu, S. Niu, X. Wen, and Z. L. Wang, *ACS Nano*, 7, 8266 (2013)

[18] K. Takei, T. Takahashi, J. C. Ho, H. Ko, A. G. Gillies, P. W. Leu, R. S. Fearing, and A. Javey, *Nat. Mater.*, 9, 821 (2010)

[19] C. Wang, D. Hwang, Z. Yu, K. Takei, J. Park, T. Chen, B. Ma, and A. Javey, *Nat. Mater.*, 12, 899 (2013)

[20] M.L. Hammock, A. Chortos, B.C.-K. Tee, J.B.-H. Tok, and Z. Bao, *Adv. Mater.*, 25, 5997 (2013)

[21] J. Park, Y. Lee, J. Hong, M. Ha, Y.-D. Jung, H. Lim, S.Y. Kim, and H. Ko, *ACS Nano*, 8, 4689 (2014)

[22] J. Kim, T. N. Ng, and W. S. Kim, *Appl. Phys. Lett.*, 101, 103308 (2012)

[23] C. Yeom, K. Chen, D. Kiriya, Z. Yu, G. Cho, and A. Javey, *Adv. Mater.*, 27, 1561 (2015)

[24] S. Lai, P. Cosseddu, A. Bonfiglio, and M. Barbaro, *IEEE Electron Device Lett.*, 34, 801 (2013)

[25] M.-E. Vlachopoulou, A. Tserepi, P. Pavli, P. Argitis, M. Sanopoulou, and K.

Misiakos, *J. Micromech. Microeng*., 19, 015007 (2009)

[26] V. Sunkara and Y.-K. Cho, *ACS Appl. Mater. Interfaces*, 4, 6537 (2012)

Chapter 4

Stretchable multifunctional sensor

4.1. Introduction

Stretchable electronics have gained huge interest, because of their versatile applications such as stretchable displays, comfortable and wearable sensing systems, epidermal electronics, electronic skins, and wearable electronics [1-13]. Among the various stretchable devices and systems, stretchable sensors which mimic the sensing ability of the human skin have been widely investigated for the realization of electronic skins, robotic skins and prosthetic skins [1,4,7-13]. To mimic the human skin, the human tactile receptors, stretchable sensor must detect the force applied to the various direction and strain. In other words, stretchable sensor must detect not only the normal force, but also the shear force and this means the 3-axis force sensing. Up to date, however, most of the stretchable sensors can detect only normal contact force, the pressure, and strain [7-13]. Most of the 3-axis force sensors have been fabricated using the silicon microelectromechanical systems (MEMS) technology [14,15] or flexible polymer MEMS technology [16]. Based on these fabrication method and materials, previously reported 3-axis force sensors are not stretchable [14-16]. Recently, polydimethylsiloxane (PDMS) based 3-axis force sensors have been developed. However, most of the sensors with PDMS are not stretchable due to the stiff metal electrode [17-21] and only a few papers reported stretchability by using liquid metal electrode [22].

In this chapter, we demonstrate the stretchable multifunctional sensor which can detect the 3-axis force, the normal force and shear force, and strain by using nanowire composite. By introducing various sensing component to the sensing system, we can obtain multifunctional sensor to mimic human tactile receptors and skin. For the 3-axis sensing, four individual capacitive sensors composed single sensing cell. Our sensor can sense and distinguish the pressure and shear force by analyzing the capacitance change of four individual capacitive sensors. For the strain sensing, flat nanowire composite was used. During the stretching process, the flat nanowire composite was deformed and this deformation resulted in the resistance change of the flat nanowire composite. Our sensor can detect the strain by analyzing the resistance change of the flat nanowire composite.

4.2. Experimental

AgNW ink (YURUI chemical, Shanghai, China, AgNW length ~20μm) was spray-coated on the glass with patterning mask. Spray-coated AgNW film was dried at 50℃ for 30min. We poured the mixture of liquid PDMS and curing agent (Sylgard 184, Dow corning. Liquid PDMS and a curing agent were mixed in the ratio 10:1 by weight) on the AgNW film and then cured it at 65℃ for 12 hours. After curing, we peeled off the the AgNW embedded PDMS from the glass and finally obtained the flat AgNW embedded PDMS electrode, the bottom electrode. PDMS dielectric layer (10:1 ratio of weight) was spin-coated onto the bottom electrode. The patterned top electrode with wavy and flat structure was obtained from the selective forming of SiO_x thin film by using patterning mask and UV/O_3 treatment. The mold PDMS was stretched uniaxially up to 40% and UV/O_3 treatment (power = 28 mW/cm^2) was conducted to form the patterned SiO_x thin film on the mold PDMS surface by using patterned mask. Then, AgNW ink (YURUI chemical, AgNW length 5~10μm) was spray-coated onto the mold PDMS. Spray-coated AgNW film was dried at 50℃ for 30min. After heat treatment, the mold PDMS was released to its initial state (zero strain) and the buckled patterns was introduced to the AgNW film and mold PDMS. Due to the mask during UV/O_3 treatment, SiO_x thin film was formed selectively and buckled structure was also selectively introduced onto the area of SiO_x. AgNW film followed well the buckled structure. We poured the mixture of liquid PDMS and curing agent on the AgNW film and then cured it at 65℃ for 12 hours. After curing, we peeled off the mold PDMS from the AgNW

embedded PDMS and finally obtained the patterned AgNW embedded PDMS electrode, the patterned nanowire composite. To bond PDMS spacer and the PDMS dielectric layer, both surfaces are activated using the oxygen plasma (CUTE-1MP, Femto Science) for 40 seconds and activated surfaces of PDMS spacer and the PDMS dielectric layer were sandwiched together. Then, we heated sandwiched sample at 80℃ for 30min and irreversible strong chemical bonding was successfully

introduced between the PDMS spacer and the PDMS dielectric layer. To fabricate the multifunctional sensor, the patterned nanowire composite and PDMS spacer were activated through the oxygen plasma treatment and they were sandwiched together to introduce the strong chemical bonding between the PDMS spacer and flat area of patterned nanowire composite. Finally we obtained the stretchable multifuctional sensor.

The microstructure of the patterned electrode was characterized by using a field emission scanning electron microscope (FE-SEM, Hitachi S-48000), a 3-dimensional surface profiler (NanoFocus) and optical microscope (EGTECH). Pressure was applied to the sensors by using IMADA force gauge with a z-aixs stage and metal weights. The capacitance of the bendable sensor was measured at 1 kHz with a 0.1 V a.c. signal by using Agilent 4284A LCR meter. The resistance of the nanowire composite was measured at 1V by using digital sourcemeter (Keithley 2420). Stretching test of the sensor was performed using a home-made stretching apparatus.

4.3. Results and Discussion

A schematic illustration of the stretchable multifuctional sensor is shown in Figure 4.1(a). Our sensor consists of the patterned nanowire composite (patterned electrode), spacers and the bottom plane (PDMS dielectric layer and flat nanowire composite). Each component of the sensor is stretchable and based on this stretchability the multifunctional sensor is also stretchable. We introduced various sensing ability to the sensor to demonstrate the multifunctionality like human skin. As shown in Figure 4.1, we introduced pressure and shear force sensing area and strain sensing area. For the pressure and shear force sensing, four individual capacitive sensors composed single sensing cell. Our sensor can sense the pressure and shear force by analyzing the capacitance change of four individual capacitive sensors. For the strain sensing, flat nanowire composite was used. During the stretching process, the flat nanowire composite was deformed and this deformation resulted in the resistance change of the flat nanowire composite. Our sensor can detect the strain by analyzing the resistance change of the flat nanowire composite.

Pressure and shear force were applied to our sensor to measure the pressure sensitivity and shear force sensitivity. Relative capacitance changes of four individual capacitive sensors ($\Delta C/C_0$, $\Delta C = C - C_0$) according to the pressure change are shown in Figure 4.2 (a). Four individual capacitive sensors showed almost same capacitance change behavior under the normal pressure as shown in Figure 4.2 (a). The pressure sensitivity, $S = 0.9 \text{ kPa}^{-1}(0\sim0.6\text{kPa}), S = 3 \text{ kPa}^{-1}(0.6\sim1.3\text{kPa}), and\ S = 0.3 \text{ kPa}^{-1}(> 1.3\text{kPa})$. We applied shear force to

the right direction as shown in Figure 4.2 (b) and measured the capacitance changes of four individual capacitive sensors. Capacitance changes of four individual capacitive sensors were different from the capacitance changes in normal

(a)

Flat AgNW
embedded PDMS

Wavy AgNW
embedded PDMS

1) Pressure & shear force sensing area
2) Strain sensing area

(b)

<Top view>

Flat

Wavy

Bonding area

Single sensing cell

(c)

<Side view>

AgNWs/PDMS

spacer   spacer

PDMS dielectric layer

PDMS

AgNWs/PDMS
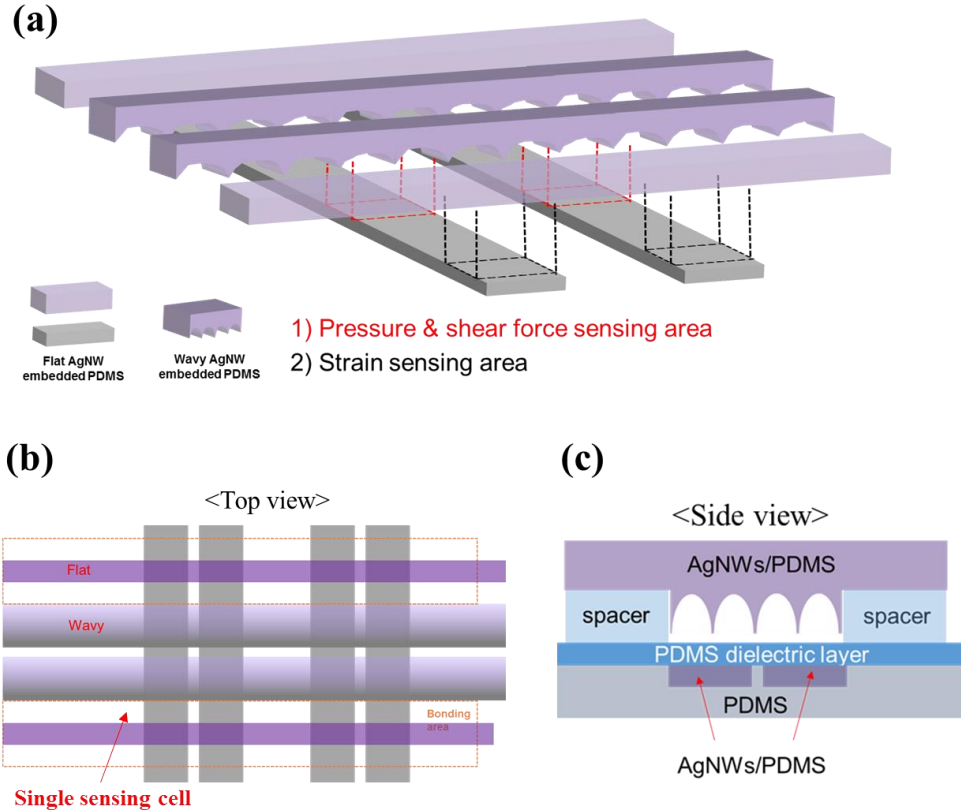
Figure 4.1 (a) Schematic image of the stretchable multifunctional sensor. (b) Top view image of the sensor. (c) Side view image of the sensor.

pressure condition. As shown in Figure 4.2 (b), when the shear force to the right direction is applied to the bump of the sensor, the bump and nanowire composite in the sensing area were deformed due to the torque generated from the shear force. The air gap on the left side of the sensing area increased, whereas the air gap on the right side of the sensing area decreased as shown in Figure 4.2 (b). As a result, the

101

capacitance values of the sensor number 1 and number 3 decreased as the shear force increased and the capacitance values of the sensor number 2 and number 4 increased as the shear force increased as shown in Figure 4.2 (b). The behavior of the capacitance change of the sensor in the same deformation condition was almost same as shown in Figure 4(b).
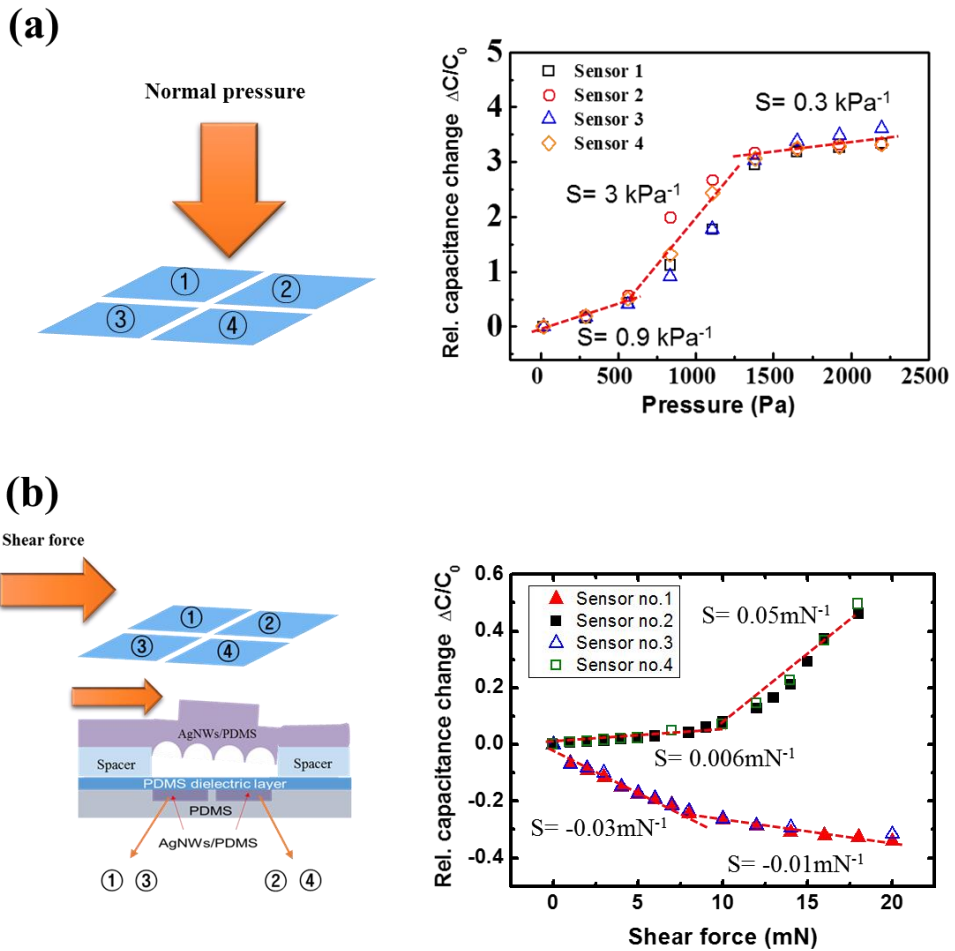
Figure 4.2 (a) Normal pressure to the sensor (left). Relative capacitance change-pressure curves of four individual capacitive sensors (right). (b) Shear force direction and the deformation of the sensor according to the shear force (left). Relative capacitance change-shear force curves of four individual capacitive sensors (right).

102

The shear force sensitivity, S ($S = \delta(\Delta C/C_0)/\delta f$, $\Delta C = C - C_0$, where C and C_0 denote the capacitance with the applied pressure and the base capacitance, respectively, and f denotes the shear force) was calcualted. The shear force sensitivity of the sensor for the left side of the sensing area, $S = -0.03 \text{ mN}^{-1}(0\sim7 \text{ mN})$ and $S = -0.01 \text{ mN}^{-1}(7\sim20 \text{ mN})$. The shear force sensitivity of the sensor for the right side of the sensing area, $S = 0.006 \text{ mN}^{-1}(0\sim8 \text{ mN})$ and $S = 0.05 \text{ mN}^{-1}(8\sim18 \text{ mN})$.

The repeated pressure and shear force were applied to the sensor, respectively, to demonstrate the stability and robust sensing ability of the sensor. We pressed our sensor with finger, several times, and measured the capacitance changes of four individual capacitive sensors as shown in Figure 4.3 (a). When we pressed the sensor with finger, all the capacitance values of four individual capacitive sensors increased up to almost same value as shown in Figure 4.3 (a). Also, the capacitance values at pressing condition were maintained constantly during the repeated pressing cycle as shown in Figure 4.3 (a). We applied shear force to the right direction repeatedly by using home-made motorized moving machine and force gauge. By attaching the force gauge onto the moving machine and moving the force gauge back and forth, we applied repeated shear force. We measured the capacitance change during the repeated shear force cycle as shown in Figure 4.3 (b). The capacitance values of the sensor number 1 decreased as the shear force increased and almost same capacitance changes were obtained to the repeated shear force (Maximum shear force is about 20mN.) as shown in Figure 4.3 (b). The capacitance values of the sensor number 2 increased as the shear force increased and almost same capacitance changes were obtained to the repeated shear force (Maximum shear force is about 20mN.) as shown in Figure 4.3 (b). These results demonstrate the robust sensing ability of the

sensor and stability to the repeated pressure and shear force.

(a)
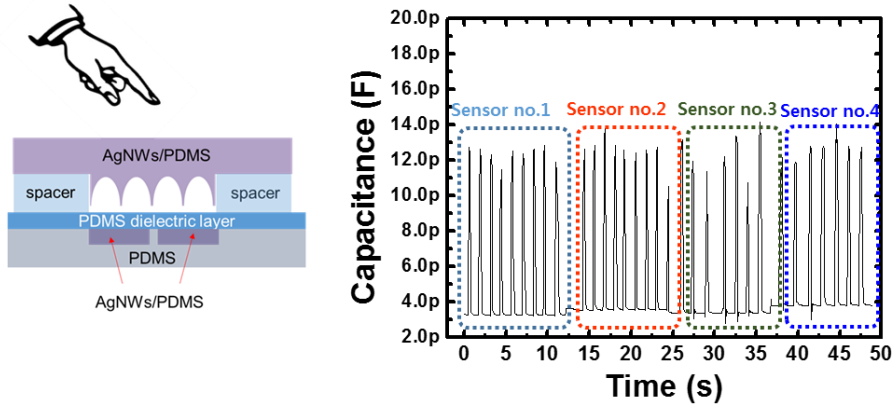
(b)
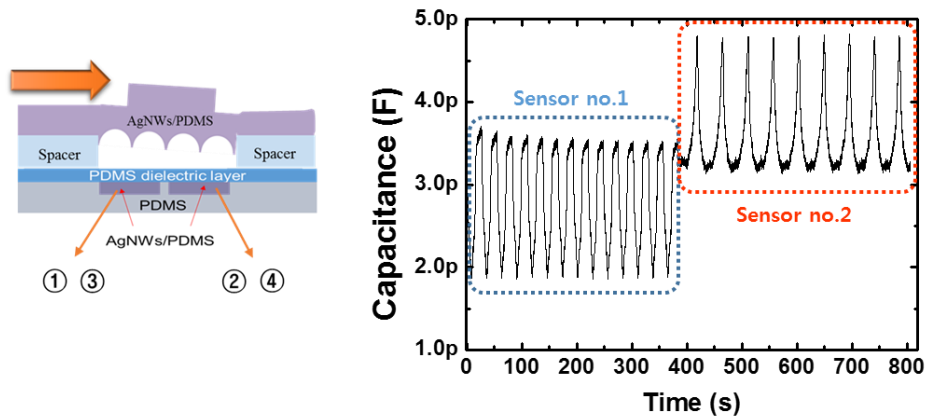
Figure 4.3 (a) Applied pressure to the sensor by touching with finger (left). Capacitance change-time curves of four individual capacitive sensors (right). (b) Shear force direction and the deformation of the sensor according to the shear force (left). Capacitance change-time curves of sensor number 1 to sensor number 2 (right).

We stretched our sensor up to 30% and measured the resistance change of the flat nanowire composite during the stretching as shown in Figure 4.4. Because the flat nanowire composite is free to the deformation when the pressure or shear force is applied to the sensor, we selected the flat nanowire composite as a resistive strain sensor. As shown in Figure 4.4 (a), the resistance of the flat nanowire composite increased as the strain increased. The gauge factor, $GF = (\Delta R/R_0)/(\Delta L/L_0)$, of the resistive strain sensor was about 2.7. We stretched the sensor up to 30% and 100 times and measured the resistance change as shown in Figure 4.4 (b). We stretched the sensor with stretching speed of 0.5mm/s. As shown in Figure 4.4 (b), the relative resistance change values were maintained stably within 10% variation during the 100-cycle test and this demonstrate that strain sensor is stable and robust to the repeated stretching.
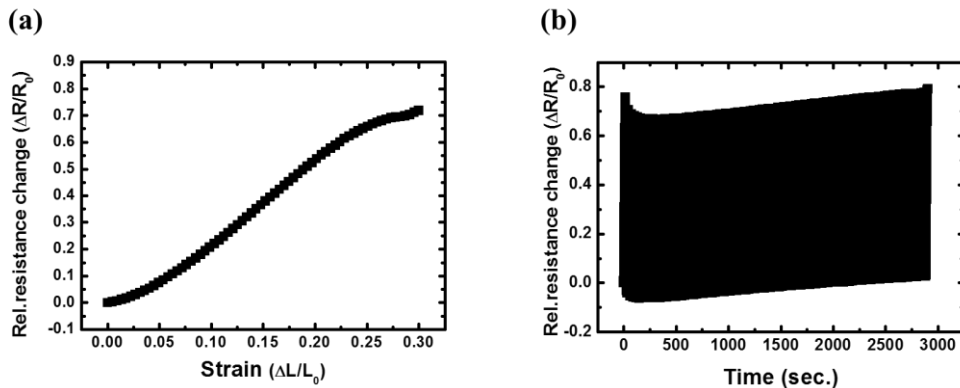
Figure 4.4 (a) Relative resistance change-strain curve of the flat nanowire composite. (b) Relative resistance change-time curve of the flat nanowire composite. We stretched the sensor up to 30% and 100 times.

4.4. Conclusion

We have fabricated stretchable multifunctional sensor which can detect the pressure, shear force, and strain. By introducing various sensing component to the sensing system, we can obtain multifunctional sensor to mimic human tactile receptors and skin. For the pressure and shear force sensing, four individual capacitive sensors composed single sensing cell. Our sensor can sense and distinguish the pressure and shear force by analyzing the capacitance change of four individual capacitive sensors. The maximum pressure sensitivity is about 3kPa^{-1} and the maximum shear force sensitivity is about 0.05mN^{-1} for increasing area and -0.03mN^{-1} for decreasing area. For the strain sensing, flat nanowire composite was used. During the stretching process, the flat nanowire composite was deformed and this deformation resulted in the resistance change of the flat nanowire composite. Our sensor can detect the strain by analyzing the resistance change of the flat nanowire composite and the gauge factor is about 2.7. Our sensor may open and broaden its application to the wearable and comfortable multifunctional sensing systems and electronic skins.

Reference

[1] A. N. Sokolov, B. C.-K. Tee, C. J. Bettinger, J. B.-H. Tok and Z. Bao, *Acc. Chem. Res.*, 45, 361 (2012)

[2] S. Kim, J. Byun, S. Choi, D. Kim, T. Kim, S. Chung, and Y. Hong, *Adv. Mater.*, 26, 3094 (2014)

[3] T. Kim, H. Song, J. Ha, S. Kim, D. Kim, S. Chung, and Y. Hong, *Appl. Phys. Lett.,* 104, 113103 (2014)

[4] D.-H. Kim, N. Lu, R. Ma, Y.-S. Kim, R.-H. Kim, S. Wang, J. Wu, S. M. Won, H. Tao, A. Islam, K. J. Yu, T.-i. Kim, R. Chowdhury, M. Ying, L. Xu, M. Li, H.-J. Chung, H. Keum, M. McCormick, P. Liu, Y.-W. Zhang, F. G. Omenetto, Y. Huang, T. Coleman, and J. A. Rogers, *Science*, 333, 838 (2011)

[5] J. Lee, S. Chung, H. Song, S. Kim, and Y. Hong, *J. Phys. D: Appl. Phys.*, 46, 105305 (2013)

[6] J. Liang, L. Li, X. Niu. Z. Yu, and Q. Pei, *Nat. Photonics*, 7, 817-824 (2013)

[7] W. Hu, X. Niu, R. Zhao, and Q. Pei, *Appl. Phys. Lett.*, 102, 083303 (2013)

[8] M. Amjadi, A. Pichitpajongkit, S. Lee, S. Ryu, and I. Park, *ACS nano*, 8, 5154-5163 (2014)

[9] J. Kim, M. Lee, H. J. Shim, R. Ghaffari, H. R. Cho, D. Son, Y. H. Jung, M. Soh, C. Choi, S. Jung, K. Chu, D. Jeon, S.-T. Lee, J. H. Kim, S. H. Choi, T. Hyeon, and D.-H. Kim, *Nat. Commun.*, 5, 5747 (2014)

[10] C. Choong, M. Shim, B. Lee, S. Jeon, D. Ko, T. Kang, J. Bae, S. Lee, K. Byun, J. Im, Y. Jeong, C. Park, J. Park, and U. Chung, *Adv. Mater.*, 26, 3451 (2014)

[11] D. J. Lipomi , M. Vosgueritchian , B. C.-K. Tee , S. L. Hellstrom , J. A. Lee , C. H. Fox , and Z. Bao , *Nat. Nanotechnol.*, 6, 788 (2011)

[12] S. Yao and Y. Zhu, *Nanoscale*, 6, 2345 (2014)

[13] F. Xu and Y. Zhu, *Adv. Mater.*, 24, 5117-5122 (2012)

[14] Z. Chu, P. M. Sarro, and S. Middlehoek, *Sens. Actuators A, Phys.*, 54, 505 (1996)

[15] B. J. Kane, M. R. Cutkosky, and G. T. A. Kovacs, *J. Microelectromech. Syst.*, 9, 425 (2000)

[16] J. Engel, J. Chen, and C. Liu, *J. Micromech. Microeng.*, 13, 359 (2003)

[17] H.-K. Lee, J. Chung, S.-I. Chang, and E. Yoon, *J. Microelectromech. Syst.*, 17, 934 (2008)

[18] G. Liang, Y. Wang, D. Mei, K. Xi, and Z. Chen, *J. Micromech. Microeng.*, 26, 045007 (2016)

[19] L. Viry, A. Levi, M. Totaro, A. Mondini, V. Mattoli, B. Mazzolai, and L. Beccai, *Adv. Mater.*, 26, 2659 (2014)

[20] R. Surapaneni, Q. Guo, Y. Xie, D. J. Young and C. H. Mastrangelo, *J. Micromech. Microeng.*, 23, 075004 (2013)

[21] H.-K. Lee, J. Chung, S.-I. Chang, and E. Yoon, *J. Micromech. Microeng.*, 21, 035010 (2011)

[22] N. Noda, K. Matsumoto, and I. Shimoyama, *Sens. Actuators A, Phys.*, 215, 123 (2014)

Chapter 5

Conclusion

In this thesis, we report pressure and strain sensing devices based on the nanowire composite composed of silver nanowires (AgNWs) and polydimethylsiloxane (PDMS). By introducing the multiscale structure which is composed of nanometer-sized rough surfaces and micrometer-sized wavy structures to the nanowire composite and fabricating the sensor with multiscale structured nanowire composite, we obtained highly sensitive pressure/strain sensors.

We used the buckled silicon oxide/PDMS as a mold to demonstrate the simple and low-cost microscale mold fabrication method and fabricated multiscale structured nanowire composite by using this mold. Owing to the peel-off stress during the peeling off process of nanowire composite from the mold, nanoscale rough surface was successfully introduced to the crest area of microscale wavy structure. The pressure sensor integrated with multiscale structured nanowire composite and polymeric dielectric layer/printed Ag electrode on plastic substrate showed highly pressure sensitivity and flexibility. We obtained maximum pressure sensitivity of 3.8 kPa^{-1} in low pressure region and very small pressure of 15 Pa can be detected by using the sensor. Sensor arrays were also demonstrated and can detect the spatial distribution of the applied pressure. We also fabricated the fingertip pressure sensing device to detect the pressure distribution of fingers, when grabbing

an object.

We fabricated pressure sensor with tunable pressure sensitivity by controlling the mechanical property of the matrix PDMS of nanowire composite. Due to the difference of the mechanical property of the matrix PDMS and the shape of the crest area of the buckled structure, the pressure sensitivity of the sensor can be easily tuned. This sensor can also detect the bending strain and is very stable to the repeated bending condition.

Based on the APTES surface functionalization and spacer, we have bonded all components of the sensor and fabricated bendable pressure sensor which can detect the pressure even in the bending state and operate stably in the bending state. By introducing the bending sensing part beside the pressure sensing part, the bendable sensor can detect both pressure and bending and distinguish the pressure and bending. We integrated the bendable sensor with the inkjet-printed SWCNT TFT for the fabrication of the pressure sensitive transistor (PST). PST can be operated in low voltage below 5V. By using the PST and commercially available electronic devices such as LED chip, resistor, OP amp and battery, we fabricated the user inter-active pressure sensing device and pulse monitoring device.

We fabricated stretchable multifunctional sensor which can detect the pressure, shear force, and strain by using only nanowire composite and PDMS. By introducing various sensing component to the sensing system, we demonstrated multifunctional sensor to mimic human tactile receptors. For the pressure and shear force sensing, four individual capacitive sensors composed single sensing cell. Multifunctional sensor can sense and distinguish the pressure and shear force by analyzing the capacitance change of four individual capacitive sensors. For the strain sensing, flat nanowire composite was used. During the stretching process, the flat nanowire

composite was deformed and this deformation resulted in the resistance change of the flat nanowire composite. By analyzing the resistance change of the flat nanowire composite, strain can be detected. Our sensor may open and broaden its application to the wearable and comfortable multifunctional sensing systems and health monitoring/sensing system.

한글 초록

본 논문에서는 피부 부착 가능하며 입을 수 있는 전자소자 구현을 위해 나노와이어 복합체를 이용한 고민감도의 압력/변위 센서에 대해 연구하였다. 이를 위해 은나노와이어와 PDMS로 구성된 다중스케일 구조의 나노와이어 복합체를 고안하였으며 이를 이용해 다기능 센서를 제조하였다. 다중스케일 구조의 나노와이어 복합체를 기반으로 한 고성능의 압력/변위 센서를 제조하였으며 이를 분석 하였다.

최근 웨어러블 전자소자로의 응용을 위해서 유연하거나 신축성 있는 압력, 변위, 온도 센서와 같은 물리 센서들이 광범위하게 연구되고 있다. 이러한 응용을 위해서는 특히 높은 민감도, 빠른 응답속도, 반복 안정성을 갖는 고성능의 압력/변위 센서들이 요구된다. 따라서 본 연구는 나노미터 사이즈의 거친 표면과 마이크로미터 사이즈의 물결 구조로 이루어진 다중스케일 구조를 갖는 나노와이어 복합체를 개발하였으며 이를 고분자 유전층과 인쇄된 은전극과 활용해 정전용량식 압력센서와 어레이를 개발하였다. 제작된 센서는 높은 압력 민감도 (S >3.8 kPa^{-1}), 빠른 응답속도 (t <0.15s), 반복 안정성 (1500회의 압력 사이클과 5000회의 굽힘 사이클)을 보였으며 압력과 굽힘을 측정할 수 있었다. 나노와이어 복합체를 이용하여 대면적의 센서 어레이를 제작할 수 있었으며 3행 3열과 5행 5열의 압력센서 어레이를 제작하였다. 센서 어레이는 단일 센서와 비슷한 민감도 특성을 보였으며 공간적으로 분포된 압력을 측정 할 수 있었다. 손가락 끝에 압력센서를 붙여 장갑형태의 센서를 구현하였으며 플라스틱 비커를 잡았을 때 손가락에서의 압력 분포를 측정 하였다.

나노와이어 복합체를 구성하는 PDMS의 배합 비율을 달리하여 압력센서의 민감도를 조절 할 수 있는 방법을 개발하였다. 5:1, 10:1, 15:1의 비율로 배합된 액상 PDMS와 가교제를 이용하여 나노와이어 복합체를 제작하였다. 배합비율에 따라 복합체의 탄성비율과 구조가 달라져서 제작된 센서의 민감도 특성이 각 배합 비율에 따라 달라지는 특성을 보였다.

굽힘 안정성과 굽힘 상태에서 압력을 측정 할 수 있는 벤더블 압력 센서를 개발 하였다. 센서에 압력 측정 영역과 굽힘 측정 영역을 넣어서 압력과 굽힘 모두를 측정 할 수 있으며 구별 할 수 있는 벤더블 센서를 개발 하였다. 고분자 유전층 위에 표면처리와 산소 플라즈마 처리를 통해서 규소 산소 간의 강한 결합을 유도하여 굽힘에서 안정적으로 동작하는 벤더블 압력 센서를 제작하였다. PDMS 스페이서를 통해 유도된 공기층으로 인해서 센서의 민감도가 9 kPa^{-1}로 크게 향상 되었다. 이로 인해 0.7 파스칼의 매우 작은 압력을 측정 할 수 있었고 0.075초 이내의 매우 빠른 응답속도를 보였다. 또한 굽힘 환경에서도 압력을 측정 할 수 있었으며 이러한 벤딩 센서를 이용하여 손목 맥박과 휴대전화의 진동을 감지할 수 있었다. 센서 어레이를 제작하였으며 굽힘 상태에서의 가해진 압력을 역으로 계산하였다. 벤더블 센서와 단일벽 탄소나노튜브 트랜지스터를 결합하여 압력 민감 트랜지스터를 개발 하였다. 압력 민감 트랜지스터는 5V이하의 동작전압에서 작동하였으며 15nW의 매우 작은 전력을 소모하였다. 압력 민감 트랜지스터와 LED 칩, 저항, 증폭기, 배터리를 활용하여 사용자 상호작용 센싱 시스템과 맥박 측정 장비를 개발 하였다.

마지막으로 수직방향과 수평방향 힘을 측정하고 변위를 측정 할 수 있는 신축성 다기능 센서를 나노와이어 복합체를 사용하여 개발 하였다. 특히 사람의 피부와 촉각 수용기를 모사하기 위해서 여러 센서 요소들을 도입하였다. 3축 방향의 힘을 감지하기 위해서 4개의 개별 정전용량 센서를 하나로 통합하였으며 각 개별 센서의 정전용량의 변화를 관측하여 압력과 전단력을 구별 할 수 있었다. 나노와이어 복합체의 스트레칭 시에 저항 변화를 통해서 변위를 감지하였다.

주요어 : 압력 센서, 변위 센서, 웨어러블 전자소자, 나노와이어 복합체, 다중스케일 구조, 신축성 전자소자

학 번 : 2012-30233